

Flocculation-assisted dewatering of fluid fine tailings using a volute screw press

by

Chen Wang

A thesis submitted in partial fulfillment of the requirements for the degree of

Doctor of Philosophy

in

Chemical Engineering

Department of Chemical and Materials Engineering
University of Alberta

© Chen Wang, 2017

Abstract

Rapid, efficient and economical water removal from fluid fine tailings represents a major challenge to many industries, including mineral processing, food processing, waste water treatment and oil sands extraction. In the absence of large-scale fine tailings processing facilities, there will be an escalating accumulation of such waste material in containment areas, which requires careful, extensive and often costly measures for hazards mitigation.

A flocculation-assisted two-stage process to continuously dewater oil sands fluid fine tailings using a volute screw press is developed. A cationic-anionic flocculant scheme was applied first to the fluid fine tailings, which flocculated essentially all suspended solids in the slurry. The concept of elastic and plastic deformations for metallic solids was extended and successfully applied to describe compression and subsequent water release characteristics of semi-solid tailings sediment. The newly developed “*controlled vertical strain test*” (CVST) enables bench-scale measurement on the theorized impact of flocculants on sediment compressive dewaterability. A new empirical parameter named “*compressive dewatering index*” (CDI) was obtained from the sediment compression response curve via the CVST method.

The flocculated slurry was introduced to the volute screw press through a series of inclined steel rings (volute plates), and carried upwards by a central auger screw. Unobstructed and self-cleaning spacing between all volute plates ensures removal of unhindered supernatant, while large flocs of sufficient mechanical strength were retained and compressed by the screw. Field test work at Canadian Natural Resources Limited

with a prototype volute screw press demonstrated successful production of stackable cake containing 55 - 60 wt% solids at 5 - 7 kg dry solids/h production rate.

The field test results showed a strong linear correlation between the CDI and the filter cake dry solids content produced by the volute screw press. Such correlation allows predictive evaluations on the volute screw press dewatering performance at bench-scale. For elastic sediments, the slope of this linear correlation is termed as the *CDI gain* of the fluid fine slurry. This intrinsic and material-specific parameter could be used to universally classify any given fine fluid mineral slurry in its dewatering difficulty by mechanical means. The findings from this study could serve as a unified theoretical framework for future research on post-flocculation dewatering of fluid fine tailings by external mechanical forces as encountered in centrifuge and filtration.

Preface

This thesis is an original work by Chen Wang.

Sections 1.1 to 1.4 in this thesis has been published previously as a review article by C. Wang, D. Harbottle, Q. Liu, Z. Xu entitled as “Current state of fine mineral tailings treatment: A critical review on theory and practice”, *Minerals Engineering* 58 (2014) 113–131. I was responsible for manuscript composition and co-authors D. Harbottle, Q. Liu, and Z. Xu assisted in manuscript edits.

Numerous sections in Chapters 2-7 are undergoing editorial reviews for publication in the *Canadian Journal of Chemical Engineering*.

Why would anyone want to spend his/her career on...tailings???

Hear me out! Because if you do, eventually:

No more ducks will perish in ponds.

No more souls will be swept away from accidental discharge.

No more settlements will be flooded by breach of containment.

Also,

No professional engineer would turn down a challenge.

Especially a challenge that took nature millennia to deal with,

and now we need it resolved in minutes.

Acknowledgements

Phase 1 (preliminary) study was carried out with the generous assistance from Prof. Sean Sanders at the University of Alberta. During the months of October 2015 to February 2016, Prof. Sanders devoted a large section of his own laboratory space for our volute screw press research. I would like to take this opportunity to again express my heartfelt gratitude to Prof. Sanders and his research team.

Insights from the early **Phase 1** study were instrumental for our subsequent success in our August 2016 **Phase 2** (field) study at Horizon Oil Sands Innovation Centre (Canadian Natural Resources Ltd.). I am also grateful for the generous help from Canadian Naturals staff at Horizon, including but not limited to: Mr. Aref Najafi, Mr. Vince Wallwork, Mr. Ashar Mirza, Mr. Reza Salehi, and Mr. Victor Maries.

The flash of insight that initiated the successful laboratory-based **Phase 3** (bench-scale) study was due in no small part to the M. Sc. thesis of Mr. Sandeep Sinha (“Mechanical dewatering of chopped alfalfa”), published in 1995 at the University of Saskatchewan.

Of course, none of the above would have been possible without the incredible amount of support and guidance from Prof. Zhenghe Xu, Prof. Qingxia Liu, as well as Prof. Jacob Masliyah and all members of the NSERC IRC in Oil Sands Engineering research group. Prof. Xu, Prof. Liu, and Prof. Masliyah hold every one of their students to the highest possible standard in academic research and integrity. It certainly felt good to have worked with like-minded individuals since day one.

Also, a big thanks to my wife and my family for putting up with my eccentric side on my lifelong quest for converting most – if not all – of Alberta’s oil sand tailings to dry stackable deposits. Your blind trust in my evidence-backed intuitions deserves a special mention. You had no clue as to where I was headed, didn’t you?

Table of Contents

Chapter 1: Introduction and Literature Review	1
1.1 Introduction.....	1
1.1.1. Fluid fine mineral tailings.....	1
1.1.2. Accumulated tailings issues.....	3
1.1.3. Current tailings treatment objectives.....	6
1.2. Theoretical considerations.....	7
1.2.1. Tailings solids and stability.....	7
1.2.1.1. Size classification.....	8
1.2.1.2. Solids mineralogy and morphology.....	13
1.2.1.3. Slurry stability.....	16
1.2.1.4. Slurry rheology.....	21
1.2.2. Enhanced settling and densification.....	24
1.2.2.1. Particle aggregation.....	25
1.2.2.2. Coagulation.....	26
1.2.2.3. Flocculation.....	28
1.2.2.4. Other methods.....	36
1.2.3. Consolidation and dewatering.....	38
1.2.3.1. Dewatering and material strength.....	39
1.2.4. Application of external energy.....	39
1.2.4.1. Evaporative and thermal treatments.....	40
1.2.4.2. Centrifugation.....	41
1.2.4.3. Filtration and electrofiltration.....	42
1.2.5. Exclusion of water.....	47
1.2.5.1. Freeze–thaw.....	47
1.2.5.2. Gelation and water absorbents.....	48
1.3. Overview of current technologies.....	49
1.3.1. Densification technologies.....	51
1.3.1.1. Traditional technologies.....	51

1.3.1.2. Assisted fines destabilization.....	53
1.3.2. Dewatering technologies.....	54
1.3.2.1. Natural drying	54
1.3.2.2. Centrifugation	56
1.3.2.3. Filtration.....	56
1.3.3. Knowledge gaps.....	59
1.4. Conclusions.....	62
1.5. Thesis objectives.....	64
1.6. Organization of thesis	65
References.....	66
Chapter 2: Volute Screw Press	77
2.1. Overview.....	77
2.2. Feed system.....	78
2.3. Dewatering press.....	79
2.4. Automatic operations.....	81
References.....	82
Chapter 3: Mechanical Dewatering of Flocculant-assisted Tailings Sediments	83
3.1. Theoretical considerations on VSP dewatering.....	83
3.1.1. Dewatering mechanisms of the VSP.....	83
3.1.2. Hypothesized outcomes of VSP dewatering.....	84
3.2. Hypothesis on elasticity and plasticity of dewatering.....	87
3.2.1. Driving forces in VSP dewatering	87
3.2.2. Elasticity and plasticity of dewatering.....	88
3.3. The controlled vertical strain test (CVST).....	89
3.3.1. CVST setup.....	89
3.3.2. Sensor calibrations	92
3.3.3. CVST generalized procedure	96
3.3.3.1. Preparing for the CVST	100
3.3.3.2. CVST experimental	101
3.3.3.3. Flocculant addition.....	106
3.3.3.4. Initial settling rate (ISR) and supernatant turbidity	106

3.3.3.5. Running the CVST.....	107
3.3.3.6. Notes on cleanup.....	111
References.....	112
Chapter 4: Volute Screw Press Field Study	113
4.1. Field study experimental.....	113
4.2. Flocculant solution preparations	115
4.3. Process start-up	115
4.4. Sample collection.....	115
Chapter 5: Controlled Vertical Strain Tests	117
5.1. Controlled vertical strain test results (10 formal cases).....	117
5.1.1. Flocculation performance	117
5.1.2. CVST stress-strain curves.....	121
5.1.2.1. Identifying the nature of a plasticity event	121
5.1.2.2. Empirical curve classification and analysis	129
5.1.2.3. Onset of compression, rupture point, and CDI results...	132
Chapter 6: Volute Screw Press Dewatering Tests	135
6.1. Effects of A-PAM and C-PAM (10 formal cases).....	135
6.1.1. Filter cake product dry solids.....	135
6.1.2. Filter cake dry solids throughput	137
6.1.3. Filtrate quality.....	139
6.1.4. Volute plate runoff losses	140
6.2. Effects of other adjustable operating parameters (6 trial cases)	143
6.2.1. Full recycle operating mode.....	143
6.2.2. Flocculant solution preparation time	144
6.2.3. Endplate gap distance	145
6.2.4. FT mixer speed	146
6.3. Process mass balance (10 formal cases)	147
6.3.1. Process and stream analyses	147
6.3.2. Detailed calculations.....	148
6.3.2.1. Assumptions.....	148
6.3.2.2. Dry solids in Dewatering Press feed (Stream 3).....	149

6.3.2.3. Mass and material flows of Dewatering Press	151
6.3.2.4. Mass and material flows in Mixing Tanks.....	153
6.3.3. Dry solids distribution in Dewatering Press	156
6.3.4. Water balance.....	158
References.....	161
Chapter 7: Predictive Modeling of VSP Filter Cake Quality	162
7.1. Correlations between CVST results and VSP filter cake quality	162
7.2. CDI gain.....	164
Chapter 8: Conclusions and Knowledge Contributions.....	165
8.1. Early VSP trials (Phase 1).....	165
8.2. Field operations (Phase 2).....	168
8.3. Lab-based CVST studies (Phase 3).....	171
8.4. Original contributions to scientific knowledge.....	174
8.5. Future work.....	175
All References.....	179
Appendix A: Some Geotechnical Considerations	190
A.1. One-dimensional consolidation test (oedometer test).....	190
A.2. Sediment dewatering characteristics prior to CVST compression regime .	191
A.3. Evolution of sediment void ratio in CVST	193

List of Tables

Table	Page
1.1 Grain size classification criteria.....	9
1.2 Examples of grain size distributions for mineral tailings of different origins.....	10
1.3 General characteristics of alumina, phosphate and copper tailings.....	15
1.4 Impact of selected flocculant and solution properties on major flocculation mechanisms.....	34
3.1 Main mechanisms of water removal from the dewatering press.....	83
3.2 Major ionic species in Horizon pond water.....	102
3.3 Formal experimental cases in field study.....	103
4.1 VSP normal operation setpoints.....	113
4.2 Trial cases in field study.....	114
5.1 Properties of point <i>O</i> and point <i>R</i> for each experiment case.....	133
6.1 Process data for runoff calculations.....	142
6.2 Operating results for six trial cases.....	143
6.3 Details of each process stream in the VSP circuit.....	148
6.4 Determination of dry solids content for Stream 3.....	151
6.5 Mass and dry solids balances for Dewatering Press.....	153
6.6 Mass and dry solids balances for Mixing Tanks (continuous basis).....	154
6.7 Average VSP operational uptime under automatic mode.....	156
6.8 Dry solids distribution in Dewatering Press.....	157
6.9 Water balance for the VSP circuit.....	160
A1 Initial sediment volumetric dry solids and void ratio for all experimental cases.....	194

List of Figures

Figure		Page
1.1	Two unit layers of kaolinite.....	16
1.2	Typical AFM interaction forces on muscovite.....	19
1.3	Interaction energies associated with the preferred “card house” structure of clays.....	23
1.4	Possible polymeric flocculant conformations following adsorption.....	30
1.5	The added benefit of dual polymer addition.....	35
1.6	Mechanisms of electrofiltration.....	45
1.7	Proposed treatment processes for oil sands MFT using filtration.....	58
2.1	Front view of the volute screw press.....	77
2.2	Overview of the volute screw press feed system.....	79
2.3	Generalized diagram of the dewatering press.....	80
2.4	Internal auger screw at the center of dewatering press.....	81
2.5	Volute plate self-cleaning cycle.....	81
3.1	Volumetric compression by the central auger screw.....	84
3.2	Desirable VSP operating conditions for sediment dewatering.....	85
3.3	Extremely undesirable VSP operating conditions for sediment dewatering.....	85
3.4	Laboratory setup for the controlled vertical strain test.....	90
3.5	Force sensor calibration setup.....	93
3.6	Force sensor calibration data.....	95
3.7	Set up of multi-purpose plexiglass cylinder for the CVST	99
3.8	Particle size distribution and cumulative size distribution for Horizon MFT.....	102
4.1	Time evolution of VSP product dry solids content after a flocculant dosage change.....	116
5.1	Initial settling rate of flocculated sediment solids.....	117
5.2	Supernatant dry solids.....	119
5.3	Initial sediment dry solids.....	120

5.4	Second plasticity event characterization for case A300-C1000.....	122
5.5	Third plasticity event characterization for case A300-C1000.....	124
5.6	Second plasticity event characterization for case A300.....	125
5.7A	Complete CVST stress-strain curves for A300 and A500.....	126
5.7B	Complete CVST stress-strain curves for A300-C1000 and A500- C1000.....	127
5.7C	Complete CVST stress-strain curves for A300-C2000 and A500- C2000.....	127
5.7D	Complete CVST stress-strain curves for A300-C3000 and A500- C3000.....	128
5.7E	Complete CVST stress-strain curves for A300-C4000 and A500- C4000.....	128
5.8	A complete and classified CVST stress-strain curve for A500-C3000....	129
5.9	Compressive dewatering indices for all 10 formal experiment cases.....	134
6.1	Impact of A-PAM and C-PAM dosages on filter cake dry solids content.....	135
6.2	Impact of A-PAM and C-PAM dosages on filter cake dry solids production rate (mass throughput).....	137
6.3	Impact of A-PAM and C-PAM dosages on filter cake dry solids production rate (volumetric throughput).....	138
6.4	Impact of A-PAM and C-PAM dosages on filtrate quality.....	139
6.5	Process flow diagram of the VSP circuit.....	147
7.1	Correlation between average sediment CDI and VSP filter cake quality	162
A1	Relations between CVST pre-compression strain and VSP cake dry solids.....	192
A2(a)	Complete stress-void ratio curves for A300 and A500.....	195
A2(b)	Complete stress-void ratio curves for A300-C1000 and A500-C1000....	196
A2(c)	Complete stress-void ratio curves for A300-C2000 and A500-C2000....	196
A2(d)	Complete stress-void ratio curves for A300-C3000 and A500-C3000....	197
A2(e)	Complete stress-void ratio curves for A300-C4000 and A500-C4000....	197

Nomenclature

A-PAM, APAM	Anionic polyacrylamide
C-PAM, CPAM	Cationic polyacrylamide
CAPEX	Capital expenditure
CDI	Compressive dewatering index
CNRL	Canadian Natural Resources Ltd.
CT	Conditioning tank
CVST	Controlled vertical strain test
DLVO	Derjaguin-Landau-Verwey-Overbeek
DP	Dewatering press
DS	Dry solids
FFT / MFT	Fluid fine tailings / Mature fine tailings
FHT	Feed holding tank
FT	Flocculation tank
inst	instantaneous flow rate
ISR	Initial settling rate
NTU	Nephelometric turbidity unit
OPEX	Operational expenditure
PAM	Polyacrylamide
RPM	Rotations per minute
SV	Sensor value
VSP	Volute screw press
W	Water

Chapter 1: Introduction and Literature Review

1.1 Introduction

1.1.1. Fluid fine mineral tailings

Fluid fine mineral tailings refer to a mixture of waste by-products generated when recovering useful and precious minerals, metals, and other resources from the ores using mineral processing and hydrometallurgical processes. After selective extraction and beneficiation of the desired materials, the mill rejects and residuals are combined to form the tailings stream. In most cases the tailings are discharged in the form of a slurry into lagoons, engineered ponds and mine sites, where solids and process fluids separate under gravity. Given sufficient time, the nearly solids-free supernatant can be recycled into the extraction process to reduce freshwater intake and minimize waste volume. In very few instances the waste tailings has been discharged directly into the environment, although this practice is heavily declining and the practice is banned in many countries under more strict guidelines of zero discharge (Power et al., 2011; Samal et al., 2013). Discharge to tailings ponds remains an inexpensive and proven technology that has been widely adopted by the mineral industry (Watson et al., 2010). However, this approach often does not provide a long term tailings management solution.

With the ever-growing demand for mineral products, coupled with deterioration and depletion of high-grade mineral ore deposits, mining of lower-grade ores that are more resource- and energy-intensive to process is becoming the norm (Crowson, 2012; Bethell, 2012; Nesbitt, 2007; Jones and Boger, 2012). In these cases, sub-micrometer ore grinding and classification become inevitable to achieve the necessary mineral liberation and

hence recovery using conventional mineral processing and hydrometallurgical processes. Unfortunately, fine grinding has also led to the reduced selectivity by the production of undesired fine gangue mineral solids. These fine solids, often only a few microns in diameter, are extremely difficult to separate from the tailings water. As a result they contribute directly to the accumulation of an alarmingly large volume of fluid waste mineral tailings that requires safe containment.

For example, typical coal preparation plants discharge 75–120 kg of dry tailings per tonne of coal processed. These tailings are in the slurry form, with total solid contents ranging between 20% and 35% (w/w) (Ryu et al., 2008; Beier and Segó, 2009; Murphy et al., 2012). In 2002, the U.S. National Research Council estimated that 70–90 million tonnes of tailings were produced annually by these facilities in the United States alone (National Research Council, 2002). Global inventory of the highly alkaline by-product (red mud) from alumina production using the Bayer process has surpassed 2.5 billion tonnes in 2007 with a predicted growth of 120 million tonnes per year, at an estimated ratio of 1–1.5 tonnes of red mud per tonne of alumina product, or 4 tonnes per tonne of finished aluminum (Kumar et al., 2006; Power et al., 2011). Production of phosphoric acid, an essential ingredient for the fertilizer ammonium phosphate, generates on average 450% of its weight as phosphogypsum (phosphate tailings) (Zhang and Stana, 2012). Given a worldwide phosphoric acid production of 40 million tonnes in 2010, about 180 million tonnes of acidic phosphate tailings require proper disposal (International Fertilizer Industry Association, 2010). At the extreme, extraction of copper generates a vastly disproportional amount of tailings. According to studies by Gordon and Bridge, 128–196 tonnes of combined copper tailings would be generated to produce 1 tonne of

copper (Gordon, 2002; Bridge, 2000). Using Gordon's data, Onuaguluchi and Eren estimated a worldwide production of 2 billion tonnes of copper tailings in 2011 (Onuaguluchi and Eren, 2012).

A notable example outside mineral processing is found in northern Alberta (Canada) where bitumen production by surface mining has been a thriving industry for over 50 years. Located north of Fort McMurray, tailings slurry impoundment has created substantial land disturbances, covering an area of at least 130 km² in 2011 (Masliyah and Czarnecki, 2011). To produce one barrel of crude bitumen, 3.3 m³ of tailings is discharged, containing 1.5 m³ of fluid fine tailings (FFT) or mature fine tailings (MFT) that accumulate in the tailings pond after supernatant recovery (Masliyah and Czarnecki, 2011). These fluid fine tailings are stable at 30% (w/w) solids content without further noticeable densification for centuries. If one assumes that the density of the crude bitumen is approximately the same as that of water, then approximately 11.6 tonnes of MFT would be generated per tonne of crude bitumen produced. Recently, the Alberta Energy Regulator (formerly Energy Resources Conservation Board, ERCB) published the latest crude bitumen production figure of 340 million barrels from surface mining activities in 2012 (Alberta Energy Regulator, 2013). That amounts to an increase of approximately 510 million cubic meters (627.3 million tonnes) of fluid fine tailings.

1.1.2. Accumulated tailings issues

The huge volumes of mineral tailings are conventionally discharged into natural or engineered depressions, surrounded by dams and dykes that are critical to the structural

integrity of the containment pond. Unfortunately, over the years there have been several incidents of dam failures and the disastrous release of tailings, which are often a result of extreme weather and/or natural disasters (WISE Uranium Project, 2012). The dam failures are a result of both geotechnical problems of the containment structure and management of the stored tailings (Jones and Boger, 2012). Several failures of fine coal tailings ponds in the United States have been documented by the U.S. National Research Council. One such disaster in West Virginia resulted in 125 fatalities and substantial environmental and property damage (National Research Council, 2002). In Ajka, Hungary, the unprecedented release of 700,000 m³ of red mud slurry in October 2010 caused numerous fatalities as well as widespread farmland and waterborne contamination (Ruyters et al., 2011). Between 1967 and 2005, eleven industrial accidents in the US involving millions of cubic meters of phosphate tailings have been reported to damage or eliminate local aquatic biota (WISE Uranium Project, 2012). In the same time period many other mining industries, for example copper, iron, and zinc have witnessed failures leading to the destruction of properties, livelihood, and the local environment. Canada's oil sands industry has also received substantial negative public reception after much-publicized cases of wildlife deaths in the tailing ponds, though no major containment breaches of the oil sand tailings have been reported (Timoney and Lee, 2009).

In addition to the disastrous consequences of accidental tailings containment failures, the structures of operational tailings impoundment are also a cause of concern for mine operators. Fine solids in mineral tailings slurry require long settling time, which necessitates the use of large land areas to accommodate mine productivity. This situation is also magnified by the formation of stable particle networks (gels). Such network

structure resists consolidation and traps a significant volume of process water that is not available for recycle. Also, certain clay minerals (such as montmorillonite) are able to absorb water into its internal structure, resulting in swelling and an increase in the apparent volume of discharged material. Those phenomena are responsible for poor water recovery from tailings, and directly contribute to increasing footprint of tailings containment structures. A growing number of studies conducted at mineral tailings containment areas suggest that mobilization of harmful substances by wind, evaporation, and seepage can affect air quality and underground water tables (Percy et al., 2012; Timoney and Lee, 2009; Jones and Haynes, 2011; Jones and Boger, 2012). Stockpiling of mineral tailings can result in undesirable interactions with the environment (e.g. acid mine drainage), and this practice has also been linked to deformities, reproduction failures, and deaths of local flora and fauna (Renault et al., 2000; Gentes et al., 2006; Lee and Correa, 2005; Ramirez et al., 2005). As the public grows increasingly aware of these environmental issues and disasters related to mineral tailings, mining projects are facing greater levels of scrutiny from government agencies in terms of sustainability and social responsibility. The familiar practice of containing mineral tailings slurry by conventional dam and dykes is no longer considered acceptable in many countries (Zhang and Stana, 2012).

In the US for example, the Florida Department of Environment Protection (FDEP) established guidelines for phosphate tailings disposal (DEP 62-673.220), which has been adopted by an increasing number of government regulators worldwide (Zhang and Stana, 2012). In essence, the FDEP requires several modifications to the conventional containment structure by using: (a) composite liner, (b) leachate control, and (c)

perimeter underdrain, with specified material properties. Top soil cover of specified nature is applied for closure of the disturbed area. This improved tailings containment setup limits the extent of contamination from the seepage. However it does little to prevent slurry overflow, structural failures, and large land area requirements.

In an effort to reduce the inventory and production of oil sands tailings, the Energy Resources Conservation Board issued in 2009 Directive 074 which required operators to convert fresh and legacy tailings to deposits of trafficable material strengths (ERCB, 2009). Recognizing the evolving and often site-specific nature of tailings management practices, the ERCB has given operators the freedom to choose their own best practice, and outlined progressive evaluation criteria that are based on the amount of fine solids captured. According to the performance assessment report issued in June 2013, operators have not been able to meet these criteria despite ongoing efforts and improvements, due to numerous issues with operations and reliability (Alberta Energy Regulator, 2012).

1.1.3. Current tailings treatment objectives

The *status quo* of mineral tailings management thus appears as follows. In response to the progressive government regulations and public sentiment, mine operators are more willing to address the environmental and social impacts of legacy tailings and conventional tailings management practices. Land reclamation efforts, for example, are ongoing in the oil sands industry (Golder Associates, 2009). However, current mineral tailings consumption technologies are usually costly, perform less robust than desired, and suffer from limited throughput, which is particularly the case for managing the growing volume of copper, oil sands, and bauxite tailings. These factors elevate the risk

associated with tailings management programs using alternative technologies that differ from the less expensive and more established “dam and dyke” approach, and discourage their execution. On the other hand, mine operators are unwilling to reduce production rates due to plant economics and generally rising demand for products, thus leading to an overall excess and accumulation of fluid mineral fine tailings.

To break this impasse, actions must be taken to target the heart of the tailings problem – fine solids, and to better understand and combat the two undesirable fundamental phenomena that are associated with it – slow consolidation and water capture, using efficient, reliable, and economical processes. This review broadly examines current scientific understandings and prevalent practices of fluid mineral fine tailings densification (thickening) and dewatering, and the scope of this work is by no means comprehensive. Rather, the authors wish to highlight some of the difficulties and aims to provide some insights into future technological developments and advancements in this challenging yet essential area.

1.2. Theoretical considerations

1.2.1. Tailings solids and stability

Mineral tailings are heterogeneous mixtures of different solids suspended in process-contaminated water that often contains multiple soluble species. Characterization of solids in mineral tailings is often considered in terms of grain size, mineralogy, and morphology. All three factors and their interactions with the aqueous species directly contribute to the observed bulk behavior of a given tailings slurry.

1.2.1.1. Size classification

By convention, mining operators classify the size fractions of solid constituents in tailings as “sand”, “silt”, and “clay” based on a variety of methods and standards.

Exact cut-off sizes for these classes can vary by applications. **Table 1.1** provides some general guidelines used in the mining industry.

Table 1.2 lists some examples of classification results and solids concentration (if available) for tailings across different sectors of the mining industry. Generally there are significant amounts of silt and clay materials whose concentrations can vary considerably within an impoundment area. Fines enrichment becomes increasingly pronounced at locations further away from the slurry discharge point (Gräfe et al., 2011), and may be minimized by alternative discharge methods as demonstrated in, for example, Al and Blowes (1999).

Table 1.1. Grain size classification criteria.

Methods and Standards	Classification Criteria			Reference
	Sand (“Coarse”)	Silt (“Fines”)	Clay (“Fines”)	
Wentworth (1922)	> 63 μm	4 – 63 μm	< 4 μm	(Sabah & Cengiz, 2004)
ISO 14688-1	> 63 μm	2 – 63 μm	< 2 μm	(ISO, 2002)
Unified Soil Classification System (USCS)	> 75 μm	< 75 μm (Distinguished by plasticity)		(ASTM, 2011)
Canadian oil sands classification system	> 44 μm	2 – 44 μm	< 2 μm	(Masliyah, <i>et al.</i> , 2011)

Table 1.2. Examples of grain size distributions for mineral tailings of different origins.

Industry	Examples	Grain Size Distributions	Reference
Coal	Fresh tailings from Tuncbilek, Turkish Coal Enterprises, Turkey	Solids: 5.85% (w/w) > 63 μm : 10% 4 – 63 μm : 62% < 4 μm : 28%	(Sabah, <i>et al.</i> , 2004)
	Sediment tailings from Coal Valley Resources Inc., Alberta, Canada	Solids: 50-55% (w/w) > 63 μm : 3% 4 – 63 μm : 31% < 4 μm : 66%	(Beier & Segó, 2009)
	Diluted tailings from BMA plant, Central Queensland, Australia	Solids: 35% (w/w) > 63 μm : 35.4% 38 – 63 μm : 6.2% < 38 μm : 58.4%	(Alam, <i>et al.</i> , 2011)
	Tailings from Colombian washing coal plant, Columbia	Solids: 5% (w/w) > 75 μm : 19.5% 37 – 75 μm : 8.6% < 37 μm : 71.9%	(Barraza, <i>et al.</i> , 2013)
Alumina	Aluminum Corporation of Shandong Ltd., China	Solids: 60.2-66.8% (w/w) > 23 μm : none 5 – 23 μm : 90.3% < 5 μm : 9.7%	(Wang, <i>et al.</i> , 2008b)
		> 23 μm : 10% (w/w) 5 – 23 μm : 40% < 5 μm : 50%	(Kalkan, 2006)

	Etibank Seydisehir Aluminum Plant, Konya, Turkey		
	Literature review	Solids: 20-80% (w/w) Range: 0.1 – 200 μm Average: 2 – 100 μm < 5 μm : 50%	(Gräfe, <i>et al.</i> , 2011)
Phosphate	Bunge Brazil SA, Araxá, Brazil	> 75 μm : 60.7% (w/w) 37 – 75 μm : 25.0% < 37 μm : 14.3%	(Oliveira, <i>et al.</i> , 2011)
Phosphate (cont'd)	Phosphate concentration plant, Guizhou Province, China	> 75 μm : 14.0% (w/w) 37 – 75 μm : 28.5% < 37 μm : 57.5%	(Xu, <i>et al.</i> , 2012)
	The Mosaic Company, United States	Fresh tailings solids: 3% (w/w) (settles and stabilizes to ~20%) < 19.95 μm : 90% < 8.96 μm : 50% < 1.73 μm : 10%	(Tao, <i>et al.</i> , 2008)
Copper	El Teniente-Codelco copper mine, Chile	> 75 μm : 66.1% (w/w) 38 – 75 μm : 30.0% < 38 μm : 3.9%	(Hansen, <i>et al.</i> , 2005)

	Abandoned processing facility, Lefke, Cyprus	> 48 μm : 50% (w/w) 1 – 48 μm : 16% < 1 μm : 34%	(Onuaguluchi & Eren, 2012)
	Carén tailings, El Teniente copper mine, Chile	Solids: 55% (w/w) > 63 μm : 11% 2 – 63 μm : 68% < 2 μm : 21%	(Smuda, <i>et al.</i> , 2008)
Oil Sands	Tailings pond MFT, Alberta, Canada	Solids: 40% (w/w) > 44 μm : 4% 2 – 44 μm : 78% < 2 μm : 19%	(Farkish & Fall, 2013)
	Mature fine tailings from Syncrude Canada Ltd., Alberta, Canada	Solids: 34% (w/w) > 44 μm : 4% 6.5 – 44 μm : 46% < 6.5 μm : 50%	(Alamgir, <i>et al.</i> , 2012)
	Typical fine tailings sample	Solids: 30-40% (w/w) > 44 μm : 10% 1 – 44 μm : 57% < 1 μm : 33%	(Voordouw, 2013)

1.2.1.2. Solids mineralogy and morphology

Many researchers have studied and characterized the solids mineralogy and morphology for some of the tailings samples listed in **Table 1.2**. Characteristics of the process water obtained from the tailings slurries were also widely published. Results presented (de Kretser et al., 1997; Sabah et al., 2004; Ofori et al., 2011) suggest that coal preparation tailings in the fines fraction consist mostly of phyllosilicate minerals, such as kaolinite, illite, muscovite, mica, and mixed-layer illite/montmorillonite clays, along with quartz. Residual coal particles are detected predominately in the coarse fraction (Sabah et al., 2004). This particular combination of fine solids is very similar to those identified from the oil sands fluid fine tailings, in which kaolinite is the dominant clay fraction, followed by illite, chlorite, and other mixed-layer clays (Masliyah and Czarnecki, 2011). However, the coarse fraction of oil sands fluid fine tailings is mostly quartz, K-feldspar, and bitumen–clay aggregates. Solids in both coal and oil sands tailings are entrained in slightly alkaline process waters, with pH ranging between 7.5–8.5 and 7.7–8.8, respectively (de Kretser et al., 1997; Allen, 2008). Concentrations of sodium ion between the two mineral tailings are generally similar (Ryu et al., 2008; Alam et al., 2011; Allen, 2008) although higher levels (in excess of 960 ppm) have been reported for coal tailings (Ofori et al., 2011). Process water from oil sands tailings contains lower amounts of calcium, magnesium, chloride and sulfate ions, thus coal tailings are, in general, more saline than its counterpart from oil sands (Allen, 2008; Ofori et al., 2011; Sabah et al., 2004; Alam et al., 2011).

In comparison, mineral tailings from the alumina, phosphate and copper industries are found to contain less clay minerals and higher proportions of metal oxides. It is often

unclear which types of mineral are enriched in either the coarse or fines fractions. The nature of the process water from these tailings is closely linked to the type of the extraction process used. Details are presented in **Table 1.3**.

Although differences exist in the composition of these tailings, the ubiquitous presence of phyllosilicate minerals is evident. Among these phyllosilicate minerals, the majority is classified as clay minerals and concentrated in the fines fractions. These materials originate from weathering of ores and have tetrahedral sheets of silicon and oxygen as the basic building block. Other types of layers are chemically bonded parallel to each tetrahedral sheet to form the unit layer for a variety of clays. For example, kaolinite is structured as repeating units of an octahedral aluminum–hydroxyl sheet bonded to the tetrahedral silicon–oxygen sheet, as illustrated in **Fig. 1.1** by Konan et al. (2007), whereas the octahedral Al–OH sheet is sandwiched between two tetrahedral Si–O sheets for montmorillonite and illite. Clays have a large surface area to volume ratio that facilitates a variety of interactions with themselves as well as with aqueous species in the slurry (Singer and Munns, 1996; Giese, 2002).

Table 1.3. General characteristics of alumina, phosphate and copper tailings.

Industry	Composition of solids	Characteristics of liquid	Reference
Alumina	Oxides of iron (III), titanium, silicon, calcium, sodium, and residual aluminum	Elevated pH (10.3–11.3) and sodium ions (average 2332 mg/L)	(Gräfe, <i>et al.</i> , 2011; Kalkan, 2006; Poulin, <i>et al.</i> , 2008; Wang, <i>et al.</i> , 2008a)
Phosphate	Oxides of calcium, iron (III), silicon (quartz and mica), residual P ₂ O ₅ , and magnesium oxide (dolomite) in some cases	Limited available data; generally acidic; concentrated in anions such as sulfite (SO ₃ ²⁻).	(Oliveira, <i>et al.</i> , 2011; Abdel-Aal, 2000; Xu, <i>et al.</i> , 2012; Zhang & Stana, 2012)
Copper	Quartz, K-feldspars, biotite, chlorite, mica, muscovite, gypsum, and dolomite, with residual amounts of copper and other metals	pH 9.2–10.2 for alkaline flotation of sulfide ores; neutral pH reported for porphyry deposit tailings; limited water salinity data	(Smuda, <i>et al.</i> , 2008; Liu, <i>et al.</i> , 2013; Hansen, <i>et al.</i> , 2005)

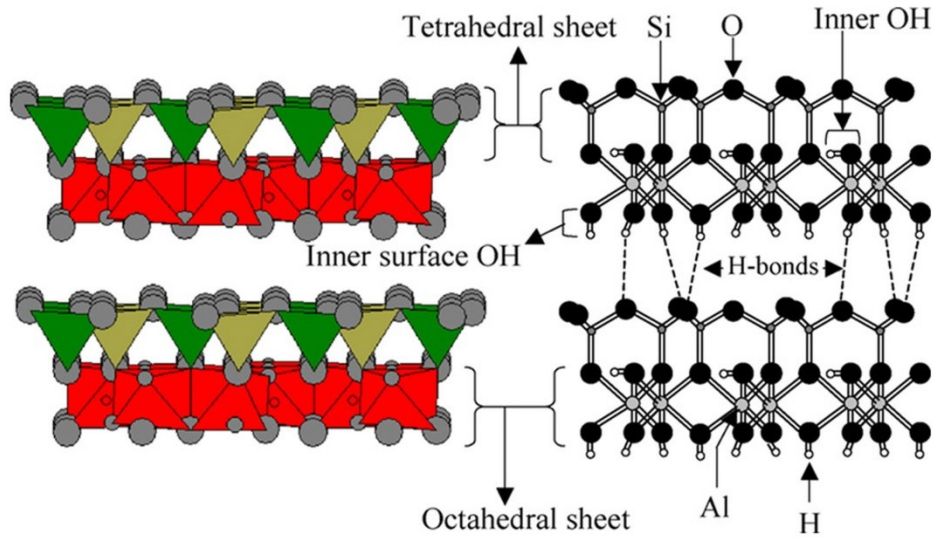


Figure 1.1. Two unit layers of kaolinite (adopted from Konan, *et al.*, 2007, with permission). Elsevier (Copyright © 2014).

1.2.1.3. Slurry stability

Mineral solids suspended in slurries physically and chemically interact with the carrier fluid and dissolved species. These interactions directly dictate the suspension bulk properties, such as stability of the solids dispersion, slurry viscosity, as well as shear and compressional yield stresses.

All solid particles in a slurry are subjected to gravitational settling at steady-state (or terminal) velocities v_∞ that can be estimated by Stoke's law for dilute suspensions. The Stoke's law established relations between the settling velocity with the gravitational field strength g , characteristic particle size D_p , particle density ρ_p , as well as carrier fluid density ρ_f and viscosity μ_f .

$$v_\infty = \frac{gD_p^2(\rho_p - \rho_f)}{18\mu_f} \quad (1.1)$$

Actual particle settling velocities will be lower than those predicted by **Eq. 1.1** due to non-spherical particle shapes and, at sufficient particle concentrations, hindrance effects from the neighboring particles. Nevertheless, Stoke's law is commonly used as a first-hand approximation to describe particle settling in stagnant media, such as tailings impoundments. From **Eq. 1.1** it is clear that particles in the coarse fraction (i.e. sand) settle much faster than silts and clays. Consequently, this differential settling results in the segregation of these two size fractions and formation of fluid fines tailings in the disposal areas (Masliyah and Czarnecki, 2011; Gräfe et al., 2011).

Suspended fine solids generally settle at negligible velocities and remain stable for extended periods of time, due to increasingly pronounced colloidal interactions and diminishing role of gravity with decreasing particle size. Stability of the fines suspension is reasonably well described by the DLVO theory that considers two principal colloidal forces. The ubiquitous and attractive van der Waals force acts between particles in close proximity, enabling particles to “stick” upon contact and remain in intimate contact. Counteracting the attractive force is a repulsive force caused by the overlap of electrical double layers surrounding the neighboring particles. This repulsive force is termed as electrical double layer repulsion. Unlike the attractive force that is only material specific, the double layer force is both material and solution dependent (electrolyte type, concentration and pH), with the repulsive potential decreasing with increasing conductivity which suppresses the charge/potential surrounding the particles, known as charge screening.

Fine solids, especially clays when dispersed in an aqueous fluid can attain surface charge through a variety of mechanisms. Isomorphous substitution, where structural cations (e.g., Si^{4+} and Al^{3+}) are exchanged by dissolved cations of equal or, more commonly, lower valence (e.g. Al^{3+} , Mg^{2+} , and K^{+}), resulting in a net negative charge on the basal surfaces of the clay particle. Many researchers had considered that surface charges on both the tetrahedral Si–O layer and octahedral Al–OH layer to be relatively constant regardless of pH (Singer and Munns, 1996; Giese, 2002), although recent research has challenged that notion and found that Al–OH layer has a pH-dependent (although less pH-sensitive as compared to the edge or metal oxide surfaces) surface charge for kaolinite (Gupta and Miller, 2010) and muscovite (Yan et al., 2011), see **Fig. 1.2**.

Protonation or de-protonation of oxides and hydroxide groups can occur at the broken edges of the layers, which results in a more pH-dependent surface charge (Singer and Munns, 1996). When the surfaces of a fine solid particle become charged in an aqueous environment via those mechanisms, it attains a surface potential and attracts a fixed (Stern) layer of counter ions (if available) on the particle surface, enveloped by a diffuse ionic layer that forms the basis of an electric double layer in such a manner that the particle appears electrically neutral in the bulk, i.e., at a large distance into the bulk. The surface potential is usually estimated by the potential at the boundary between the Stern and diffuse layers, known as zeta potential and often determined from electrophoretic mobility measurements. Thickness of the double layer, κ^{-1} , is defined as the distance from the particle surface into the aqueous phase at which the surface potential decays to $1/e$ (~ 0.368) of its magnitude. The value of electrical double layer thickness is inversely

related to the concentration c_i and valence Z_i of the dissolved i^{th} counter ions as shown in Eq. 1.2.

$$\kappa^{-1} = \sqrt{\frac{\epsilon k T}{e^2 N_A \sum_i Z_i^2 c_i}} \quad (1.2)$$

where ϵ is the permittivity of suspending media, k is the Boltzmann constant, T is the system temperature, e is the elemental charge, and N_A is the Avogadro number. On close approach, two similarly charged particles will experience increasing repulsion as their electrical double layers overlap.

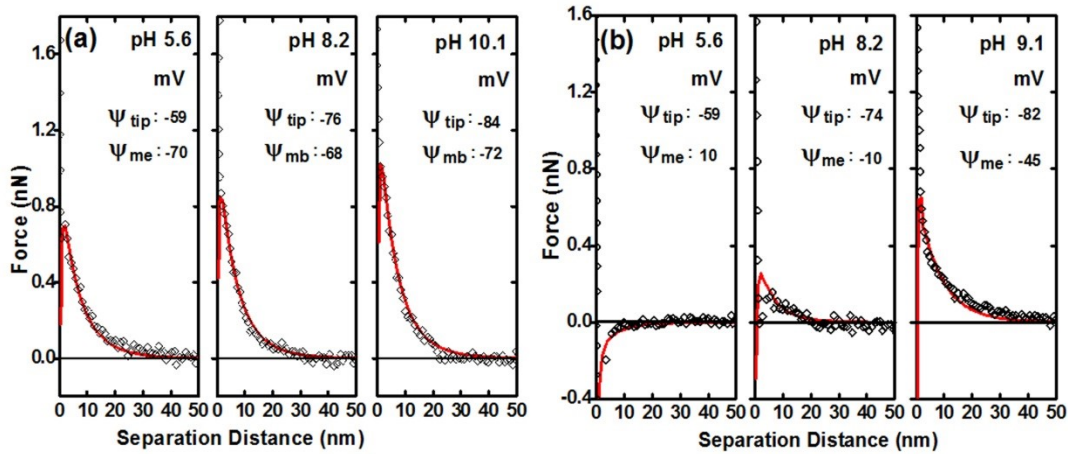


Figure 1.2. Typical AFM interaction forces on muscovite in 1 mM KCl solution of varying pH confirm the pH independent surface potential of the Si-O basal plane (a) (pH 5.6–10.1), and the pH dependent Al-OH/Si-O edge surface (b) with charge reversal measured between pH 5.6 (positive) and pH 8.2 (negative). The layered structure of muscovite, octahedral layer of gibbsite sandwiched between Si-O-Si tetrahedral layers, was suitably prepared for AFM measurement by cleaving the basal plane and exposing

the edge surface using an ultramicrotome cutting technique. Adopted from Yan, *et al.* (2011), with permission. American Chemical Society (Copyright © 2014).

However, given the pH-dependence and anisotropy of surface charge for the irregular-shaped clay minerals, as well as their interactions with a myriad of dissolved species in typical industrial process water, additional non-DLVO interactions and complex dispersion stability behaviors can be expected and have indeed been reported (Masliyah and Czarnecki, 2011; Johnson et al., 2000). Hydration and steric interactions stemming from adsorbed layers of water and macromolecules increase the mutual repulsion between suspended particles, while surfactant-modified or naturally hydrophobic particle surfaces experience an additional attraction to surfaces of similar nature – hydrophobic force (Israelachvili, 2011). The total interaction potential between two suspended particles can be calculated in terms of interaction energies with respect to their separation distance, as shown by Masliyah and Czarnecki (2011) for two spheres experiencing van der Waals and double layer interactions. A more thorough treatment involving “hard-sphere” and steric interactions is presented by Tadros (2011). Often, as two suspended particles approach each other, an energy barrier to the primary energy minimum, which corresponds to permanent particle attachment or strong aggregation, can be observed. In addition, a secondary energy minimum also exists before the energy barrier that results in weak and reversible aggregation (Elimelech et al., 1995). In addition, Tadros (2011) showed the effect of electrosteric stabilization where no primary energy minimum exists. Magnitude of the energy barrier directly corresponds to the stability of the dispersion in a quiescent environment.

For an energy barrier of $20kT$ and a given κ^{-1} , only one in an estimated 1 million inter-particle collisions due to thermal motion of two identical 1 μm particles can result in a successful aggregation (Elimelech et al., 1995). In this case, collisions between particles are highly inefficient for aggregation, and suspended particles are stabilized by their strong mutual repulsion at constant temperature.

Although the efficiency of particle collisions is a major determining factor for aggregate formation, the total number of successful aggregations formed per unit time is a product of both the collision efficiency and frequency of collisions in the same time frame.

Application of additional collision frequency via increased kinetic energy, as well as lowering the magnitude of the energy barrier can greatly improve the formation rate of aggregates, which increases the apparent particle size D_p . As indicated in **Eq. 1.1**, the rate of particle sedimentation can be improved, and the suspension is subsequently destabilized as the apparent particle size increases due to particle aggregation.

Techniques to destabilize fine solids suspensions will be discussed in detail in **Section 1.2.2**.

1.2.1.4. Slurry rheology

Suspended solids in a slurry are known to alter the rheological properties of the slurry, whose effects are strongly dependent on the net interaction between particles (Tadros, 2011; Harbottle et al., 2011a, b). Strong net repulsive interactions amongst the fine solids result in a stable dispersion with minor modifications to slurry viscosity. In this case, no shear yield stress is developed. On the other hand, if the solids experience strong net attractive interactions (i.e. at primary interaction energy minimum without energy

barriers), they will readily aggregate into a single, tightly-bound solid mass, leading to very high shear yield stress of the slurry. However, it is often the case in which the particles, or a fraction of the particles are weakly interacting, more so for clays due to their pH-dependent and anisotropic distribution of surface charges. Consequently, the solids aggregate at larger separation distances where the secondary interaction energy minimum occurs to form loose and porous aggregates. For clays, a “card house” structure is often observed at intermediate pH and for low aspect ratio clays, where the dominant inter-particle orientation consists of basal plane-edge surface interaction due to anisotropic surface charge characteristics of basal planes and edge surfaces, as shown in **Fig. 1.3** (Johnson et al., 2000; Gupta et al., 2011; Yan et al., 2013). At high pH, the charge repulsion between the negatively charged basal plane and edge surface is sufficient to stabilize the particles in the suspension. However, as the pH is lowered the edge surface undergoes charge reversal leading to a net attraction between the basal plane and edge surface. The strength of the attraction is shown to increase as the pH is lowered from pH 8 to pH 5.6. Clay anisotropy should be carefully considered to provide meaningful interpretation of slurry/sediment rheology (Yan et al., 2013).

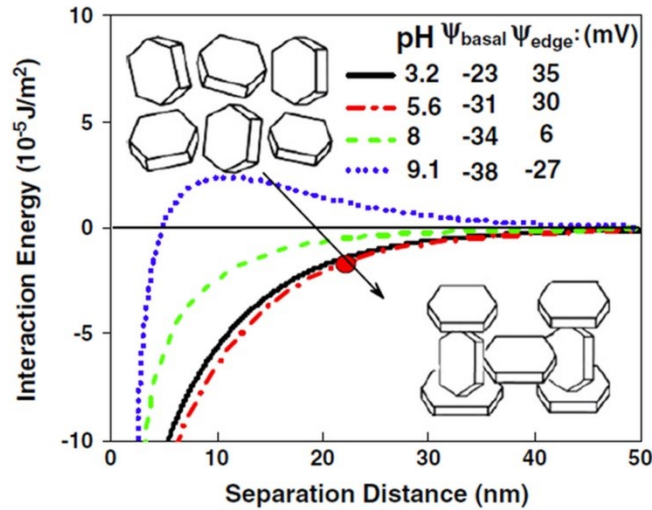


Figure 1.3. Interaction energies associated with the preferred “card house” structure of clays. Basal-edge attachments are favored across a wide spectrum of system pH values (adopted from Yan et al. (2013), with permission. Elsevier (Copyright © 2014).

Since the aggregation process is reversible, a few interesting rheological behaviors are observable: (a) the slurry viscosity decreases with increasing shear, as more loose aggregates are fractured than formed per unit time; (b) when at rest, a shear yield stress is developed as the aggregates obtain structural integrity; and (c) under constant shear, the competing processes of shear fracturing and weak aggregation reaches steady state, thus the slurry viscosity decays to an equilibrium value. As a result, most fine solids suspensions become pseudoplastic and exhibit thixotropic behavior upon agitation.

For a given type of fines slurry, its steady state viscosities at different shear rates and shear yield stress increase with increasing solids concentration. An example is provided by Boger (2009) for red mud. The development in slurry viscosity can be substantially enhanced by introducing certain minerals, as shown by Masliyeh and Czarnecki (2011),

in which a small quantity (1% w/w) of montmorillonite is shown to significantly thicken the 40% (w/w) kaolinite suspension. As montmorillonite is susceptible to swelling by absorption of water between its unit layers, its presence is expected to reduce the amount of free (unbound) water in the slurry and increase the effective solids volume fraction, both of which directly contribute to the increased slurry viscosity. Amounts of dissolved ions and counter ions (Leong and Boger, 1990; Johnson et al., 2000; Penner and Lagaly, 2001), pH (Leong and Boger, 1990; Johnson et al., 2000), and adsorbed surfactants or other macromolecules (Harbour et al., 2007) are also able to modify the interactions between particles, thus directly affecting their rheological properties.

Generally it is undesirable to have high concentrations of fine solids in a slurry due to the entrapment of large amounts of water within the network of loose aggregates, that subsequently interact to form a 3-dimensional gel. In oil sands ores, clay-sized materials of >16% w/w, or ultra-fine particles (sized less than 0.3 μm) of >1.5% w/w, were shown to exceed the gel concentration, causing plant operational issues when present in an extraction slurry (Tu et al., 2005).

1.2.2. Enhanced settling and densification

This section provides a general review of the available techniques for accelerating the sedimentation of dispersed fine solids. Fine solids suspension, a by-product of the gravity settling of typical mineral tailings, entraps a significant amount of valuable process water and prevents direct and timely re-use of water and reclamation of disposed fluid fine tailings. From the above discussions, it is clear that the urgency and importance of fine solids separation from liquids cannot be understated. However, due to the highly

dispersive nature of the solids, gravity sedimentation is usually ineffective and destabilization of the suspended solids by aggregation is often a necessary first step. Naturally, accelerated settling will occur after particle aggregation, followed by the densification of the settled solid sediments.

1.2.2.1. Particle aggregation

Aggregation refers to the attachment of two entities via physical and/or chemical mechanisms, and its kinetics is generally determined by collision frequency and efficiency in a given suspension. Perikinetic aggregation occurs in a static suspension through Brownian motion with efficiency directly related to the interaction energy barrier between the solid particles. Upon agitation, the orthokinetic collision frequency becomes dependent on fluid shear and aggregate size for entities larger than 1 μm . The orthokinetic collision is less pronounced for smaller particles and aggregates, where the effect of temperature is still more significant (Masliyah and Bhattacharjee, 2006).

Collision efficiency can be improved by applying relatively high rate of shear to overcome the energy barrier in an orthokinetic setting. However hydrodynamic (viscous) interactions between two particles at close approach are known to reduce the probability of attachment (Elimelech et al., 1995).

Within the scope of this article, it is desirable to form aggregates from suspended solids in the silt and clay size fractions. In such system the apparent particle size can be increased so that both perikinetic and orthokinetic aggregations contribute to destabilizing the suspension. As discussed in **Section 1.2.1**, particle aggregations occurring at the secondary interaction energy minimum result in aggregates that are

porous, easily disrupted, and have large capacities for process water entrainment. Thus aggregates in the primary energy minimum, or strong aggregation, are more favored for their high compactness and integrity. For industrial fine solids suspensions that are typically highly stabilized, it is apparent that either increasing the solids kinetic energy or decreasing the magnitude of the energy barrier is necessary for successful particle attachment. In practice, additional kinetic energy is usually imparted to particles by mechanical mixing, combined with the introduction of coagulating and/or flocculating agents that serve to reduce the interaction energy barrier. The terms “coagulation” and “flocculation” are often used interchangeably in literature. In this article, however, coagulation is defined as particle aggregation brought by the addition of inorganic salts to reduce electrostatic double layer repulsive force, whereas flocculation refers to the same phenomena induced by organic polymers or other macromolecules that bridge the particles. In flocculation, therefore, the interaction of polymer with particles and conformation of polymers play a more decisive role than colloidal forces between the particles in destabilizing colloidal suspensions.

1.2.2.2. Coagulation

The addition of inorganic salts is well-known for its effectiveness at destabilizing fine solids suspensions (Hogg, 2000). Coagulation and sedimentation of suspended particles have been employed extensively in the water treatment industry, where a variety of chemical agents such as alum, lime, ferric chloride, and pre-hydrolyzed chemicals are used.

It is generally recognized that upon addition to aqueous environments, inorganic salts undergo hydrolysis into the corresponding cations and anions, forming a variety of monomeric and polymeric products that depend on the type, valency and dosage of ions, solution pH, and temperature (Duan and Gregory, 2003). At concentrations below bulk saturation, surfaces of negatively-charged fine particles electrostatically attract hydrolyzed metal cations, screening the surface charge for other particles. Quantitatively, an increase of ionic concentration leads to a reduced thickness of the electric double layer as indicated by **Eq. 1.2**, resulting in a more rapid decay of the repulsive double layer interaction with increasing inter-particle distances. Therefore for simple systems, the attractive van der Waals interaction becomes more prevalent at very small separation distances between two particles, reducing the energy barrier and hence increasing the probability of particle aggregation. At a critical coagulation concentration (CCC), the magnitude of the energy barrier reaches zero, where the suspension destabilizes spontaneously. The value of CCC for a given electrolyte depends strongly on its valency, and can be estimated by the Schulze–Hardy rule (Masliyah and Czarnecki, 2011). As well, depending on the suspension pH, metallic salts such as alum can precipitate on the dispersed solids and nucleate into amorphous metal hydroxide patches (Duan and Gregory, 2003). These neutral or positively-charged patches are attracted to oppositely-charged bare particle surfaces. Further increasing the ionic concentration will cause increased coverage of the adsorbed ions on the solid surfaces and shrinkage of the electric double layer. On the other hand, addition of excess salts gradually results in charge reversal of solid surfaces, which re-stabilizes the suspension.

Although charge screening by ionic species can improve inter-particle collision efficiency, the corresponding rates of aggregation reported by Duan and Gregory (2003) are very slow for dilute (50 mg/L) kaolinite suspensions. They attributed the slow rate of particle aggregation to the low collision frequency due to the low population and small size of the constituent particles, and to the limited particle enlargements offered by the hydroxide precipitates. However, using the same suspension with ferric chloride as the coagulating agent, Ching et al. (1994) accelerated the rate of particle aggregation at shear rates of 94 s^{-1} and greater. Although frequency of inter-particle collisions can be improved by this manner at low coagulant dosages, in practice the coagulant is overdosed to achieve rapid and widespread precipitation of the amorphous metal hydroxide, which enmeshes and captures most of the suspended fine particles as it moves downward via “sweep flocculation” (Duan and Gregory, 2003). Under such conditions, the mechanisms of particle aggregation are, in principle, thought to be similar to “bridging” of particles with polymeric flocculants, which will be discussed in the next section.

1.2.2.3. Flocculation

The aggregation of fine particles by polymeric and other macromolecular additives (flocculants) is utilized in many applications both in and outside mineral processing, and has attracted immense academic interest (Smith-Palmer and Pelton, 2012). Common flocculants include polyacrylamide (PAM), poly(diallyldimethyl ammonium chloride) (PDADMAC), polyethylene oxide (PEO), chitosan-based polymers, etc. The flocculants can be synthesized for a variety of molecular weight (MW), electric charge type and charge density to suit specific requirements. Additional structural modifications can also

be incorporated to produce novel flocculants of interesting properties, such as the temperature-sensitive poly(N-isopropyl acrylamide) (poly-NIPAM) (O'Shea et al., 2010), and impregnation of positively charged colloidal $\text{Al}(\text{OH})_3$ particles in PAM, the latter being referred to as the hybrid flocculant Al-PAM (Alamgir et al., 2012).

Perhaps the sole constraint to the seemingly endless types of modifications is the adsorption behavior of the polymer product on fine solids upon introduction into a given suspension, which is well-described by Smith-Palmer and Pelton (2012). In essence, segment(s) of the polymer flocculant is (are) convectively and/or diffusively transported to the solid–water interface where irreversible solid–polymer attachment can occur non-specifically (e.g., van der Waals or electrostatic attraction) or specifically (e.g., hydrogen bonding), followed by polymer re-orientation. In some cases polymer–solid adsorption does not occur at all due to, for example, electrostatic repulsion between hydrolyzed PAM and negatively charged silica or bitumen-coated solid surface at their experimental conditions, as shown by Klein et al. (2013). The rate of polymer adsorption is generally faster for lower molecular weight flocculants, setting up the barrier governed by the surface coverage that prevents further polymer adsorption. Once adsorbed, the polymer conformation depends on a number of factors, some of which are discussed next. Several possible conformations are shown by Alagha et al. (2013) in **Fig. 1.4**.

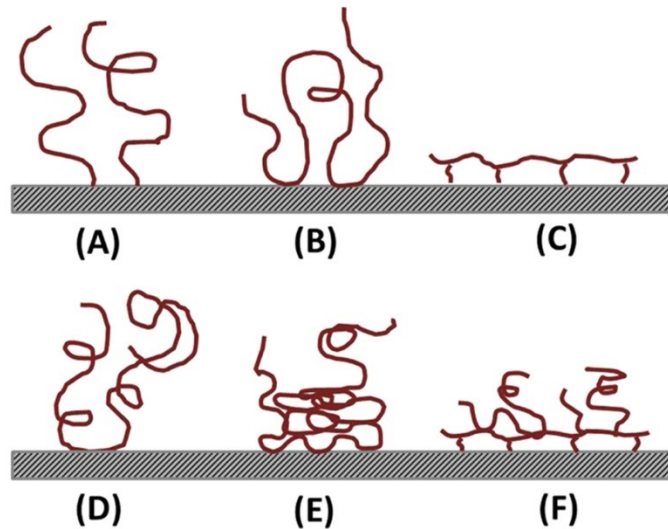


Figure 1.4. Possible polymeric flocculant conformations following adsorption (adopted from Alagha et al. (2013), with permission. Copyright © 2014 American Chemical Society).

- Polymer–solids interaction: strong attraction will result in the polymer collapsing onto the solid surface (**Fig. 1.4** cases C and F), and weak attraction leads to the polymer extending away from its anchor points (cases A, B, and D).
- Polymer–water interaction: strong affinity to water will encourage the polymer chain to maximize its contact area with water, resulting in conformations of polymer brushes (e.g. case A, B, and D); relatively hydrophobic polymers, on the other hand, will minimize their contact area in water resulting in mushroom-like conformations (F).
- Polymer self-interaction: excessive attraction between functional groups on the polymer chain will favor self-collapse and the formation of loops and coils (e.g. case E).

- Polymer chain stiffness: stiffer polymers, such as highly charged polymers, will have increased resistance to changes in their conformations (A & C).

Since the selection criterion for optimum removal of fine solids from aqueous suspensions is to quickly capture fines, the following conditions would have to be satisfied based on the above qualitative observations. Interactions between polymer and solids should be weakly attractive, since electrosteric or steric stabilization can occur (for charged and neutral polymers, respectively) if the polymers are strongly attracted to and hence fully cover the solids. Strong repulsion between the polymer and solids, on the other hand, can drastically reduce the collision efficiency between solids and polymers, as previously mentioned. When present in aqueous environments, the flocculant should have some degree of hydrophilic nature such that it is soluble in water and its extension into the aqueous phase in the form of loops is favorable. The extent of self-interaction should be minimized in order to promote greater contact points for solids capture, and levels of chain stiffness should be balanced between the preservation of chain integrity under fluid shear and sufficient mobility for chain re-orientation.

Once a properly-chosen polymer is attached to a solid particle, polymer brushes and loops extend from its anchor points into the aqueous phase and serve as connectors for the aggregation of additional solids via bridging, charge neutralization, and charged patch flocculation. Complex flocculation utilizing compounds such as cofactors (co-additives) for PEO-induced flocculation are common in the paper industry (Gaudreault et al., 2005), and can involve sophisticated reaction and aggregation pathways in combination with the aforementioned mechanisms. As more solids accumulate on the polymer chain, the

particle–polymer aggregate attains a much larger apparent particle size that readily settles under gravity.

Particle bridging is generally considered an attractive interaction in addition to the van der Waals attraction, with interaction energy formulated by Ji et al. (2013) in terms of inter-particle distance for two spherical particles that depends strongly on the adsorbed polymer conformations (in terms of their contour length) and adsorption-specific parameters. Connecting particles in electrostatically- stabilized fine suspensions requires that the length of the extending polymer chains or loops meets or exceeds the combined electric double layer thickness of two particles, which precludes the use of short-chain polymers as flocculant unless electrolytes are present in significant quantities. Generally this mechanism is prevalent for polymers of low charge density (usually identified by “anionicity” or “cationicity”). This phenomenon also takes place in “sweep flocculation”. Due to an excess of metal salts, waterborne metal hydroxide complexes are able to grow into large fractal structures that essentially act as an inorganic polymer. As a result, in addition to charge neutralization and electric double layer compression that usually accompanies coagulation, bridging of suspended particles and their subsequent flocculation are therefore possible.

At higher (>30%) charge densities, polymers strongly adhere to oppositely charged solids neutralizing the surface charge (Smith-Palmer and Pelton, 2012). This leads to the polymers collapsing on the solid surface, which is especially detrimental at high flocculant dosages. However, incomplete surface coverage occurs at low dosages, where the attached polymer “patches” are able to attract and flocculate other oppositely charged particles. Thus in practice it is critically important to determine the optimum

dosage for a given type of flocculant to maximize solids attachment, while exercising due diligence in flocculant distribution to avoid local overdose (Masliyah and Czarnecki, 2011). The charged patch flocculation mechanism bears similarities to the precipitation of amorphous metal hydroxides on solid surfaces in coagulation. Additionally, when present in large concentrations, water-soluble flocculants that do not interact with solid surfaces can also induce aggregation via depletion flocculation. Since regions sandwiched between adjacent solid particles are energetically unfavorable for the presence of non-adsorbing flocculants, concentration gradients would exist between these regions and bulk solution, which produces an osmotic flow that drains water out of the flocculant-depleted regions and slowly propels particles closer to each other. At close inter-particle distances, the osmotic driving force is counteracted by the electric double layers on each particle, thus resulting in weak and reversible aggregation. Often for industrial applications it is only necessary to consider flocculation by bridging, charge neutralization, and charged patch mechanisms as they operate much more effectively and faster than depletion flocculation. As an example for negatively charged particles flocculated by cationic polymers, Smith-Palmer and Pelton (2012) provided a summary of important factors that can affect the performance of these mechanisms as shown in **Table 1.4**.

Table 1.4. Impact of selected flocculant and solution properties on major flocculation mechanisms (adopted from Smith-Palmer and Pelton, 2012, with permission. Copyright © 2014 Taylor & Francis Group, LLC).

Condition of increasing	Mechanism		
	Charge neutralization	Charge patch flocculation	Bridging
Polymer Concentration	Destabilization	Destabilization then restabilization	Destabilization then restabilization
Polymer MW	Negligible	Small increase	Increase
Polymer Charge Density	Increase	Increase	Increase then decrease
Electrolyte Concentration	Increase	Decrease	Increase

Though the application of polymers for fine particle flocculation has proven largely successful, the anisotropic and irregular nature of the dispersed particles often necessitates additional measures to complement and improve the efficacy of single-polymer systems. Introduction of additional coagulant and/or flocculant that specifically binds to particle surfaces of different nature (**Fig. 1.5**) offers the opportunity to increase the compactness and size of the solids–polymer aggregates, both of which further improve the rate of slurry clarification (Yuan and Shaw, 2007; Alagha et al., 2013). Changes in adsorption conformations via external inputs are also possible for “smart” flocculants such as poly-NIPAM, whose hydrophobicity is found to be heavily influenced by slurry temperature (Franks et al., 2009; Li et al., 2007). Thus below the hydrophobic

transition temperature, poly-NIPAM is hydrophilic and can be deployed similarly as a PAM. Increasing the system temperature past transition will cause the adsorbed poly-NIPAM to minimize its contact area with water and therefore shrink in size, which reduces the solids–polymer aggregate size but increases the density of the aggregates. This switchable feature has been demonstrated to form sediments of lower moisture content than PAM. Application of such novel polymers for tailings management (among a variety of purposes) in the mining industry is an exciting field of work and has gained attraction over the last 10 years.

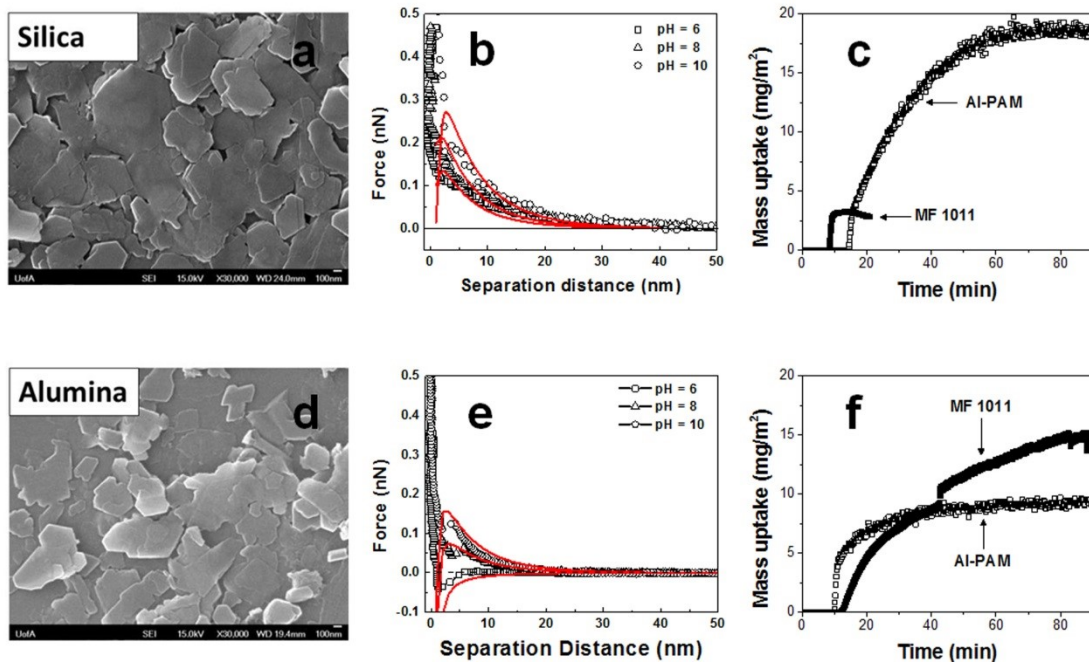


Figure 1.5. The added benefit of dual polymer addition is demonstrated when measuring polymer adsorption on anisotropic basal planes of kaolinite. Adopted from Alagha et al. (2013), with permission. Copyright © 2014 American Chemical Society. SEM micrographs of deposited kaolinite nanoparticles on silica and alumina piezo-electric sensors show a near uniform coverage with basal planes mostly exposed (a and d). To

determine the preferential arrangement of the kaolinite nanoparticles on the sensor surface AFM force curves between a silicon nitride probe and the deposited particle layer were measured in Milli-Q® water at pH's 6, 8 and 10. A purely repulsive interaction on the silica sensor confirms exposure of the tetrahedral silica basal plane, while the pH dependent charge (repulsion pH 8 and 10, attraction pH 6) confirms the predominant exposure of the octahedral alumina basal plane (b and e). Measuring the adsorption properties of anionic (MF 1011) and cationic-hybrid (Al-PAM) flocculants on the two basal planes of kaolinite by quartz crystal microbalance – dissipation monitoring, preferential uptake of Al-PAM and MF 1011 is measured on the tetrahedral silica and octahedral alumina basal plane, respectively (c and f). From the adsorption properties it is anticipated that large compact flocs formed by electrostatic interaction with Al-PAM will bridge smaller flocs through the hydrogen bonding of the octahedral basal plane by MF 1011 (Alagha et al., 2013). Dual polymer studies have been shown to form larger more compact flocs of the highest settling rate and lowest supernatant turbidity (data unpublished).

1.2.2.4. Other methods

Although suspension destabilization by aggregation via coagulation or flocculation is currently of industrial prevalence, many studies on alternative methods for enhanced particle settling have been published up to date. Some examples are presented here.

In 1955, Whitmore demonstrated that settling of a dispersed suspension can be enhanced by introducing neutrally buoyant particles (Whitmore, 1955). Among other researchers, experiments by Venkataraman and Weiland (1985) confirmed this phenomenon and

suggested thickening of settled phases. The underlying physics and associated dynamic models were reviewed by Kulkarni et al. (1993). In summary, the buoyant particles flow against gravity and produce “convection fingers” that generate a downward velocity, which propels the suspending solids to the bottom, subject to restrictions on buoyant and dispersed particle concentrations (as well as feed flow rate) that discouraged its potential for industrial applications. Interestingly, insights gained from these studies have led to the development of the inclined plate settler, which has been commercially deployed in, for example, particle size classification in the oil sands industry (Davis et al., 1989; Nasr-El-Din et al., 1990).

As fine solids generally have pH-dependent surface charges in a suspension, formation of aggregates can also be promoted by the addition of acids or bases to reduce the surface charge, thereby lowering the extent of mutual repulsion and promote destabilization. Instead of using large (and often costly) amounts of acids and bases, treatments with alternative acidifying or alkalising agents, many of them being waste materials, have shown promise. For example, Zhu et al. (2011) investigated the injection of CO₂ into combined oil sand tailings (sand and fines), and determined conditions that significantly improved solids settling and sediment compaction without segregation of fines and sand. They have demonstrated a pH reduction from 8.2–8.4 to 5.9–6.2 in two samples that was attributed to the dissolution of CO₂ and subsequent formation of carbonic acid. Similarly, effective red mud neutralization was demonstrated by Jones and Haynes (2011) whom also noted its benefit on the quality of recycled process water. This type of approach appears beneficial and environmentally sound. Sequestration of other industrial flue gases (SO_x, NO_x, etc.) on suspension destabilization could also be investigated.

1.2.3. Consolidation and dewatering

After initially destabilizing the dispersed fine solids from a slurry, the settled solids form a water-saturated sludge of variable strength. It is often necessary to expel additional water from the sediment for further volume reduction and increase in mechanical strength of the sediment to meet the regulatory specifications for safe deposition. Historically, the mining industry has taken several key steps towards sustainable waste management practices on a broad scale (Jones and Boger, 2012). Subsequently, established guidelines and best practices (without universal geotechnical targets) became readily available for the dewatering and deposition of fine mineral tailings. As the most stringent extension to *status quo* regulations, the ERCB specifies minimum trafficable shear strengths of 5 kPa for consolidated oil sands tailings that has been deposited for 1 year, and 10 kPa after 5 years (ERCB, 2009). We urge other mining industries to establish similar standards suitable for respective types of tailings. Since the residual process water is physically contained inside the pores of the settled sediment, external energy is usually required to counteract the capillary pressure and further desiccate the solids. Energy demand increases further if it is desired to remove water that has been chemically bound to particle surfaces (Morey, 2013). Other processes utilize the difference of physical or chemical properties between water and the bulk solids to achieve their separation. This section reviews the general principles associated with each of these approaches.

1.2.3.1. Dewatering and material strength

Mechanical strength of a fine solids suspension can be characterized in terms of its shear yield stress (resistance against flow) and compressive yield stress (resistance against compression), both of which grow exponentially with increasing solid content.

Depending on the mineralogy, exact size distribution, and interactions between particles, a red mud sample that is typically fluid-like at less than 40% (w/w) solids can develop hundreds to thousands of Pascals in shear yield stress, and more than 18 kPa of compressive yield stress when dewatered to 60% (w/w) solids (Nguyen and Boger, 1998). Likewise, a sample of 10% (w/w) phosphate tailings with shear yield stress of 2.6 Pa consolidates, with external efforts, to a sludge of about 700 Pa at 48% (w/w) solids, although the accompanied increase in its compressive yield stress was unknown (Tao et al., 2008). However, permeability of the congregated fine material decreases rapidly as the material consolidates and blocks paths of least resistance for entrained water, which significantly slows down the rate of further water removal. Additional strategies to counteract the decrease of material permeability and water release are usually incorporated as part of any commonly encountered dewatering process.

1.2.4. Application of external energy

Fine solids sludge formed from sedimentation and densification processes contains, in most cases, water trapped between randomly-oriented, thin-layered amorphous particles in the silt and clay size ranges. The small size and high surface area-to-volume ratios of fine particles suggest the existence of a myriad of internal nano-scale capillaries capable of storing large quantities of water. Consequently, sludge desaturation would require

input of energy to work against the enormous capillary pressure as well as time-dependent compressive yield stress of the solid structure. Typical external energy sources are thermal, mechanical, electric, and their combinations or variants.

1.2.4.1. Evaporative and thermal treatments

Water removal by natural desiccation of fine mineral tailings has always been a key component of any land-based tailings management program. Initially, the fine solids sludge is deposited over a large area and exposed to natural elements that can assist (heat, wind, freeze–thaw cycles – see **Section 1.2.5**) or hinder (rain and snow) drying. Clearly, this method is best suited for arid or semi-arid regions. Desiccation of the topmost fraction occurs relatively quickly and induces the formation of surface cracks due to shrinkage from water evaporation. This results in changes to the material permeability and exposes additional material for drying, though some clay minerals are able to self-repair desiccation cracks when subjected to moisture (Rayhani et al., 2007). However, material fractions at depths of more than ~0.5 m do not experience significant natural drying even after a prolonged period of time, as demonstrated by Masala and Dhadli (2012). Mechanical means are often required to break or remove the top layers for additional exposure. Dedicated tailings drying by, e.g. calcination, is seldom applied unless the products are of economic value. Review of alternate red mud applications in China and India by Liu et al. (2009) and Samal et al. (2013), respectively, provided good examples where the waste material is thermally treated to produce quality construction materials such as cement and fired bricks. Similarly, the kaolinite-rich oil sand fine tailings can also be processed in this manner into a cementing material for concrete

(Wong et al., 2004), although to the best of our knowledge, no large-scale production efforts are proposed at this time.

1.2.4.2. Centrifugation

When placed in a rotating body of rotation radius r at an angular velocity ω , fine solid sludge is subjected to an enhanced gravitational field that further compresses the sediment layer and releases pore water. The magnitude of such effect is termed relative centrifugal force (RCF) given in **Eq. 1.3** in terms of the gravitational acceleration constant g .

$$RCF = \frac{r\omega^2}{g} \quad (1.3)$$

As the solid sediment gradually loses its entrained water, the compressive yield stress of the sediment increases exponentially that counteracts the applied compression force. Thus at a constant RCF value, a given sludge will, in time, consolidate to a corresponding equilibrium solids concentration. Centrifugation is sometimes used also for densification purposes. A comprehensive description of relevant particle sedimentation processes for industrial centrifuges is provided by Leung (1998). The consolidation process is irreversible as the bulk mass generally will not spontaneously re-disperse upon termination of rotation. Theriault et al. (1995) reported insignificant modifications of the equilibrium concentration by a variety of chemical, physical, and enzymatic treatments on MFT. Continuous centrifugation is currently applied in oil sands industry to remove fine solids from diluted bitumen in froth treatment. It is also used for enhanced moisture removal from fine and ultrafine coal in coal preparation plants. Use of centrifugation in

the Utah oil sands pilot projects to treat extraction tailings was shown to successfully produce stackable solid deposits and drastically reduce the requirement for fresh water (Mikula et al., 2008). The construction of a large-scale centrifugal tailings dewatering plant is currently underway in Syncrude Canada (COSIA, 2013). Commercial applications of centrifuges for treating wet mineral tailings are limited elsewhere in the industry.

1.2.4.3. Filtration and electrofiltration

Filtration is a widely practiced solid–liquid separation technique. In dead-end filtration, the feed material is placed on a porous filter medium (paper, cloth, or membrane), followed by introduction of a pressure gradient across the filter via vacuum, a hyperbaric gas, or mechanical press, that would drain out the entrained liquid while leaving behind a solid cake on the filter media. In this case the flow of filtrate is once-through and orthogonal to the filtration area. For cross-flow filtration the pressurized feed is directed parallel to the filter media, thus requiring recycle of feed flows to effectively treat the same volume of material. Mechanisms of water removal involved in filtration and compression stages are discussed by Mahmoud et al. (2010) and in detail by Dick et al. (1980) and Lockhart and Veal (1996). At a given pressure gradient and filtration area, the rate of dewatering, or filtrate flux, is a complex function of the suspension and solids properties, such as solids concentration, size distribution, surface charge, and hydrophobicity. These effects are reviewed by many researchers (Lockhart and Veal, 1996; Sung and Turian, 1994; Besra et al., 2000; Wakeman, 2007).

Filtration of materials that are predominately fine solids is extremely difficult, as demonstrated by Sung and Turian (1994) with ~400 mesh (<37 μm) coal particles, due to their high specific resistance (low permeability) and compressive yield stress in a consolidated filter cake. The authors concluded that the amount of fine particles is a determining factor on the moisture of the solid cake. Indeed, Wakeman (2007) showed that the specific resistance of the filter cake is inversely related to the second power of particle size. To effectively filter fines-rich feed, either: (a) cake thickness must be controlled and minimized (Lockhart and Veal, 1996), or (b) particles will need to be coagulated and/or flocculated to promote their effective size and reduce resistance to filtration. The latter approach has seen an increasing number of experimental work and applications in treating fine coal tailings (Alam et al., 2011), red mud (Power et al., 2011), and oil sand tailings (Xu et al., 2008; Alamgir et al., 2012; Wang et al., 2010), although polymer dosage control is critical for final cake moisture when flocculants are used (Lockhart and Veal, 1996). Surfactants can also be applied at proper dosages to render the particles hydrophobic and hence increase the recession rate of water from the filter cake (Stroh and Stahl, 1990; Morey, 2013).

Reduction of water viscosity also leads to improved filtrate flux, usually achieved by application of hyperbaric steam. Many authors (Peuker and Stahl, 1999; Bott and Langeloh, 2001; Morey, 2013) advocate the advantages of using hyperbaric steam that include: (a) its rather unique and stable dewatering front – that is a gradual movement of a sharp interface between steam-saturated, heated filter cake and remaining water-saturated section, allowing for predictive modeling and better process control; (b) a very dry cake that can be obtained even at continuous operations, as shown by Bott and

Langeloh (2001); (c) ability to extract solubilized species into the filtrate, and (d) thermal disintegration or vaporization of adsorbed contaminants. A serious drawback with this method is its dependence on the material permeability (Morey, 2013), therefore the movement of the dewatering front is anticipated to be very slow for unconditioned fine tailings, limiting its potential treatment capacity.

Augmentation to conventional filtration operations that must process fine and ultrafine materials can be realized by the application of magnetic, acoustic, electrical, and electro-acoustic energy sources. An excellent review on electric field-assisted mechanical filtration (electrofiltration) was given by Mahmoud et al. (2010). The electrofiltration method takes advantage of the electrical nature of the solid surfaces and induces electrophoresis of solids, electro-osmosis of water, as well as migration of dissolved ionic species towards the electrodes. In electrofiltration the cathode and anode are immersed in the feed material in such a way that the particle electrophoresis is directed away from the filter media. In such a configuration, according to Yukawa et al. (1976), the resultant motion of particles would fully oppose the hydraulic transport of particles towards the filter media when a critical electric field is established. This phenomenon would certainly be beneficial to treating negatively-charged fine solids suspensions as the electroosmotic flow of cation-rich water is countercurrent to the electrophoresis of solids, as presented by Mahmoud et al. (2010) in **Fig. 1.6**. Thus, formation of low-permeability fine solids cake can be resisted while filtration progresses. Such approach was demonstrated to accelerate the initial rate of dewatering on a quartz sand suspension with D_{50} of 2 μm and electric field parallel to filtrate flow, though limited improvement was found in the final cake moisture content (Weber and Stahl, 2002). Theoretical modeling by Raats et al.

(2002) showed an increased effectiveness of electrofiltration relative to conventional filtration of treating a concentrated sludge primarily consisted of micron and sub-micron sized particles. Indeed, a recent study by Loginov et al. (2013) with 23.4% (w/w) sodium bentonite ($D_{50} = 3 \mu\text{m}$) in orthogonal electric field showed similar results as Weber and Stahl (2002). Further enhancements in filtration rate were demonstrated by the optimized addition of lime. Utilization of rotating electrodes, low frequency alternating current (AC), and interrupted input instead of direct current (DC) has shown promise to further improve dewatering rate and performance (Chen and Mujumdar, 2002).

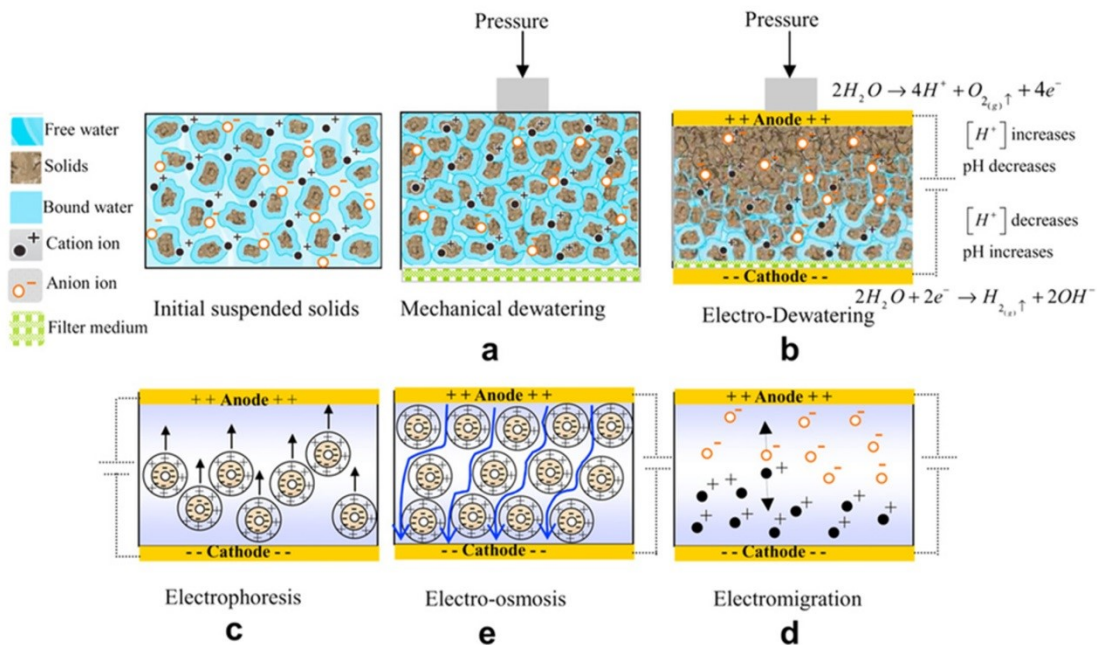


Figure 1.6. Mechanisms of electrofiltration (adopted from Mahmoud et al. (2010), with permission. Copyright © 2014 Elsevier).

Other studies have been carried out for similar systems and investigated several beneficial and detrimental side-effects of electrofiltration, which are summarized by

Mahmoud et al. (2010). Electrochemical reactions at the cathode and anode increases and decreases local pH, respectively, which directly affects surface properties of the fine solids. It is foreseeable that, for example, a kaolinite slurry undergoing electrofiltration will gradually coagulate as they migrate toward the anode, and kaolinite particles would still be mobile at the filter media (cathode). In terms of preventing filter cake formation (and thus accelerated dewatering), this trait would be a valuable asset. However, as the operational electric voltages are typically much higher than that required for the electrolysis of water, gas formation will take place at both electrodes. Hydrogen and oxygen gas bubbles are potentially an explosive mixture, and they can also increase the void fraction and electrical resistance of the feed material. As a result, the rate of electrokinetic processes diminishes, contributing to an increased local heating at the electrodes. The resistance heating, on the other hand, reduces the water viscosity and surface tension, both playing a positive (although limited) role in improving the rate of solid–liquid separation. For electrofiltration, periodic cathode cleaning is necessary for saline suspensions due to ion reduction and deposition of potentially insoluble hydroxides. Finally, the anode material is subject to oxidative corrosion, thus it is imperative to have relatively inert materials, such as those used by Raats et al. (2002), to ensure the longevity of the process and trouble-free operations. These complications may have hindered the progress on systematic studies using pilot and full-scale equipment, and created difficulties in fully assessing its performance (Mahmoud et al., 2010).

1.2.5. Exclusion of water

Water retained by a non-soluble porous medium generally has quite different physical and chemical properties from the containment material, which can theoretically be utilized to achieve dewatering. In cold regions for example, volume enlargement of ice and the exclusion of impurities from ice crystal growth have been successfully applied to treat pulp mill and oil sands wastewaters (Gao et al., 2004). Though not yet applied on an industrial scale, developments in gelation materials that can nucleate or attach to suspended solids (but not water), and absorbents that specifically accept water into their molecular structure also offer new possibilities to effective dewatering.

1.2.5.1. Freeze–thaw

The basis of the freeze–thaw as a method to treat mineral tailings, and especially fine tailings, is briefly considered as follows. Solidification of pore water physically rejects interstitial mineral and ionic impurities from the ice crystal network towards spaces already occupied by mineral solids, which forces their aggregation. As the network grows, the corresponding volumetric expansion further compresses these aggregates and over-consolidates them, while increasing the average pore size (Proskin et al., 2010). Therefore upon subsequent thawing, the entrained water experiences increased permeability and seepage can occur under gravity that leads to an overall reduction in sludge volume. Although beneficial from a dewatering viewpoint, freeze–thaw also leads to reduced material compressibility, which may necessitate further treatments for safe deposition (Beier and Segó, 2009). However, the undrained shear strength is observed to improve drastically for coal tailings and MFT due to the compressive stress exerted by

the ice phase. Although an extensive study of freeze–thaw on Florida phosphate tailings was reported (Stancyzyk et al., 1971), no published work could be found on the freeze–thaw treatment of other types of mineral tailings. Since this treatment method is seasonal and strongly depends on actual weather conditions in winter times, the benefits of freeze–thaw may be realized better if it is incorporated to other complementary dewatering technologies.

1.2.5.2. Gelation and water absorbents

Utilization of gelation agents to selectively bind and remove suspended solids is also an interesting area of research. Chaiko et al. (1998) applied a combination of alkali silicate and an organic gelling agent to extract nearly all colloidal particles from a suspension. Upon aging at 70–90 °C, syneresis of gel components initiates rapid and spontaneous exclusion of water along with the dissolved salts from the rest of the slurry components. Iwata (2003) deposited sodium alginate on surfaces of the colloidal particles and added the mixture drop-wise to calcium chloride solution that led to the formation of calcium alginate gel. Gravitational drainage and mechanical press are subsequently applied to expel water while effectively retaining the solids inside the gel. Since both studies used slurries of unspecified solids concentration, the effectiveness of these gelation agents on dewatering of concentrated sludge remains to be investigated.

Recently, Farkish and Fall (2013) demonstrated the potential of a water absorbent polymer on the consolidation of MFT. At a dosage of 3% (wt. absorbent/wt. MFT) and 7 days of conditioning, the granular cross-linked polyacrylate material is shown to readily absorb water and leave behind a residual with up to ~80% (w/w) solids and close to 9 kPa

of undrained shear strength. Further dewatering and structural strength enhancements can be achieved via freeze–thaw cycles and natural drying. Thermal treatment is used to regenerate the material. However the performance of the recycled absorbent was found to gradually deteriorate. As water is ubiquitous in mineral tailings, clearly opportunities exist in the development and application of high-capacity and regenerative water absorbents as a viable dewatering method.

1.3. Overview of current technologies

Improved empirical and semi-empirical understandings on the nature of the fine mineral tailings constituents, their mutual interactions, and role of the conditioning agents have led to a gradual transition of fine tailings handling practices, from outright waste dumping and tailings containment to the development and acceptance of several mature densification and consolidation technologies by mining industries worldwide. Some of these technologies were adopted from historical approaches, such as coagulation by alum and filtration for water purification purposes. Others, such as the paste thickener, were invented as late as the 20th century as a result of advancements in the fundamental scientific knowledge of, for example, colloidal suspensions, flocculants, and fluid mechanics. Descriptions and brief evaluations of these widely established technologies are presented in this section. More detailed technology evaluations are publically available via the Oil Sands Tailings Technology Deployment Roadmap (Consortium of Tailings Management Consultants, 2012). However, substantial performance variations do exist from case to case, which reflect the inadequacy of our current understandings and highlight several key knowledge gaps between theory and practice. Indeed, industrial

densification and consolidation equipment is almost exclusively built on the basis of laboratory and pilot plant test data as well as existing operation experience, instead of a fundamental, descriptive theoretical model at this time. Ongoing efforts from the scientific community and the mining industry on the path forward to reduce the environmental footprint of tailings are also discussed.

Concentration of finely dispersed mineral slurries has traditionally been focused on treating the beneficiated value products utilizing equipment such as hydrocyclones, thickeners, filters, and centrifuges to remove excess water for better material handling and reduce costs for transportation (Wu et al., 2010). The same technologies were adopted, with modifications, by the mining industry as a starting point for fine mineral tailings treatments. Some of these technologies are sufficiently advanced and have been applied commercially, including densification technologies (consolidated and thickened tailings), as well as technologies for dewatering (natural drying and centrifugation). In other sectors of the industry, mechanical, vacuum, or hyperbaric filtration technologies also stood the test of time and became prevalent (Wu et al., 2010). Much effort has been devoted to evolutionary enhancements on these mature technologies (e.g. electrofiltration) with varying degrees of success. As a result, new and revolutionary technologies (e.g. gelation and absorbents) are relatively scarce and have seen limited standalone or integrated applications. Current technologies are feasible, but not all of them are economically practical to treat such large volumes of fluid fine tailings on a daily basis, especially in highly variable and extreme climate conditions. However, fundamental research will continue to help the industry identify and improve these technologies to the point where commercialization will eventually become practical due

to the need to meet government regulations such as those set by ERCB Directive 074. With continuing effort of industry, for example, technologies such as thin lift drying, flocculation-enhanced centrifugation and/or filtration will mature to become reality. It should be noted that at present there is no ‘silver-bullet’ to resolve huge fluid fine tailings problems, rather a combination of technologies, such as flocculation-assisted centrifugation and filtration with co-deposition integrated into thin lift drying and/or rim ditching is likely to succeed.

1.3.1. Densification technologies

1.3.1.1. Traditional technologies

Conventional pond storage. The practice of storage or impoundment of mineral tailings and fine mineral tailings in an engineered structure still remains popular as one of the least expensive treatment options for most mines (Watson et al., 2010). Gravity sedimentation of solids occurs within the impoundment structure. Due to extremely long residence time to handle solids in the silt and fines size range, large pond sizes are typically required. Self-consolidation of solids forms a sediment layer and separates from the process water, both of which can be withdrawn for further processing and usage. Typical outgoing solids concentrations are in the range of 30–55% (w/w), depending on suspension conditions (Watson et al., 2010) as discussed in **Section 1.2.1**. Wu et al. (2010) noted that the conventional treatment method is of ‘‘high capacity, low maintenance, and low operating cost’’, in agreement with comments made by Watson et al. (2010), who also indicated the conventional method is the sole reliable technology for plants with high production rates classified by the authors as >100,000 tonnes/day (tpd).

Hydrocyclones. Traditionally, hydrocyclones are widely used in the mineral processing industry as an inexpensive and compact device for particle classification and concentration purposes. As a high capacity device, hydrocyclone can typically process feed up to 7200 m³/h and enrich solids up to 50% (w/w) at underflow discharge (Ortega-Rivas, 2012). Operating principles of a hydrocyclone is similar to centrifuges in which a centrifugal force is produced from rotation of slurry, except that hydrocyclones do not have moving parts. As a slurry containing particles of different sizes enters the hydrocyclone, the swirling motion of the fluid flow tends to spin the coarse and dense particles towards the vessel wall while retaining the finer and lighter particles in the center. Wall erosion by solid particles is attributed as the greatest threat to hydrocyclone operations and demands considerable attention in maintenance. Fortunately, advancements in erosion simulation software have led to numerous new equipment designs that significantly reduce vessel wear (Wu et al., 2010).

Satisfactory separation of dispersed fine solids from water in a hydrocyclone has been difficult due to a lack of generating sufficiently clear overflow (Franks et al., 2005; Consortium of Tailings Management Consultants, 2012). Recent developments suggest that improvements may be achieved with hydrocyclone units in smaller diameter (Yang et al., 2013), or operated under modified process conditions, e.g., cyclic flow (Zhao et al., 2008), and application of an electric field (Nenu et al., 2010), though care must be taken to avoid underflow blockage for small units. Experimental work on utilizing these performance enhancements in hydrocyclone for treating fine mineral tailings slurry has yet been published at this time.

1.3.1.2. Assisted fines destabilization

Coagulation-based technologies. Commercial installations of a densification technology utilizing coagulants on fine tailings are best demonstrated by the so called composite or consolidated tailings (CT) process, also known as non-segregating tailings (NST) process, in the oil sands industry. In essence, fresh extraction tailings are classified in a hydrocyclone, and the coarse underflow is mixed with chemical (coagulant) treated MFT (or fresh fluid fine tailings) to create a non-segregating mixture that settles quickly and releases water efficiently (Masliyah and Czarnecki, 2011). The CT leaving the process typically has solid concentrations of 57–60% (w/w) which requires further dewatering measures to meet targets set by ERCB Directive 074. In other mining operations, a version of the NST can also be realized if cement or a binder material is added to fine tailings, forming a paste to prevent segregation and improve material strength (Watson et al., 2010). Capital investments for CT installation can be expensive (Consortium of Tailings Management Consultants, 2012), and major operating cost is by coagulant/binder addition and energy demand from fluid transport. In addition, the process requires high degrees of control over feed properties, which is reflected from the reported poor reliability in actual CT operations with regards to, for example, product quality (Alberta Energy Regulator, 2012; BGC Engineering Inc., 2010).

Flocculation-based technologies. The thickened tailings (TT) and paste thickener processes involve the addition of polymeric flocculants to the feed material, followed by means of proper mixing and, in some cases, clarification inside a thickener. Typical underflow solid concentrations have been reported to be 25–55% (w/w) for oil sand fine tailings (Masliyah and Czarnecki, 2011; Consortium of Tailings Management

Consultants, 2012), and 50–70% (w/w) for other mineral tailings with conventional and high-rate thickeners at the lower end and above 65% (w/w) for high-density paste thickeners (Watson et al., 2010). Since its inception in 1973 at Kidd Creek, Canada, commercial applications of TT are gaining popularity. The largest TT project currently in operation is reported to have a capacity of 95,000 tpd, located in northern Chile. Procurement, operation, and maintenance of specialized equipment and flocculants are often required to pursue this option, which can amount to significant costs.

The immediate benefits of using technologies described in **Section 3.1.2.** are near-complete fine solids capture and potential cost savings realized from smaller tailings impoundment structures and water recycle, which offsets, to some extent, increased capital and operating costs from additional equipment, piping, and slurry transportation. Since the extent of water removal in some cases is restricted by available slurry pumping and pipeline transportation technologies (Jones and Boger, 2012), additional dewatering measures are generally necessary. Applications would be favored for mining operations where land or water resources are restricted, and discouraged where exists, for instance, high energy cost, unfavorable project economics, and/or less stringent regulations on mine waste discharge.

1.3.2. Dewatering technologies

1.3.2.1. Natural drying

Thin-lift drying. This technology applied to oil sands extraction tailings involves deposition of treated tailings products, such as pond sediments, CT, or TT, in thin layers

that are subjected to gravity drainage, natural desiccation, and freeze–thaw cycles. Inclined surface is generally used to enhance water release and collection, and the angle of inclination is highly dependent on the rheological properties of the product, ranging from 0.5% to 2.0% for pond sediments and 3.0–10.0% for paste tailings (Watson et al., 2010). Perimeter underdrains are typically in place to control seepage of process water. Successive layers are deposited on the previous layers once sufficient drying is achieved and the material becomes self-supportive. This technology and its variants are also widely applied in the alumina industry to treat red mud, where it is termed as “dry stacking” (Power et al., 2011). Although inexpensive to operate, this technology requires substantial land area due to long residence time for the deposited layer to reach desirable dryness and strength suitable for subsequent deposition and/or reclamation, which creates limitations to the volume of tailings that can be timely treated.

Deep in-pit deposition (rim ditching). In comparison with thin-lift drying, deep tailings deposition discharges the treated tailings into deep engineered pits. Natural desiccation and freeze–thaw of topmost layers occur relatively quickly, whereas underdrains, vertical (wick) drains, perimeter rim ditching, and other mud farming operations help to remove water from the deeper sections via exposure, gravity drainage, and self-weight consolidation (BGC Engineering Inc., 2010). Though labor-intensive, successful applications of deep in-pit deposition have been reported for dewatering phosphate tailings in Florida (Carrier, 2001). Geotechnical tests are ongoing to evaluate the strength and trafficability of oil sand tailings deposits over long periods of time. In particular, results from Shell’s Tailing Testing Facility appear promising after 5 years in operation (Masala and Dhadli, 2012).

1.3.2.2. Centrifugation

The continuous solid bowl scroll decanter centrifuge is widely used in mineral processing (Consortium of Tailings Management Consultants, 2012). Pre-treatment of fine tailings is necessary prior to centrifugation for efficient fine solids capture and would eliminate the need for excessively high rate of rotation, which translates to the increase in the treatment throughputs. An application example of a horizontal decanter centrifuge to treat flocculated MFT is given by Masliyah and Czarnecki (2011), in which 270 m³/h feed is enriched to a solid product of 60% (w/w), while recovering high quality process water of <1% (w/w) solids. Based on the past experience, adequate process controls will be required to maintain feed solids concentration targets. Capital investments and operation and maintenance costs of centrifugation for oil sands tailings treatment are expected to be significant due to fast-moving mechanical parts.

1.3.2.3. Filtration

Various mechanical, vacuum, and pressure filtration installations are common for dewatering coal tailings and red mud (Bethell, 2012; Power et al., 2011), but have rarely been applied in oil sands. Dry disposals of coal tailings are becoming increasingly common and generally performed with belt filter presses and plate-and-frame filters (Bethell, 2012). Belt filter presses require feed pre-treatment, usually by flocculation, and produce solid products that depend on the particle size distribution of the feed. Typical capacities are 3.6–10 tonne per hour per meter of belt width for fine tailings, which produces products of 45–65% (w/w) solids. In belt press filtration, large loss of fine

solids (up to 40% w/w of total solids) can occur if feed material is predominately clay-sized (Fenzel, 2012). In 2004, the capital and operating costs are also estimated by Fenzel (2012) to be Australian (AU) \$0.49/ tonne and AU \$1.84/tonne of solids to be treated, respectively. Although cost-effective, the relatively low product solid concentration and product consistency may be unsatisfactory. On the other hand, other filter presses such as plate-and-frame are more expensive but enables near-complete solids capture, which also gives a final product of 18–30% (w/w) surface moisture only (Prat, 2012). Limited data on the filtration rate suggest a flux of 110–140 kg/m²-h to achieve a surface moisture of 21–23% (w/w) for a South African metallurgical coal tails (Prat, 2012), and similarly for a sample of Pennsylvania anthracite refuse (Verma and Klima, 2010). As a result, large filtration areas are required to accommodate high-rate processing plants. Laboratory investigations on the pressure filtration of oil sands MFT revealed that higher throughputs can be achieved by proper fine solids flocculation and the selection of a two-stage filtration process (Wang et al., 2010; Alamgir et al., 2012). **Fig. 1.7** compares single stage filtration (plain region) and two-stage filtration (i.e. flocculation and thickening followed by filtration as shown by shaded region) for processing MFT. With appropriate dilution of MFT, the filtration time to achieve 23% (w/w) cake moisture can be reduced from 25 min to 10 min by operating a two-stage filtration process. The two-stage process is favorable since it filters only the thickened sediment. With appropriate choice of flocculant (Al-PAM), large mushroom-like flocs are formed that favor rapid dewatering under applied pressure. Reuse of the clarified supernatant as dilution water ensures that the process produces a net gain of water for recycling, as well as reducing the chemical

loading to achieve minimum filtration times. With this configuration it is less critical to have effective flocculation of fines.

To date, few operators have reported commercial applications of pressurized steam filtration, and even fewer for electric field-enhanced filtration. An encouraging prototype setup employing the combined principles of centrifugation and pressure filtration are shown to continuously process 120 L/min of fine coal slurry to products of less than 20% moisture, even when the feed material is dominated by particles of less than 25 μm (Keles et al., 2010). However its effectiveness on treating fine coal refuse and other fine mineral tailings remains to be investigated.

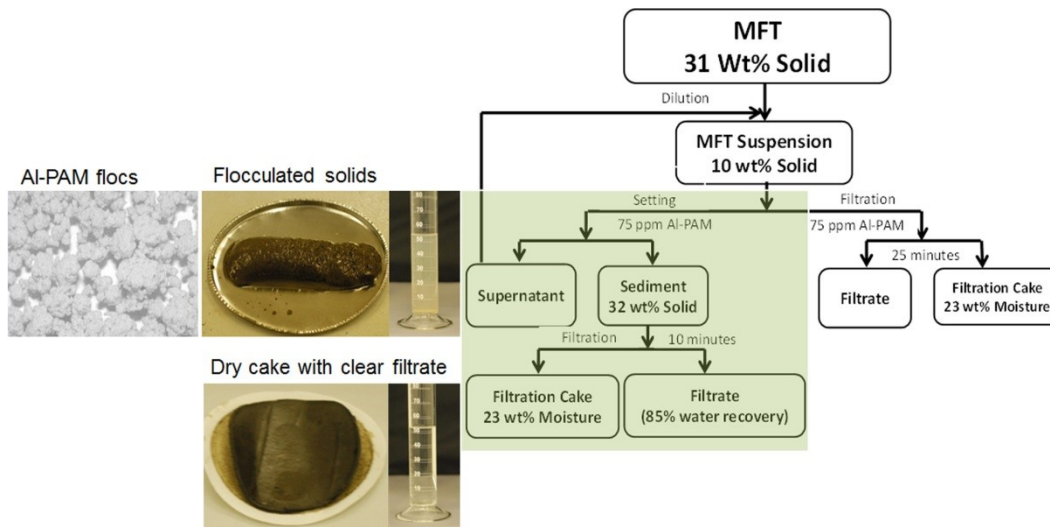


Figure 1.7. Proposed treatment processes for oil sands MFT using filtration. Shaded rectangle indicates the preferred option. Process as well as product visuals “Flocculated slurry” and “Filtered sediment” are adopted from Alamgir et al. (2012), with permission. Copyright © 2014 Elsevier. Product visual of Al-PAM flocs adopted from Wang et al. (2010), with permission. Copyright © 2014 John Wiley and Sons.

1.3.3. Knowledge gaps

There are many proposed short-term and long-term solutions to alleviate or eliminate the accumulation of fine mineral tailings via enhanced solids sedimentation as well as sludge desaturation. Unfortunately over time, only a few have managed to maintain the delicate balance of process efficiency and economics, and not all of these methods are considered commercially robust or reliable at present time. As discussed previously, this is a direct consequence stemming from the generally decreasing ore grade and loss of mineral selectivity with current mechanized mining and hydrometallurgical beneficiation processes, both of which introduce degrees of variability across tailings streams in terms of key physical and chemical properties. Due to their complex nature, current theories on the fundamental properties and conditioning of fine mineral tailings mostly follow empirical or semi-empirical approaches performed with ideal (single solid component) slurries and less commonly, real tailings. Conclusions drawn from existing studies are difficult to extrapolate for *a priori* industrial equipment selection, design, and operation. For most, if not all industrial applications dealing with fine tailings, sound industry expertise coupled with extensive performance data and evaluations from lab- and pilot-scale tests are mandatory before their full-scale implementation. Unfortunately, even for the most veteran processes and techniques it is still difficult to perform reliable on-line measurements to determine changes in response to variations in important and relevant feed property parameters. It is a common practice to adjust necessary equipment controls in time by grabbing and analyzing samples at fixed time intervals, which occasionally causes operational problems ranging from off-spec products to equipment blockage. More comprehensive analysis on this aspect can be found in a recent document entitled

Oil Sands Tailings Technology Deployment Roadmap (Consortium of Tailings Management Consultants, 2012). This five-part roadmap focused extensively on current and potential technologies/operational guidelines, accumulating information not just from oil sands but from the global minerals and mining sector. The report, compiled through the collaborative efforts of many technical and industrial experts assessed numerous technologies that were categorized based on their current status of deployment and feasibility. We encourage readers of greater interest in this aspect to review the roadmap for more details on individual technologies.

An option available to mine operators is to develop protocols for selective mining to reduce the amount of fine tailings production, however its implementation may be costly and the practice is unnecessary in the long-term. The demand for mineral products continues to grow with no end in sight, even the leanest of ore deposits will become economically attractive to mine. Additionally, it should be noted that although tailings processing and environmental management are generally a minor component of the CAPEX and OPEX profile of a major mining operation, it represents resolving a huge liability issue to mining companies. This potential liability would limit the growth of the industry and further development of the valuable resources due to potential catastrophic disaster of dam structure failures and/or long term land disturbances that present potential risks to wildlife. Resolving such issue is a major step towards responsible development of our valuable natural resources. Thus efforts should be concentrated on facing the tailings problems head-on instead of delaying the inevitable long-term issues. For the foreseeable future, instead of treating fine mineral tailings as a black box, emphasis should be given to advancements in fundamental science for improved comprehension of their

macroscopic properties and behaviors. This will certainly serve to better refine current treatment techniques, as well as greatly assisting the development of next-generation techniques that can revolutionize the management of fine mineral tailings.

Since the subject of interest involves a myriad of micron- and nano-sized solid particles, it is essential to address several aforementioned key microscopic properties: e.g. size distribution, mineralogy, and morphology, using standardized characterization methods and procedures, both of which can greatly benefit from improvements to measurement technologies and devices. Also, it is of utmost importance to study the fundamental molecular-scale interactions between solid materials of different mineralogy and morphology across a spectrum of grain sizes in water, and with any chemical additives in the complex solution environments with inevitable soluble species and contaminants. Similarly important is to characterize morphology as well as geotechnical and mechanical properties of the particle aggregates. Foreseeably, the 'silver bullet' to managing fine mineral tailings would involve an array of subprocesses that recognizes these complexities from a fundamental level. There is no single 'silver bullet'. The 'silver bullet' would most likely be an entire process of its own with innovative integration of chemicals and process configurations with the rest of the mining operations.

Current research efforts utilizing ideal and model slurries must continue while special attention should be given to establishing relevant connections to real tailings. In the meantime, available microscopic properties and observations should be carefully leveraged to achieve quantitative conversion between microscopic behaviors from/to essential macroscopic parameters to fundamentally address and model commonly encountered phenomena such as:

- In enhanced settling: a unified sedimentation-consolidation model addressing fluid–solid state transitions (BGC Engineering Inc., 2010).
- In dewatering: fluid transport through immiscible, compressive, porous media.
- In slurry transport and disposal: rheological and depositional behavior of thickened tailings, pastes, and dried solids; optimizing transportation equipment and strategies of tailings feed and products.
- Slurry conditioning: molecular interactions between suspended solids, additives, and contaminants; impact of these molecular interactions on enhanced settling, dewatering, and modification of slurry bulk properties; design and synthesis of novel chemical additives; optimized addition and mixing guidelines/strategies.
- Process control and reliability: real-time monitoring of important slurry properties.

Additionally it may be of interest for mine operators to explore alternate uses for unfinished/finished tailings products.

1.4. Conclusions

In the mining industry, accumulation of large amounts of fine mineral tailings is still an ongoing issue due to increasing demand of mineral products and insufficient means to consume the associated tailings that are generated by mega-scale mining operations. In many cases the tailings are conventionally stored in engineered ponds that are susceptible to accidental discharges and a host of environmental issues that pose significant risk to the public and surrounding areas.

Much effort has been devoted to fundamentally investigate the two key technical issues (slow settling and water capture) involved with fine tailings by addressing their sedimentation, consolidation, stability, and rheological behaviors. Coagulation and flocculation are effective at destabilizing fine solid suspensions, both of which can greatly accelerate solid–liquid separation under the correct conditions. More energy will be needed to further consolidate the solid sediment and release additional water. Specialty reagents that specifically remove water or solids also show some promises. Performance of actual densification and dewatering technologies varies by application. At this time, extensive laboratory and field tests are mandatory before implementation. This is a consequence of our limited understandings on the actual feed material, as difficulties exist when extending the current fundamental understandings to predictively describe actual tailings samples. It is highly desirable to establish links between their microscopic characterization parameters and observable bulk behavior. Opportunities exist in further refinements and extensions of current scientific models to better describe actual fine mineral tailings. Evidently, better theoretical models improve and assist industrial efforts when processing fine tailings, or solid slurries in general with similar nature, positively affecting a wide range of activities such as equipment design and scale-up, modification and retrofitting, operation and process control, product quality assurance, and ultimately reliability of the process. All of these serve to reduce technical and financial risks of brownfield and greenfield fine tailings treatment technologies, by improving the robustness for existing applications, and the performance certainty for emerging projects.

Compared with the *status quo* scenario (interpreting fine tailings as a black box), where over-production and under-utilization of tailings have created a vicious cycle of waste accumulation that is prone to environmental damage, the fundamental approach – although difficult at first – helps to drive a virtuous cycle that gradually reduces and eliminates fresh and legacy fine mineral tailings. As noted by Jones and Boger (2012), in the past 30 years or so, growing mutual cooperation between mine operators, global research teams and forums, as well as equipment suppliers to address the challenging issues brought by fine mineral tailings is very encouraging and extremely valuable. These efforts are indispensable for significant contributions to our understandings of the tailings problem while further improving the sustainability of the entire mining industry. Insights gained from such multidisciplinary exchanges of knowledge offer great potential to the advancements in other related research areas.

1.5. Thesis objectives

A promising technology for the treatment of waste slurry containing fine particulates has been brought to Canada for the first time. This technology, named “volute screw press” (VSP), combines the principles of flocculation, continuous filtration, and automatic filter medium cleaning in operation. Application of such a device to the treatment of Canada’s oil sands tailings would bring groundbreaking and revolutionary changes to this field. Among the many beneficial consequences, use of the volute screw press solves a critical problem with conventional tailings filtration efforts – filter media fouling and blockage by fines and bitumen.

The objectives of this work are as follows:

- To demonstrate the VSP is a viable method to treat MFT.
- To present a systematic theoretical analysis on the dewatering principles of the VSP.
- To study the responses of polymer-flocculated MFT sediments to the dewatering mechanisms brought by the VSP.
- To predictively model the VSP solid product (filter cake) dry solids content based on sediment response parameter(s).

The project was executed over three phases:

- **Phase 1:** early VSP trials at the University of Alberta
- **Phase 2:** on-site VSP testing at the Innovation Centre of the Horizon Oil Sands, Fort McMurray (Canadian Natural Resources Limited)
- **Phase 3:** on-campus systematic sediment study at the University of Alberta

1.6. Organization of thesis

Main body of this thesis is divided into eight chapters.

Chapter 1 – a basic scientific and technological overview and analysis of the recent overall status of fine mineral tailings treatment, which has been published in *Minerals Engineering*.

Chapter 2 – descriptions of the VSP device.

Chapter 3 – presentation of a semi-empirical theory on the mechanical dewatering of flocculated MFT sediments. This chapter also includes all experimental materials and methods used in the **Phase 3** (bench-scale) study.

Chapter 4 – materials and experimental methods used in the **Phase 2** (field) study.

Chapter 5 – presents bench-scale study results and discussions.

Chapter 6 – provides results, observations and discussions from the field study.

Chapter 7 – establishes predictive modeling of the VSP filter cake product quality based on results from **Chapter 5** and **Chapter 6**.

Chapter 8 – concludes this thesis, outlines contributions to original knowledge and suggests relevant future work.

References

- Abdel-Aal, E.-S.A., 2000. Recovery of phosphoric acid from Egyptian Nile Valley phosphate tailings. *Miner. Eng.* 13 (2), 223–226.
- Alagha, L. et al., 2013. Probing adsorption of polyacrylamide-based polymers on anisotropic basal planes of kaolinite using quartz crystal microbalance. *Langmuir* 29, 3989–3998.
- Alamgir, A., Harbottle, D., Masliyah, J., Xu, Z., 2012. Al-PAM assisted filtration system for abatement of mature fine tailings. *Chem. Eng. Sci.* 80, 91–99.
- Alam, N., Ozdemir, O., Hampton, M.A., Nguyen, A.V., 2011. Dewatering of coal plant tailings: flocculation followed by filtration. *Fuel* 90, 26–35.
- Alberta Energy Regulator, 2012. Directive 074 (Supplemental Information, Tailings Management Assessment Report (2011/2012)). <http://www.aer.ca/rules-andregulations/directives/directive-074> (accessed 2013).

Alberta Energy Regulator, 2013. ST98: Alberta's Energy Reserves & Supply/Demand Outlook. <http://www.aer.ca/data-and-publications/statistical-reports/st98> (accessed 2013).

Allen, E.W., 2008. Process water treatment in Canada's oil sands industry: I. Target pollutants and treatment objectives. *J. Environ. Eng. Sci.* 7, 123–138.

Al, T.A., Blowes, D.W., 1999. The hydrogeology of a tailings impoundment formed by central discharge of thickened tailings: implications for tailings management. *J. Contam. Hydrol.* 38, 489–505.

ASTM, 2011. D2487-11 Standard Practice for Classification of Soils for Engineering Purposes (Unified Soil Classification System). http://enterprise.astm.org/filtrexx40.cgi?+REDLINE_PAGES/D2487.htm (accessed 2013).

Barraza, J., Guerrero, J., Piñeres, J., 2013. Flotation of a refuse tailing fine coal slurry. *Fuel Process. Technol.* 106, 498–500.

Beier, N.A., Sego, D.C., 2009. Cyclic freeze–thaw to enhance the stability of coal tailings. *Cold Reg. Sci. Technol.* 55, 278–285.

Besra, L., Sengupta, D., Roy, S., 2000. Particle characteristics and their influence on dewatering of kaolin, calcite and quartz suspensions. *Int. J. Miner. Process.* 59, 89–112.

Bethell, P.J., 2012. Dealing with the challenges facing global fine coal processing. In: Bethell, P.J., Arnold, B.J., Klima, M.S. (Eds.), *Challenges in Fine Coal Processing, Dewatering, and Disposal*. Society for Mining, Metallurgy, and Exploration Inc., Englewood, Colorado, pp. 33–45.

BGC Engineering Inc., 2010. Oil Sands Tailings Technology Review (OSRIN Report No. TR-1). Oil Sands Research and Information Network, University of Alberta, School of Energy and the Environment, Edmonton, Canada.

Boger, D.V., 2009. Rheology and the resource industries. *Chem. Eng. Sci.* 64, 4525–4536.

Bott, R., Langeloh, T., 2001. Synergy effects with steam pressure filtration. *Chem. Ing. Tech.* 73, 1323–1327.

Bridge, G., 2000. The social regulation of resource access and environmental impact: production, nature and contradiction in the US copper industry. *Geoforum* 31, 237–256.

Carrier, W.D., 2001. Rapid Clay Dewatering Phase II: Field-Scale Tests. Florida Institute of Phosphate Research, Bartow, Florida.

Chaiko, D.J., Kopasz, J.P., Ellison, A.J.G., 1998. Use of sol–gel systems for solid/liquid separation. *Ind. Eng. Chem. Res.* 37, 1071–1078.

Chen, G., Mujumdar, A.S., 2002. Application of electrical fields in dewatering and drying. *Dev. Chem. Eng. Miner. Process.* 10, 429–441.

Ching, H.-W., Tanaka, T.S., Elimelech, M., 1994. Dynamics of coagulation of kaolin particles with ferric chloride. *Water Res.* 28, 559–569.

Consortium of Tailings Management Consultants, 2012. Alberta Innovates – Energy and Environment Solutions, Featured Reports, Tailings Roadmap and Action Plan. <http://www.ai-ees.ca/reports.aspx> (accessed 2013).

COSIA, 2013. Centrifuges Used to Release Water from Fluid Fine Tailings. <http://www.cosia.ca/projects/tailings/centrifuges-used-to-release-water> (accessed 2013).

Crowson, P., 2012. Some observations on copper yields and ore grades. *Resour. Policy* 37, 59–72.

Davis, R.H., Zhang, X., Agarwala, J.P., 1989. Particle classification for dilute suspensions using an inclined settler. *Ind. Eng. Chem. Res.* 28, 785–793.

de Kretser, R., Scales, P.J., Boger, D.V., 1997. Improving clay-based tailings disposal: case study on coal tailings. *AIChE J.* 43, 1894–1903.

Dick, R.I., Ball, R.O., Novak, J.T., 1980. Sludge dewatering. *CRC Crit. Rev. Environ. Control* 10, 269–337.

Duan, J., Gregory, J., 2003. Coagulation by hydrolysing metal salts. *Adv. Colloid Interf. Sci.* 100–102, 475–502.

Elimelech, M., Gregory, J., Jia, X., Williams, R.A., 1995. *Particle Deposition and Aggregation Measurement, Modelling and Simulation*. Butterworth-Heinemann, USA.

ERCB, 2009. Directive 074: Tailings Performance Criteria and Requirements for Oil Sands Mining Schemes. <http://www.aer.ca/rules-and-regulations/directives/directive-074> (accessed 2013).

Farkish, A., Fall, M., 2013. Rapid dewatering of oil sand mature fine tailings using super absorbent polymer (SAP). *Miner. Eng.* 50–51, 38–47.

Fenzel, M.S., 2012. Belt filter press in coal tailings dewatering—a comprehensive economic, design, and process analysis. In: Bethell, P.J., Arnold, B.J., Klima, M.S. (Eds.), *Challenges in Fine Coal Processing, Dewatering, and Disposal*. Society for Mining, Metallurgy, and Exploration Inc., pp. 309–327.

- Franks, G.V., Li, H., O'Shea, J.-P., Qiao, G.G., 2009. Temperature responsive polymers as multiple function reagents in mineral processing. *Adv. Powder Technol.* 20, 273–279.
- Franks, G.V., Yates, P.D., Lambert, N.W., Jameson, G.J., 2005. Aggregate size and density after shearing, implications for dewatering fine tailings with hydrocyclones. *Int. J. Miner. Process.* 77, 46–52.
- Gao, W., Smith, D., Segó, D., 2004. Treatment of pulp mill and oil sands industrial wastewaters by the partial spray freezing process. *Water Res.* 38, 579–584.
- Gaudreault, R., van de Ven, T.G., Whitehead, M., 2005. Mechanisms of flocculation with poly(ethylene oxide) and novel cofactors. *Colloids Surf. A: Physicochem. Eng. Aspects* 268, 131–146.
- Gentes, M.-L., Waldner, C., Papp, Z., Smits, J.E., 2006. Effects of oil sands tailings compounds and harsh weather on mortality rates, growth and detoxification efforts in nestling tree swallows (*Tachycineta bicolor*). *Environ. Pollut.* 142, 24–33.
- Giese, R.F., 2002. *Colloid and Surface Phenomena in Clays and Related Materials*. Marcel Dekkar Inc., New York, USA.
- Golder Associates, 2009. *Reclamation and Closure in Oil Sands Development Areas*. http://www.golder.ca/en/modules.php?name=Newsletters&op=viewarticle&sp_id=114&page_id=1100&article_id=124 (accessed 2013).
- Gordon, R.B., 2002. Production residues in copper technological cycles. *Resour. Conserv. Recycl.* 36, 87–106.
- Gräfe, M., Power, G., Klauber, C., 2011. Bauxite residue issues: III. Alkalinity and associated chemistry. *Hydrometallurgy* 108, 60–79.
- Gupta, V. et al., 2011. Particle interactions in kaolinite suspensions and corresponding aggregate structures. *J. Colloid Interf. Sci.* 359, 95–103.
- Gupta, V., Miller, J.D., 2010. Surface force measurements at the basal planes of ordered kaolinite particles. *J. Colloid Interf. Sci.* 344, 362–371.
- Hansen, H.K., Yianatos, J.B., Ottosen, L.M., 2005. Speciation and leachability of copper in mine tailings from porphyry copper mining: influence of particle size. *Chemosphere* 60, 1497–1503.
- Harbottle, D., Biggs, S., Fairweather, M., 2011a. Fine particle turbulence modulation. *AIChE J.* 57 (7), 1693–1699.

- Harbottle, D., Fairweather, M., Biggs, S., 2011b. The minimum transport velocity of colloidal silica suspensions. *Chem. Eng. Sci.* 66, 2309–2316.
- Harbour, P.J., Dixon, D.R., Scales, P.J., 2007. The role of natural organic matter in suspension stability: 1. Electrokinetic–rheology relationships. *Colloids Surf. A: Physicochem. Eng. Aspects* 295, 38–48.
- Hogg, R., 2000. Flocculation and dewatering. *Int. J. Miner. Process.* 58, 223–236.
- International Fertilizer Industry Association, 2010. <http://www.fertilizer.org>.
<http://www.fertilizer.org/ifa/HomePage/STATISTICS/Production-and-trade> (accessed 2013).
- ISO, 2002. ISO 14688-1:2002 Geotechnical Investigation and Testing – Identification and Classification of Soil – Part 1: Identification and Description.
http://www.iso.org/iso/catalogue_detail.htm?csnumber=25260 (accessed 2013).
- Israelachvili, J.N., 2011. *Intermolecular and Surface Forces*, third ed. Elsevier Inc..
- Iwata, M., 2003. Solid–liquid separation by use of particle immobilization in calcium alginate gel. *Sep. Sci. Technol.* 38, 837–850.
- Ji, Y., Lu, Q., Liu, Q., Zeng, H., 2013. Effect of solution salinity on settling of mineral tailings by polymer flocculants. *Colloids Surf. A: Physicochem. Eng. Aspects* 430, 29–38.
- Johnson, S.B. et al., 2000. Surface chemistry–rheology relationships in concentrated mineral suspensions. *Int. J. Miner. Process.* 58, 267–304.
- Jones, B.E.H., Haynes, R.J., 2011. Bauxite processing residue: a critical review of its formation, properties, storage, and revegetation. *Crit. Rev. Environ. Sci. Technol.* 41, 271–315.
- Jones, H., Boger, D.V., 2012. Sustainability and waste management in the resource industries. *Ind. Eng. Chem. Res.* 51, 10057–10065.
- Kalkan, E., 2006. Utilization of red mud as a stabilization material for the preparation of clay liners. *Eng. Geol.* 87, 220–229.
- Keles, S. et al., 2010. Development of the centribaric (TM) dewatering technology. In: *Proceedings from International Coal Preparation Congress*, pp. 488–495.
- Klein, C., Harbottle, D., Alagha, L., Xu, Z., 2013. Impact of fugitive bitumen on polymer-based flocculation of mature fine tailings. *Can. J. Chem. Eng.* 91, 1427–1432.

- Konan, K.L. et al., 2007. Surface properties of kaolin and illite suspensions in concentrated calcium hydroxide medium. *J. Colloid Interf. Sci.* 307, 101–108.
- Kulkarni, S.G., Ramarao, B.V., Hassett, J.M., Tien, C., 1993. Dynamic modeling of the sedimentation of concentrated bidispersed suspensions. *Sep. Technol.* 3, 12–24.
- Kumar, S., Kumar, R., Bandopadhyay, A., 2006. Innovative methodologies for the utilisation of wastes from metallurgical and allied industries. *Resour. Conserv. Recycl.* 48, 301–314.
- Lee, M.R., Correa, J.A., 2005. Effects of copper mine tailings disposal on littoral meiofaunal assemblages in the Atacama region of northern Chile. *Mar. Environ. Res.* 59, 1–18.
- Leong, Y.-K., Boger, D.V., 1990. Surface chemistry effects on concentrated suspension rheology. *J. Colloid Interf. Sci.* 136, 249–258.
- Leung, W.-F., 1998. *Industrial Centrifugation Technology*. McGraw-Hill, New York.
- Li, H., Long, J., Xu, Z., Masliyah, J.H., 2007. Flocculation of kaolinite clay suspensions using a temperature-sensitive polymer. *AIChE J.* 53, 479–488.
- Liu, W., Yang, J., Xiao, B., 2009. Review on treatment and utilization of bauxite residues in China. *Int. J. Miner. Process.* 93, 220–231.
- Liu, Y.-C. et al., 2013. Leaching kinetics of copper flotation tailings in aqueous ammonia/ammonium carbonate solution. *Can. J. Chem. Eng.* 91, 770–775.
- Lockhart, N.C., Veal, C., 1996. Coal dewatering: Australian R&D trends. *Coal Prep.* 17, 5–24.
- Loginov, M., Citeau, M., Lebovka, N., Vorobiev, E., 2013. Electro-dewatering of drilling sludge with liming and electrode heating. *Sep. Purif. Technol.* 104, 89–99.
- Mahmoud, A., Olivier, J., Vaxelaire, J., Hoadley, A.F., 2010. Electrical field: a historical review of its application and contributions in wastewater sludge dewatering. *Water Res.* 44, 2381–2407.
- Masala, S., Dhadli, N., 2012. Correlations of shear strengths of soft oil sands tailings assessed by different in situ methods. In: *Proceedings from 3rd International Oil Sand Tailings Conference*, Edmonton, Canada.
- Masliyah, J.H., Bhattacharjee, S., 2006. *Electrokinetic and Colloid Transport Phenomena*. Wiley-Interscience, Hoboken, NJ.

- Masliyah, J.H., Czarnecki, J., Xu, Z., 2011. Handbook on Theory and Practice of Bitumen Recovery from Athabasca Oil Sands: Theoretical Basis, vol. I. Kingsley Knowledge Publishing, Canada.
- Mikula, R., Munoz, V., Omotoso, O., 2008. Centrifuge options for production of dry stackable tailings in surface mined oil sands tailings management. In: Proceedings from Canadian International Petroleum Conference, Calgary, AB, Canada.
- Morey, B., 2013. Dewatering. In: Kirk–Othmer Encyclopedia of Chemical Technology. John Wiley and Sons Inc., pp. 310–339.
- Murphy, C., Bennett, C., Olinger, G., Cousins, B., 2012. Alternatives to coal mine tailings impoundment – evaluation of three dewatering methods at rockspring coal mine. In: Proceedings from Water in Mineral Processing, Seattle, WA, pp. 301–309.
- Nasr-El-Din, H.A., Masliyah, J.H., Nandakumar, K., 1990. Continuous gravity separation of concentrated bidisperse suspensions in an inclined plate settler. *Int. J. Multiph. Flow* 16, 909–919.
- National Research Council, 2002. Coal Waste Impoundments: Risks, Responses, and Alternatives. National Academy Press, Washington, DC.
- Nenu, R., Hayase, Y., Yoshida, H., Yamamoto, T., 2010. Influence of inlet flow rate, pH, and beads mill operating condition on separation performance of submicron particles by electrical hydrocyclone. *Adv. Powder Technol.* 21, 246–255.
- Nesbitt, C.C., 2007. Waste reduction in metals manufacturing. In: Environmentally Conscious Materials and Chemicals Processing. John Wiley & Sons Inc., pp. 33–58.
- Nguyen, Q., Boger, D., 1998. Application of rheology to solving tailings disposal problems. *Int. J. Miner. Process.* 54, 217–233.
- O’Shea, J.-P., Qiao, G.G., Franks, G.V., 2010. Solid–liquid separations with a temperature-responsive polymeric flocculant: effect of temperature and molecular weight on polymer adsorption and deposition. *J. Colloid Interf. Sci.* 348, 9–23.
- Ofori, P. et al., 2011. Shear-induced floc structure changes for enhanced dewatering of coal preparation plant tailings. *Chem. Eng. J.* 172, 914–923.
- Oliveira, M.S., Santana, R.C., Ataíde, C.H., Barrozo, M.A., 2011. Recovery of apatite from flotation tailings. *Sep. Purif. Technol.* 79, 79–84.
- Onuaguluchi, O., Eren, Ö., 2012. Recycling of copper tailings as an additive in cement mortars. *Constr. Build. Mater.* 37, 723–727.

- Ortega-Rivas, E., 2012. Hydrocyclones. In: Ullmann's Encyclopedia of Industrial Chemistry. Wiley-VCH Verlag GmbH & Co. KGaA, Weinheim, pp. 208–233.
- Penner, D., Lagaly, G., 2001. Influence of anions on the rheological properties of clay mineral dispersions. *Appl. Clay Sci.* 19, 131–142.
- Percy, K., Hansen, M., Dann, T., 2012. Air quality in the Athabasca oil sands region 2011. In: *Developments in Environmental Science*. Elsevier Ltd., pp. 47–91.
- Peuker, U.A., Stahl, W., 1999. Scale-up of steam pressure filtration. *Chem. Eng. Process.* 38, 611–619.
- Poulin, É., Blais, J.-F., Mercier, G., 2008. Transformation of red mud from aluminium industry into a coagulant for wastewater treatment. *Hydrometallurgy* 92, 16–25.
- Power, G., Gräfe, M., Klauber, C., 2011. Bauxite residue issues: I. Current management, disposal and storage practices. *Hydrometallurgy* 108, 33–45.
- Prat, G., 2012. Dewatering fine coal and tailings with a filter press. In: Bethell, P.J., Arnold, B.J., Klima, M.S. (Eds.), *Challenges in Fine Coal Processing, Dewatering, and Disposal*. Society for Mining, Metallurgy, and Exploration Inc., pp. 279–292.
- Proskin, S., Segó, D., Alostaz, M., 2010. Freeze–thaw and consolidation tests on Suncor mature fine tailings (MFT). *Cold Reg. Sci. Technol.* 63, 110–120.
- Raats, M., van Diemen, A., Laven, J., Stein, H., 2002. Full scale electrokinetic dewatering of waste sludge. *Colloids Surf. A: Physicochem. Eng. Aspects* 210, 231–241.
- Ramirez, M., Massolo, S., Frache, R., Correa, J.A., 2005. Metal speciation and environmental impact on sandy beaches due to El Salvador copper mine, Chile. *Mar. Pollut. Bull.* 50, 62–72.
- Rayhani, M., Yanful, E., Fakher, A., 2007. Desiccation-induced cracking and its effect on the hydraulic conductivity of clayey soils from Iran. *Can. Geotech. J.* 44, 276–283.
- Renault, S., Zwiazek, J., Fung, M., Tuttle, S., 2000. Germination, growth and gas exchange of selected boreal forest seedlings in soil containing oil sands tailings. *Environ. Pollut.* 107, 357–365.
- Ruyters, S. et al., 2011. The red mud accident in Ajka (Hungary): plant toxicity and trace metal bioavailability in red mud contaminated soil. *Environ. Sci. Technol.* 45, 1616–1622.

- Ryu, C., Finney, K., Sharifi, V.N., Swithenbank, J., 2008. Pelletised fuel production from coal tailings and spent mushroom compost – Part I: Identification of pelletisation parameters. *Fuel Process. Technol.* 89, 269–275.
- Sabah, E., Cengiz, I., 2004. An evaluation procedure for flocculation of coal preparation plant tailings. *Water Res.* 38, 1542–1549.
- Sabah, E., Yuzer, H., Celik, M., 2004. Characterization and dewatering of fine coal tailings by dual-flocculant systems. *Int. J. Miner. Process.* 74, 303–315.
- Samal, S., Ray, A.K., Bandopadhyay, A., 2013. Proposal for resources, utilization and processes of red mud in India – a review. *Int. J. Miner. Process.* 118, 43–55.
- Singer, M.J., Munns, D.N., 1996. *Soils: An Introduction*, third ed. Prentice-Hall Inc., New Jersey, USA.
- Smith-Palmer, T., Pelton, R., 2012. Flocculation of particles. In: Somasundaran, P., Hubbard, A. (Eds.), *Encyclopedia of Surface and Colloid Science*. Taylor & Francis, pp. 2584–2599.
- Smuda, J., Dold, B., Spangenberg, J.E., Pfeifer, H.-R., 2008. Geochemistry and stable isotope composition of fresh alkaline porphyry copper tailings: implications on sources and mobility of elements during transport and early stages of deposition. *Chem. Geol.* 256, 62–76.
- Stancyzyk, M., Field, I., Collins, E., 1971. *Dewatering Florida Phosphate Pebble Rock Slime by Freezing Techniques*. US Bureau of Mines, Washington, DC (Report of Investigations 7520).
- Stroh, G., Stahl, W., 1990. Effect of surfactants on the filtration properties of fine particles. *Filtr. Sep.* 27, 197–199.
- Sung, D.-J., Turian, R.M., 1994. Chemically enhanced filtration and dewatering of narrow-sized coal particles. *Sep. Technol.* 4, 130–143.
- Tadros, T., 2011. Interparticle interactions in concentrated suspensions and their bulk (rheological) properties. *Adv. Colloid Interf. Sci.* 168, 263–277.
- Tao, D., Parekh, B., Honaker, R., 2008. *Development and Pilot-Scale Demonstration of Deep-Cone (TM) Paste Thickening Process for Phosphatic Clay Disposal*. Florida Institute of Phosphate Research, Bartow, Florida.
- Theriault, Y. et al., 1995. The effect of chemical, physical and enzymatic treatments on the dewatering of tar sands tailings. *Fuel* 74, 1404–1412.

- Timoney, K.P., Lee, P., 2009. Does the Alberta tar sands industry pollute? The scientific evidence. *Open Conserv. Biol. J.* 3, 65–81.
- Tu, Y. et al., 2005. Recovery of bitumen from oilsands: gelation of ultra-fine clay in the primary separation vessel. *Fuel* 84, 653–660.
- Venkataraman, S., Weiland, R.H., 1985. Buoyant-particle-promoted settling of industrial suspensions. *Ind. Eng. Chem. Process Des. Dev.* 24, 966–970.
- Verma, S., Klima, M.S., 2010. Evaluation of a pilot-scale plate-and-frame filter press for dewatering fine anthracite refuse. In: *Proceedings from International Coal Preparation Congress*, pp. 516–524.
- Voordouw, G., 2013. Interaction of oil sands tailings particles with polymers and microbial cells: first steps toward reclamation to soil. *Biopolymers* 99, 257–262.
- Wakeman, R., 2007. The influence of particle properties on filtration. *Sep. Purif. Technol.* 58, 234–241.
- Wang, S., Ang, H., Tadé, M., 2008a. Novel applications of red mud as coagulant, adsorbent and catalyst for environmentally benign processes. *Chemosphere* 72, 1621–1635.
- Wang, X., Feng, X., Xu, Z., Masliyah, J.H., 2010. Polymer aids for settling and filtration of oil sands tailings. *Can. J. Chem. Eng.* 88, 403–410.
- Wang, X. et al., 2008b. Particle characteristics and rheological constitutive relations of high concentration red mud. *J. China Univ. Min. Technol.* 18, 0266–0270.
- Watson, A. et al., 2010. A comparison of alternative tailings disposal methods – the promises and realities. In: *Proceedings from Mine Waste, Perth, Australia*.
- Weber, K., Stahl, W., 2002. Improvement of filtration kinetics by pressure electrofiltration. *Sep. Purif. Technol.* 26, 69–80.
- Whitmore, W.L., 1955. The sedimentation of suspensions of spheres. *Br. J. Appl. Phys.* 6, 239–245.
- WISE Uranium Project, 2012. Chronology of Major Tailings Dam Failures. <http://www.wise-uranium.org/mdaf.html> (accessed 2013).
- Wong, R. et al., 2004. Calcined oil sands fine tailings as a supplementary cementing material for concrete. *Cem. Concr. Res.* 34, 1235–1242.
- Wu, Z.H. et al., 2010. Dewatering and drying in mineral processing industry: potential for innovation. *Dry. Technol.* 28, 834–842.

- Xu, Y., Dabros, T., Kan, J., 2008. Filterability of oil sands tailings. *Process Saf. Environ. Prot.* 86, 268–276.
- Xu, Z., Zhang, Q., Lin, H., Qiu, Y., 2012. Application of reverse flotation to recover phosphate minerals from plant tailings. In: El-Shall, H.E., Miller, J.D., Zhang, P. (Eds.), *Beneficiation of Phosphates: New Thought, New Technology, New Development*. Society for Mining, Metallurgy, and Exploration Inc., pp. 275–279.
- Yang, Q., Li, Z., Lv, W., Wang, H., 2013. On the laboratory and field studies of removing fine particles suspended in wastewater using mini-hydrocyclone. *Sep. Purif. Technol.* 110, 93–100.
- Yan, L., Englert, A.H., Masliyah, J.H., Xu, Z., 2011. Determination of anisotropic surface characteristics of different phyllosilicates by direct force measurements. *Langmuir* 27, 12996–13007.
- Yan, L., Masliyah, J.H., Xu, Z., 2013. Understanding suspension rheology of anisotropically-charged platy minerals from direct interaction force measurement using AFM. *Curr. Opin. Colloid Interf. Sci.* 18, 149–156.
- Yuan, X., Shaw, W., 2007. Novel processes for treatment of syncrude fine transition and marine ore tailings. *Can. Metall. Quat.* 46, 265–272.
- Yukawa, H. et al., 1976. Analysis of batch electrokinetic filtration. *J. Chem. Eng. Jpn.* 9, 396–401.
- Zhang, P., Stana, R., 2012. Phosphogypsum management and utilization: a review of research and industry practice. In: El-Shall, H.E., Miller, J.D., Zhang, P. (Eds.), *Beneficiation of Phosphates: New Thought, New Technology, New Development*. Society for Mining, Metallurgy, and Exploration Inc., pp. 309–322.
- Zhao, L., Jiang, M., Wang, Y., 2008. Experimental study of a hydrocyclone under cyclic flow conditions for fine particle separation. *Sep. Purif. Technol.* 59, 183–189.
- Zhu, R. et al., 2011. Role of dissolving carbon dioxide in densification of oil sands tailings. *Energy Fuels* 25, 2049–2057.

Chapter 2: Volute Screw Press

2.1. Overview



Figure 2.1. Front view of the volute screw press.

A prototype volute screw press (model ANK-101) was purchased from Amcon China, a Sino-Japanese company specializes in sludge dewatering (Amcon China, 2016). As visualized in **Fig. 2.1**, a typical VSP comprises of three major components: a) process tanks, mixers, and flocculant transport (feed) system; b) dewatering press; and c) control modules. In operation, the feed slurry enters the 34.5-L feed holding tank (FHT) from the bottom, and overflows into the adjacent 38.4-L conditioning tank (CT) via a V-weir. The first flocculant (typically anionic polyacrylamide, A-PAM) solution is introduced in the

CT to induce initial flocculation by a twin-blade constant speed mixer. Next, the conditioned slurry underflows towards the 86.6-L flocculation tank (FT), where the second flocculant (typically cationic polyacrylamide, C-PAM) solution was added to further flocculate remaining dispersed particles and primary flocs aided by a tri-blade adjustable speed mixer. Finally, the flocculated slurry overflows through a rectangular weir into the dewatering press (DP) under natural gravity action. Separation of supernatant and compression of sediment solids occur at the internal spacing between the central auger screw and an assembly of circular stainless steel rings (volute plates). Additional axial compression is provided by the circular outlet compression plate (end plate) located at a maximum 2-mm gap from the discharge outlet of the VSP.

2.2. Feed system

Figure 2.2 is a schematic overview of the VSP feed system that involves three tanks, each with distinctive roles. The first FHT allows gravitational separation between light and heavy phases. In the context of oil sands tailings treatment, this is useful to preventatively settle out fugitive coarse sand, large bitumen aggregates, or other massive particles that may cause abrasion and other operational problems to the downstream DP. The second is a similar-sized CT equipped with a 180-RPM mechanical mixer, which is intended to quickly induce initial flocculation by A-PAM flocculant for the subsequent operations. The third and largest FT uses a mechanical mixer of wide, slow-moving (up to 60 RPM) blades to induce the second stage flocculation by the C-PAM and clarify the supernatant, producing desired feed stream characteristics for the downstream DP unit. A

level controller located in the FT ensures fully automatic stable operations which will be discussed further.

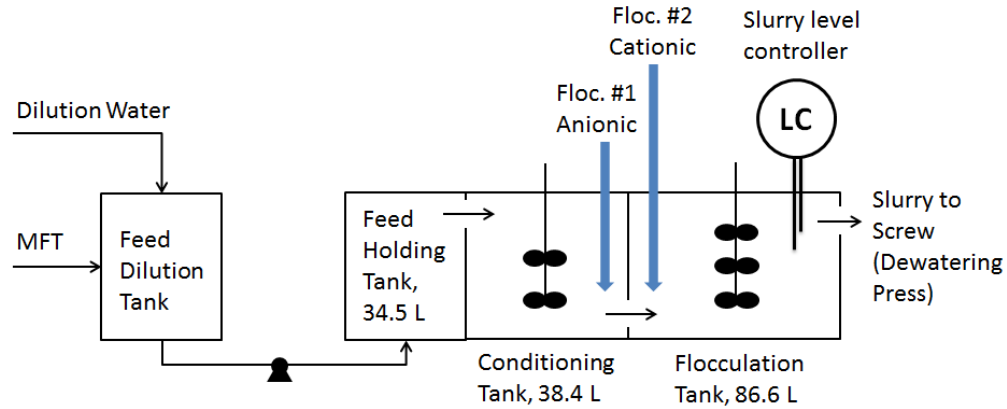


Figure 2.2. Overview of the volute screw press feed system.

2.3. Dewatering press

Figure 2.3 shows a generalized diagram of the VSP dewatering press (DP). For our prototype VSP, its DP consists of 360 volute plates and an internal auger screw located through the center of all volute plates shown in **Fig. 2.4**, which is driven by a 0.1 kW variable speed motor operating typically at 1.6 RPM. The DP is installed at an 11.3° inclination from feed to outlet to further facilitate supernatant drainage through the openings between adjacent volute plates (drainage slits). As the solids are moved up-forward towards the discharge end by the auger screw, the gradually decreasing pitch on the screw provides the primary means of compression and dewatering.

With the exception of the 20 volute plates near the DP discharge outlet, each volute plate plus four washers of a chosen thickness are sandwiched between two (slightly larger) immobile plates. Such a setup ensures the volute plate at the center of the 3-plate layer always has a contact point with the auger screw, which allows movement of the center

plate as the screw rotates. Such arrangement ensures that an arc on any given mobile (center) plate constantly extends away from the center of the screw shaft, while the remainder of the mobile plate pulls towards the center of the shaft. As shown in **Fig. 2.5**, when the auger screw rotates, the screw-plate contact point moves in a circular pattern, which continuously remove any fugitive material (runoff) trapped within the drainage slits.

Adjustment of inter-plate washer thickness allows operators to control the inter-plate axial separation distance in the DP. Larger inter-plate distances would improve supernatant flow at a cost of increased fugitive solids flow through the larger spacing (thus decreased supernatant quality), and vice versa.

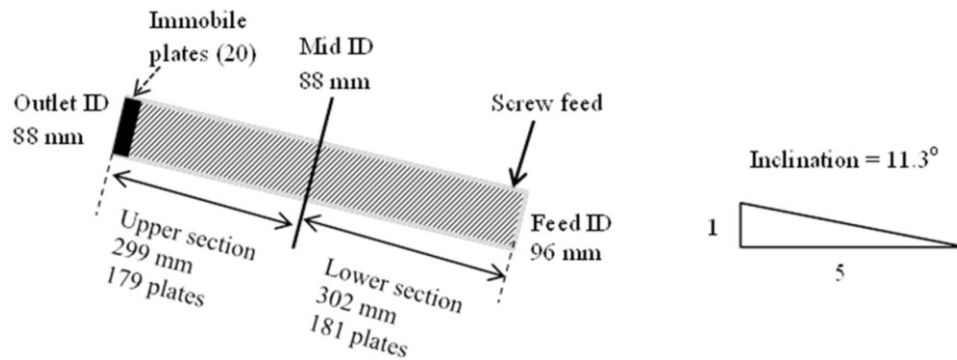


Figure 2.3. Generalized diagram of the dewatering press.

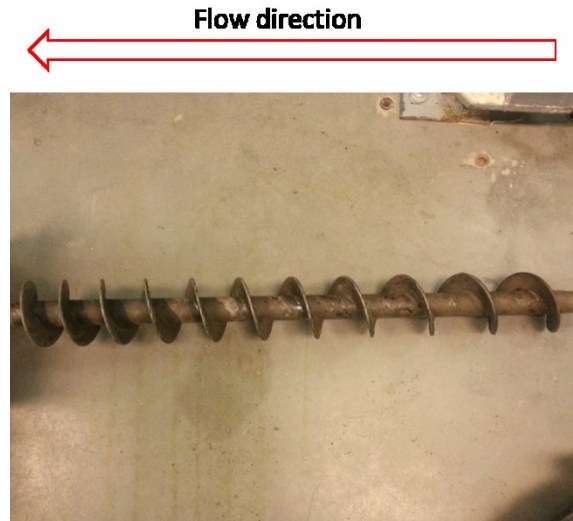


Figure 2.4. Internal auger screw at the center of dewatering press.

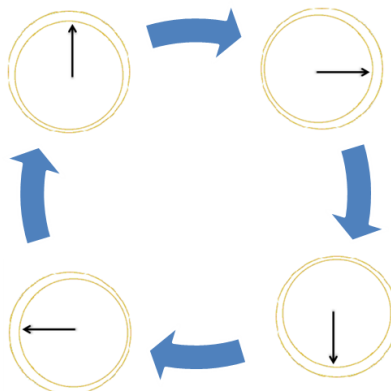


Figure 2.5. Volute plate self-cleaning cycle. Colored annuli denote the overlapping region between each mobile and immobile volute plate in the DP. Arrows inside annuli denote the screw-plate contact point.

2.4. Automatic operations

The FT slurry level controller as shown in **Fig. 2.2** can be used to achieve fully automatic VSP operations with little operator oversight. In essence, the controller detects two signals: 1) high slurry level, and 2) low slurry level. When the high level signal is

triggered, the controller shuts off slurry feed as well as both anionic and cationic flocculant feeds. Mixers in the CT and FT, and the DP auger screw remain in operation to reduce the slurry level inside FT. All elements of the VSP are turned on as soon as the controller detects low slurry level.

It is clear that in contrast to the conventional filtration processes, the VSP requires no dedicated filter medium other than the volute plates. In operation, radial movement among alternating volute plates (driven by the central auger screw) continuously cleans the inter-plate spacing along the entire assembly. This feature effectively eliminates both bitumen fouling and fines blockage on the filter medium that are commonly encountered by existing tailings filtration efforts. Successful applications of the VSP include municipal waste treatment, livestock and general biological waste sludge dewatering, food and industrial painting waste disposal, and so on.

References

Amcon China, 2016. Overseas Subsidiaries - amcon inc.. [Online], Available at: <http://en.amcon.co.jp/company/group/> [Accessed January 2016].

Chapter 3: Mechanical Dewatering of Flocculant-assisted Tailings Sediments

Chapter 3 establishes a semi-empirical theoretical framework to fundamentally describe the mechanical dewatering characteristics of flocculated MFT sediments. A bench-scale test system was developed to provide experimental data for theory verification.

3.1. Theoretical considerations on VSP dewatering

3.1.1. Dewatering mechanisms of the VSP

In the VSP dewatering press (DP) unit, the main mechanism for dewatering is provided by the decreasing pitch of the central auger screw, which is further complemented by the numerous drainage slits among the volute plates assembly. **Table 3.1** provides an overview of both features.

Table 3.1. Main mechanisms of water removal from the dewatering press.

Central auger screw – pitch per stage (mm)									
Stage 10 (outlet)	Stage 9	Stage 8	Stage 7	Stage 6	Stage 5	Stage 4	Stage 3	Stage 2	Stage 1 (feed)
35	40	45	50	55	60	65	70	75	80
Volute plate assembly – drainage slits per stage (average 175 µm/slit)									
Stage 10 (outlet)	Stage 9	Stage 8	Stage 7	Stage 6	Stage 5	Stage 4	Stage 3	Stage 2	Stage 1 (feed)
3	26	30	34	36	40	44	46	50	0

Based on relevant measurements from the VSP, the volumetric compression by the central auger screw has been determined as shown in **Fig. 3.1**. Given a perfectly “compressible” slurry feed, one would expect about 50% volumetric expulsion of water solely from screw compression. Additional water removal (from gravity sedimentation, for example) is facilitated by the drainage slits as well.

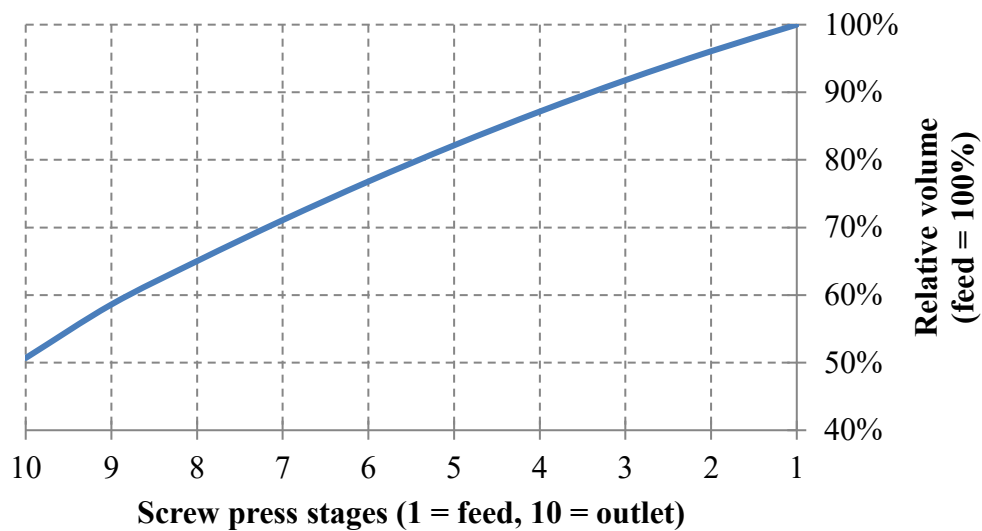


Figure 3.1. Volumetric compression by the central auger screw.

3.1.2. Hypothesized outcomes of VSP dewatering

Two types of dewatering outcomes were hypothesized in terms of the dry solids content of the solid cake product. **Figure 3.2** shows the process flow of the DP unit at good (desirable) VSP operating condition. On the other hand, **Fig. 3.3** is indicative of an extremely poor (undesirable) operating condition.

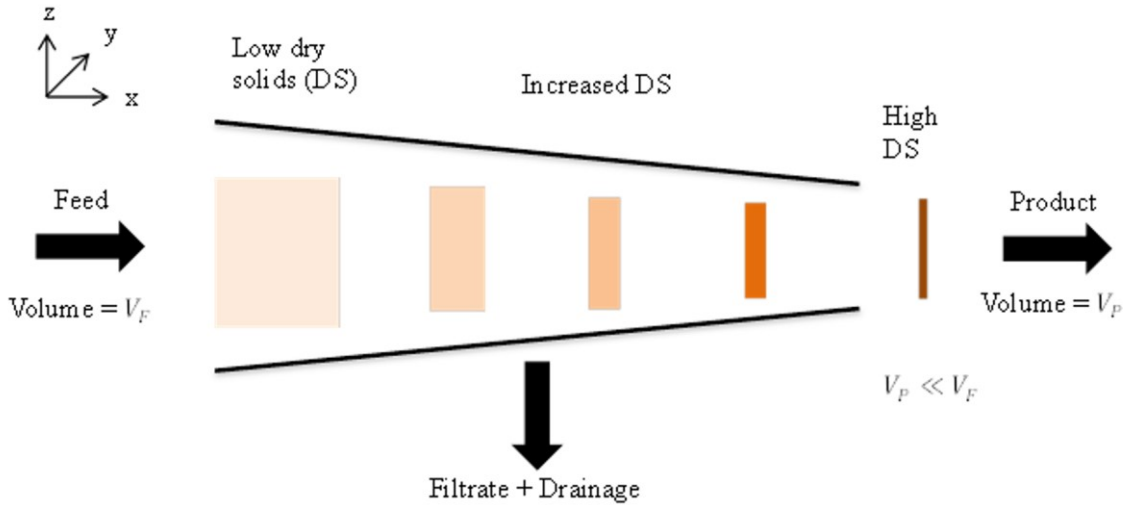


Figure 3.2. Desirable VSP operating conditions for sediment dewatering. Dry solids is abbreviated as DS. Here, $V_P \ll V_F$ conceptually indicates maximum possible filtrate and drainage release.

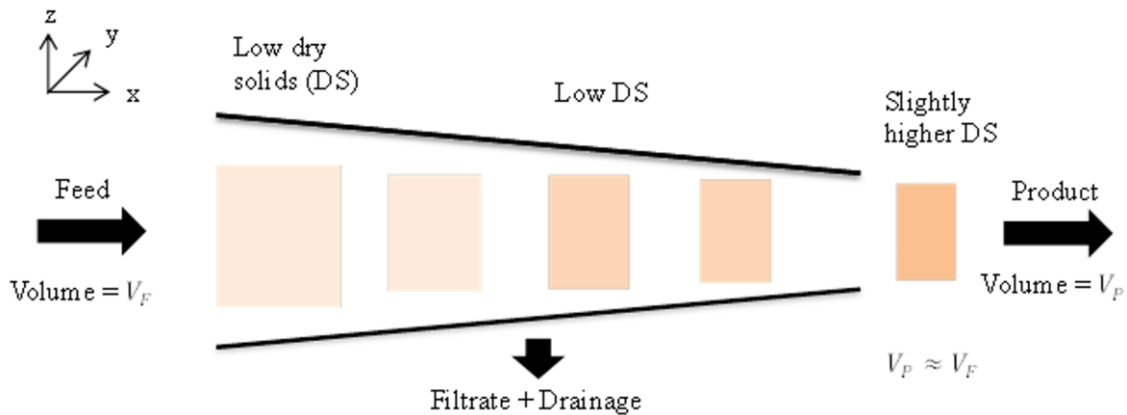


Figure 3.3. Extremely undesirable VSP operating conditions for sediment dewatering. Dry solids is abbreviated as DS. Here, $V_P \approx V_F$ conceptually indicates minimal filtrate and drainage release.

Figure 3.2 represents a case of significant water expulsion from the flocculated MFT sediment. As discussed in **Chapter 2**, the self-cleaning design of the volute plates essentially removes any build-up material (solids, bitumen, etc.) between the drainage

slits in normal operations. Such a feature allows unhindered filtrate separation from the MFT sediments, which is a critically necessary condition for the continuous production of dryer MFT cakes towards the discharge end. However, if the MFT sediment responds little in volumetric reduction upon mechanical compression, as shown in **Fig. 3.3**, the dewatering capabilities of the VSP would be severely limited – even with the self-cleaning volute plates.

In other words, two necessary conditions given below are required to achieve a desirable operating system shown in **Fig. 3.2**.

- a. Flocculated MFT sediment must respond to mechanical compression via expulsion of water and corresponding volumetric reduction (strength of flocs, open structure of flocs, size distribution of sediment internal water channels and minimal suspended interstitial fines). This parameter is highly dependent on the feed material, types of flocculant, process conditions (pH, ions, etc.), as well as mixing characteristics, as discussed in **Chapter 1**.
- b. There must be sufficiently clean and large openings on the filter medium for the expressed water to be rapidly removed (non-fouling filter medium).

As condition *b* is intrinsic of the VSP design (i.e. self-cleaning volute plates), therefore it is apparent that successful volumetric reduction of flocculated MFT sediments is the sole factor to obtain dry stackable solid cake product in the VSP. Such a goal has been highly sought after by the oil sands industry. The next section introduces some theoretical considerations of MFT sediments undergoing mechanical compression.

3.2. Hypothesis on elasticity and plasticity of dewatering

3.2.1. Driving forces in VSP dewatering

Energy must be supplied to the flocculated sediment for water removal. The required energy rapidly increases when most water is contained inside capillary pores (e.g. raw MFT). Therefore, one may establish that, with a fixed amount of energy for dewatering, the final product solids content will depend on two factors. Namely, these are the initial pore structure of flocculated tailings sediment, and any changes brought to the pore structure from the given dewatering process. However, neither of these characteristics is trivial to accurately quantify at present time. Relevant fundamental studies in this area are looking into the characteristics of water channels inside polymer-amended FFT/MFT, for example with Synchrotron-based computerized tomography (CT) scan (Boxill, 2015), as well as high resolution X-ray micro tomography (Chen, et al., 2015). As work progresses in the field of fundamental sediment modeling, there exists a need for new and improved engineering techniques which can identify flocculant-assisted FFT/MFT sediments in terms of their dewaterability with great certainty. For each dewatering application, in order to correctly predict outcomes of dewatering, care must be taken to consider the underlying physical phenomena involved in dewatering.

If one focuses on the special case of the VSP, in which mechanical energy is supplied to flocculated sediment via compression, there are three plausible consequences. In order to dissipate the excess energy and achieve a state of equilibrium, the sediment can convert the energy to bulk movement (flow), rejection of interstitial water (volumetric reduction), and to some extent, increasing internal energy (heating). As the DP of VSP is essentially an open system for compression, sediment temperature is not expected to significantly

increase. Therefore the scenarios of flow and volumetric reduction are considered the dominant energy dissipation mechanisms for the MFT sediment in this work.

3.2.2. Elasticity and plasticity of dewatering

Sediment experiences compressional stress when subjected to mechanical compression as in the DP unit of the VSP. Responses to such stress dictate the extent of compressional dewatering. When subjected to the same amount of compressional stress over the same period of time in the same test system, Sediment A will contain less water than Sediment B if Sediment A experiences more degree of volumetric reduction *and* less likely to flow out of the test system than Sediment B. This type of stress response bears many similarities to those encountered in textbook examples of material science. A material is said to be more *elastic* if this material is resistant to shape change upon the introduction of compressional or tensile stress. When the perfect elastic deformation takes place, the amount deformed (volumetric reduction/elongation, or strain) is linearly proportional to the external stress. On the other hand, a perfectly *plastic* material will immediately yield upon external stress and produces no resultant strain.

Based on the above considerations, it is appropriate to extend the concept of elasticity and plasticity for metallic solids to compressive dewatering of flocculant-assisted tailings sediments in an effort to predictively describe the dewatering outcomes of the volute screw press. Sediment that is elastic upon compressive dewatering will reduce its volume by releasing water in order to dissipate the excess stress whilst being contained. In contrast, sediment that is plastic for dewatering cannot reduce its volume and must be displaced out of containment to achieve a state of equilibrium.

It is also anticipated that such classification and characterization of flocculated sediments can provide a useful theoretical framework for future fine tailings dewatering studies.

Desirable polymer flocculant characteristics (in terms of molecular weight [MW], charge type and density, degree of branches, etc.) can be designed to maximize sediment dewatering elasticity and achieve superior compressional dewatering, for example.

It is therefore highly desirable to design the controlled vertical strain test (CVST) and to verify the above hypothesis of linking the mechanical properties with the water removal efficiency from the flocculated sediments, which is the main subject of the next section.

3.3. The controlled vertical strain test (CVST)

3.3.1. CVST setup

Due to the material- and labor-intensive nature of running the pilot-scale VSP, it was of great interest to scientifically forecast the VSP dewatering outcome for any given combination of A-PAM, C-PAM, and MFT prior to using the actual VSP device. This became the main motivation on the development and utilization of the controlled vertical strain test (CVST) method, by which the flocculants can be quickly screened followed by selective testing of the more promising combinations on the VSP.

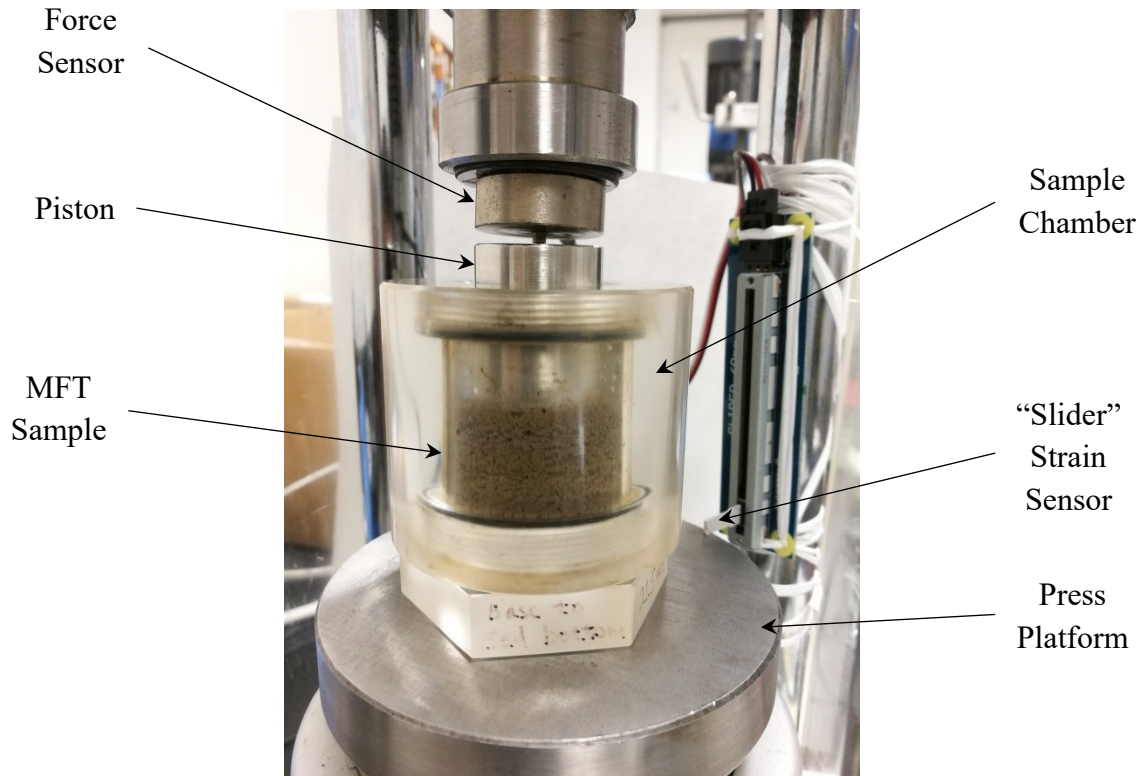


Figure 3.4. Laboratory setup for the controlled vertical strain test.

Figure 3.4 shows the laboratory setup for the investigation of compressional stress-strain relations of MFT sediments. The setup consists of a 200-kg force sensor and a vertical displacement sensor mounted within a 40-MPa laboratory pellet press. The flocculated MFT sediment is contained in a special plexiglass chamber (inner diameter [ID] 25.44 mm) and below a stainless steel piston (diameter 25.34 mm), in which the open apertures will be elaborated in **section 3.3.3**. During the CVST experiments, the press platform rises (in a controlled manner) relative to the stationary force sensor, which causes the piston to compress vertically against the softer MFT sediment inside the sample chamber (hence the name of the test). Signals from the force sensor are processed and amplified via an external Wheatstone bridge, whose output (F) is monitored and recorded by a custom LabVIEW program. Compressional stress (σ) applied to the sediment sample is

easily calculated by **Eq. 3.1**, using the constant cross-sectional area of compression (A) of the piston.

$$\sigma = \frac{F}{A} \quad (3.1)$$

A separate slider-type sensor was used to estimate the volumetric compression (strain, ε) experienced by the sediment sample upon the introduction of the compressive stress σ . This sensor is essentially a resistor whose resistance varies with the absolute position of the slider (zero to 60 mm). Sensitivity of the slider is one-thousandth (1/1000) along the entire 60-mm displacement, or 60 μm . For the setup in **Fig. 3.4**, the sensor is mounted vertically such that its slider is always in contact with the pellet press platform. Sensor value at initial position is 999 – although in practice it is best to “prime” or “initialize” the sensor to a value of ~ 990 , in order to avoid deadband at bottom-most slider position (i.e. the slider is able to move but sensor value remain at 999).

To determine the strain ε after the sample experiences a compressive stress σ , the constant area of compression (A) is also used. This result in the strain ε depends only on the vertical height of the sample before compression, and the vertical displacement occurred during compression. For each experiment, four values from vertical displacement sensor have to be recorded to determine ε .

1. The baseline signal ($SV1$) is recorded after priming or initializing the sensor.
2. Second value ($SV2$) is the height at sediment-air interface in the sample chamber.

3. Baseline reset ($SV3$) is generated by resetting the slider back in contact with the platform after determination of $SV2$. Note that $SV3$ is not necessary the same as $SV1$ due to sensitivity, but their values should differ by a maximum of 1 (one).
4. Final sediment height ($SV4$) is obtained after the CVST is complete.

Based on appropriate measurements of the sample chamber, it is possible to obtain ε as follows. **Equation 3.2** calculates the initial height of the sample (H_i) while **Eq. 3.3** determines the maximum ε produced (ε_{max}). Due to the nature of the current CVST setup, ε progresses in uniform, discrete steps in time throughout the test (see **section 3.3.3**).

$$H_i(mm) = \left(\frac{SV1 - SV2}{1000} * 60 \right) - 21.5 \quad (3.2)$$

$$\varepsilon_{max}(mm) = \frac{SV3 - SV4}{1000} * 60 \quad (3.3)$$

3.3.2. Sensor calibrations

It was not necessary to calibrate the vertical displacement slider sensor as it becomes ready to use after driver software installation. On the other hand, user calibration of the 200-kg force sensor was required prior to its application in CVST. A simple setup was devised for this task, as shown in **Fig. 3.5**.



Figure 3.5. Force sensor calibration setup. Left: methods of force generation and measurement. Right: close-up view of the sensor and the protective aluminum block during calibration.

Difficulties arise when one attempts to accurately generate up to 200 kg (1962 N) of compressive force across a 2.54-mm diameter sensor tip. Fortunately this goal can be realized with a sufficiently large and sturdy screw-based item with space for incorporating the force sensor. Thus a C-clamp (**Fig. 3.5**, left) from our lab was selected. Measurement of such large forces was made possible with a common weight scale. An aluminum block was placed in between the sensor tip and the scale to ensure the sensor tip (which is under enormous pressure) does not penetrate fully into the plastic weight scale surface. The sensor output becomes invalid once full tip penetration occurs, because

a portion of the compressive force would be distributed to the sensor chassis and away from the sensor tip.

Prior to calibration, several laboratory co-workers were asked to step on the bathroom scale and assess its accuracy. Their feedback suggests good agreement within ± 1 kg of their actual body masses. Thus the proposed calibration method was deemed sufficiently appropriate.

During calibration, the sensor was securely taped to the flat edge at the end of the screw on the C-clamp. The aluminum block was placed on top of the bathroom scale on a flat surface, whose reading was tared. Next, the C-clamp containing the force sensor was placed across the block-scale-surface assembly, with the tip of the force sensor pointed towards the block. Afterwards the C-clamp screw was fastened and the sensor tip was in contact against the block, generating a force reading on the scale (**Fig 3.5**, right). At each chosen force, sensor output data was collected each second for 10 seconds, whose averaged value was used for subsequent analysis. To eliminate any contributions from the self-weight of C-clamp while the flat edge of the screw was still relatively loose (which distorted force readings for 10 kg and 20 kg measurements), the C-clamp was manually held in an upright position for these cases. Once the flat edge of the screw was securely fastened (force ≥ 30 kg), the C-clamp became upright and contributed to the compressive force exerted on the sensor tip.

Figure 3.6 shows the sensor output value (SV) against applied compressive force (F) up to 1275.3 N (130 kg, upper limit of the bathroom scale). Perfect linearity between these two variables is evident. Therefore, even though the calibration data did not reach the

upper limit of the sensor (1962 N), one can extrapolate the linear relation within the sensor measurement limit with full confidence. Using this correlation, the custom-built LabVIEW force measurement program directly outputs F in Newtons by **Eq. 3.4**.

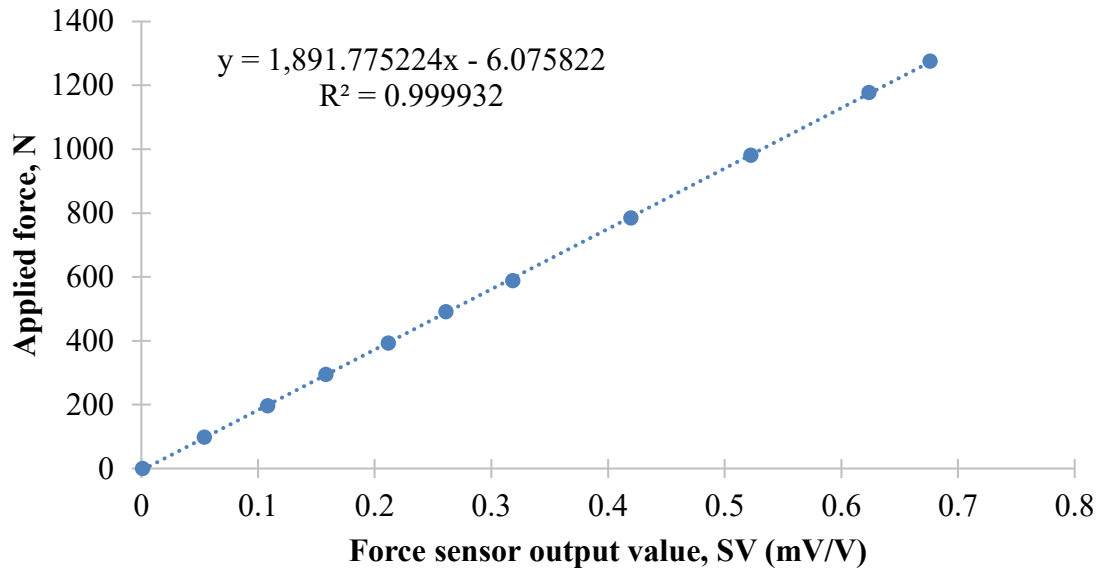


Figure 3.6. Force sensor calibration data.

$$F(N) = 1891.775 * SV - 6.076, \quad 0 \leq F \leq 2400 \quad (3.4)$$

Note the LabVIEW program extends the correlation further from 1962 N by ~20% (relative to the maximum force) for two reasons. First, the program incorporates a basic functionality common in all computer programs – error traps. Here, this feature essentially acts as a filter to discard any data outside a specified range. It was discovered that the force sensor generates an enormous first reading ($\sim 10^{300}$) when called by the program – likely from its power-up and initialization. Thus it was necessary to exclude

this data so that one may observe the correct waveform plot in real time during the CVST (see **section 3.3.3**); otherwise the first data point unnecessarily expands the vertical axis and makes everything else appear as a flat line.

Second, to properly use the error trap, it was necessary to buffer the maximum limit slightly higher than the intended maximum value to maximize collection of valid data. A buffer zone of 20% was chosen according to the safe overload limit (20%) provided by the sensor manufacturer.

3.3.3. CVST generalized procedure

The following pre-requisites are required for those who would like to run the CVST.

1. A compression mechanism that can generate at least 10 MPa of stress.
2. For the mechanism described in #1, it must be able to produce user-controlled vertical strain to the sediment sample, with movement precision in the order of 100 μm .
3. A MFT sediment containment apparatus with the following characteristics.
 - a. It should be able to safely withstand at least 10 MPa of compressive stress.
 - b. Hollow space within the device to deposit sediment sample.
 - i. The hollow space should be designed such that only one end of the space is open to atmosphere. The other end should be impermeable to water at a pressure of 10 MPa.
 - c. A piston made with stainless steel, or other types of materials that deforms less than 1 mm vertically under 10 MPa of compressive stress.

- i. The piston must be of the same geometric shape (in 3 dimensions) as the hollow space stated in condition 3(b).
 - ii. The piston cross-section must be marginally smaller than the cross-section of the hollow space stated in condition 3(b). This is used to simulate the functionalities of the VSP drainage slits.
 - iii. Difference in cross-section dimensions of the piston and hollow space, as stated in condition 3(c)(ii), should be in the range of 100-200 μm .
4. A device with at least one USB 2.0 (or higher) port. Each of the two sensors used in the CVST needs a separate port. Use a USB hub if there is only one available port on the device.
5. Familiarity with both force and slider sensors and their related accessories (hardware, software, wire connections, precision, measurement range, overload limits, troubleshooting, etc.). Refer to Phidgets website for details (www.phidgets.com).
6. Use of a real-time monitoring and data collection program for the force sensor. Currently only the LabVIEW version exists, so users must create their own program if they wish to use other programming languages.
7. For the latter situation described in #6, users should have basic computer programming skills with commonly-used languages such as C-suite (C++, C#...), Visual Basic, Python, LabVIEW, etc. Users are also required to interface the force sensor to their measurement program. See support database on Phidgets website for assistance.

The above conditions #1 to #6 are the minimum required items for all CVST users.

Fulfillment of condition #7 is highly recommended as it can be crucially valuable in the debugging and error diagnostics for the measurement program.

The author of this work determined that all seven of the aforementioned conditions were met during the early development of the CVST method. Conditions #1 and #2 were realized by the existing 40-MPa pellet press, whose platform (see **Fig. 3.4**) can be raised manually with a hydraulic oil lever. Based on historical data, a full swing of the lever (upright-to-horizontal) produces $110 \pm 10 \mu\text{m}$ of vertical strain, which is suitable for condition #2. For practical purposes, it was decided to execute a full lever swing for 1 s (which produces strain), and return the lever to its starting upright position during the next 1 s (which produces no strain). This method produces a uniform step-up in sample strain every 2 s. In order to obtain a smooth stress-strain curve for analytical purposes, the step-up strain profile and the corresponding stress response profile were subjected to two-period time averaging. Such data treatment essentially transformed the actual step-up strain profile to a constant rate of strain application of $55 \pm 5 \mu\text{m}$ per second. For future improvement of the CVST setup, the author suggests the use of a programmable precision linear actuator ($\geq 10 \text{ MPa}$ rated) to maximize user controls and accuracy over the vertical strain production.

To fulfill condition #3, a custom-designed multi-purpose plexiglass cylinder setup was fabricated with the generous assistance from the CME Machine Shop on campus. **Fig. 3.7** shows the front view of the plexiglass cylinder.

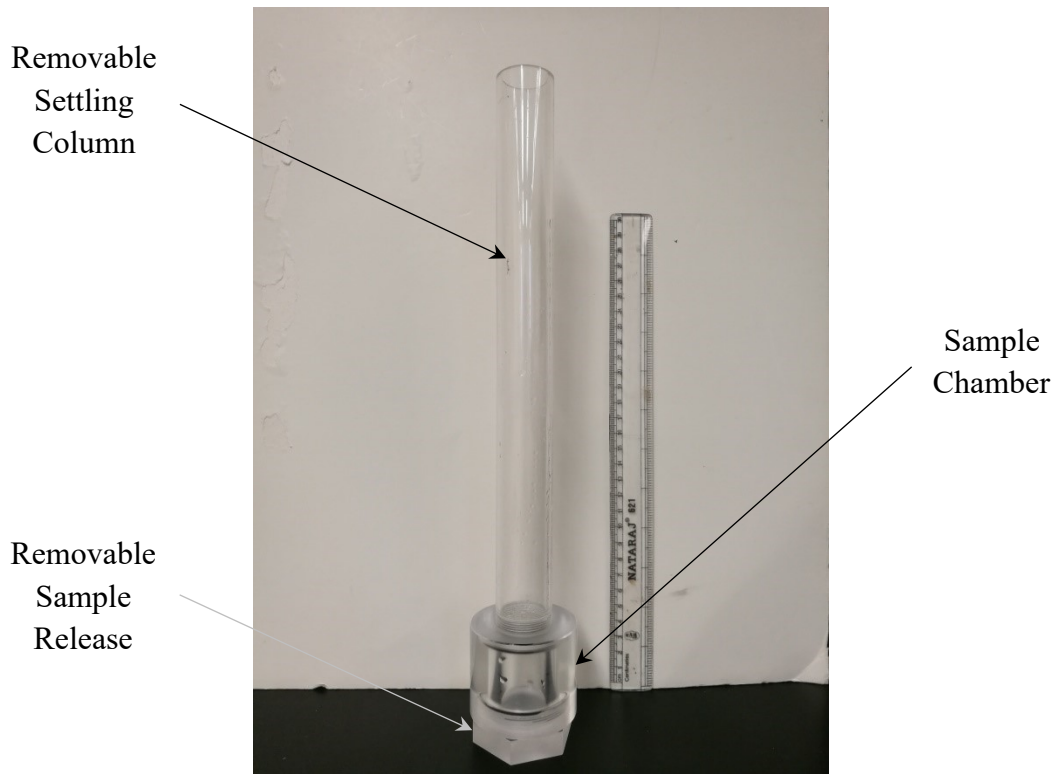


Figure 3.7. Set up of multi-purpose plexiglass cylinder for the CVST.

Since the stainless-steel piston (cylindrical, diameter 25.34 mm) was already available in the laboratory, the sediment containment apparatus was designed to accommodate a 25.44 mm-diameter cylindrical hollow space. A water-proof removable sample release at the bottom of the sample chamber was chosen to facilitate cleanup, as well as to easily take out the contained sediment for further analysis. Experiences from early development work indicated the necessity of forming the entire flocculated MFT sediment inside the sample chamber (in-situ settling). This minimizes the inevitable errors arising from transferring and sub-sampling ex-situ sediments into the sample chamber. Therefore, it was decided to install a removable and water-proof settling column (ID 25.44 mm) above the sediment chamber to achieve in-situ settling of sediments. Vertical heights along the

column were subsequently marked with a straightedge ruler for the determination of solids initial settling rate (ISR).

In addition, as the author was already skilled in basic programming, conditions #4 to #7 were fulfilled as the CVST development progressed.

3.3.3.1. Preparing for the CVST

First, connect both force sensor and vertical strain (slider) sensor to a USB-enabled device. Check connections of both sensors by opening the Phidgets Control Panel. There should be two items on the list.

- “PhidgetBridge 4-input”, for the force sensor, and
- “Phidget InterfaceKit 2/2/2”, for the slider sensor.

If any one of the two items is missing, the user should stop and diagnose hardware connections and software installation.

Next, double-click on “Phidget InterfaceKit 2/2/2” to start monitoring of the slider sensor. Ensure the “Ratiometric” box is ticked and adjust “Change Trigger (Deadband)” to 1. Initialize the slider sensor by slowly moving its slider to the bottom-most position. One of the boxes under “Analog In” should read 999. This will be the sensor output value of the vertical strain sensor. Close the oil release valve on the pellet press and swing the lever until sensor output value changes to ~990. Carefully and slightly lift the slider, and slowly press the slider down till bottom of the slider is in contact with the press platform. Record the current sensor output value as SVI .

To ensure the plexiglass cylinder setup is fully water-proof, slightly wet all threads and rubber rings with tap water, then carefully fasten top settling column and bottom sample release. Visually check the rubber ring at bottom to ensure uniform rubber coverage. Very importantly, verify that any part of the rubber ring has not been twisted during fastening. Also, no portion of the rubber ring shall extend into the central hollow space. If any one of these three conditions is not met, the sediment sample may leak out under stress, which will invalidate the corresponding CVST measurement.

3.3.3.2. CVST experimental

Mature fine tailings (MFT) and pond water were supplied by Horizon Oil Sands (Canadian Natural Resources Limited) at ~30 wt% and ~0.5 wt% dry solids respectively. Particle size distribution and cumulative size distribution of the Horizon MFT were analyzed by Mastersizer 3000 (Malvern Instruments, UK), as shown in **Fig. 3.8**. The MFT has a D_{50} of 5 μm and a D_{90} of 17 μm , which indicates a near-absence of $> 44 \mu\text{m}$ sand particles as well as significant $< 2 \mu\text{m}$ clay fraction. In fact, the clay-to-water ratio was calculated to be about 0.23 (Ng & Xu, 2017). These factors suggest that Horizon MFT would be nearly impossible and impractical to dewater by gravitational sedimentation alone.

Ion chromatography was used to obtain concentrations of dominant ionic species in the Horizon pond water, as listed in **Table 3.2**. Elevated concentrations of sodium and chloride ions suggest saline ore body at Horizon. On the other hand, the relatively low calcium ion concentration could necessitate higher amounts of coagulants or flocculants for effective solid-water separation.

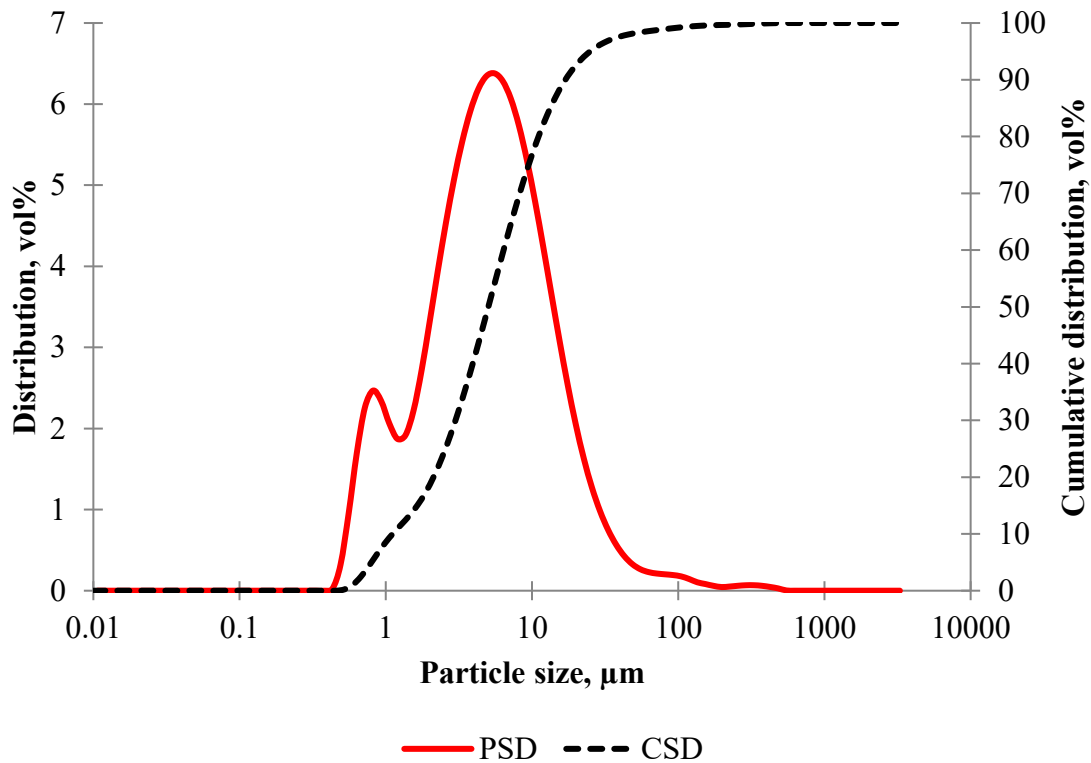


Figure 3.8. Particle size distribution (PSD, left) and cumulative size distribution (CSD, right) for Horizon MFT.

Table 3.2. Major ionic species in Horizon pond water.

Ion	Na ⁺	K ⁺	Mg ²⁺	Ca ²⁺	Cl ⁻	SO ₄ ²⁻
Concentration, ppm	667	16	9	14	498	221

A promising combination of one anionic polyacrylamide (A-PAM) and one cationic polyacrylamide (C-PAM) was obtained from BASF Canada. The A-PAM named Magnafloc 336 is of medium anionic charge density and an average molecular weight

(MW) of 11.5 million Da (Ng & Xu, 2017), while the C-PAM named Zetag 8110 has been better characterized to contain 10% cationic charge density with an average MW of 12.7 million Da (Wang, et al., 2016).

Two A-PAM dosages were chosen based on advance work prior to the CVST: 300 or 500 grams of dry PAM powder per tonne of dry solids processed (g/t or ppm dry solids).

Follow-up addition of C-PAM varied from zero to 4000 g/t at 1000 g/t intervals. This results in a total of ten (10) formal experimental cases, as shown below in **Table 3.3**. At first glance, these dosages may seem high, and in some cases, astronomically high and non-economical. However, as this study involves the very first application of an unproven technology for MFT treatment, extreme emphasis was placed on proving the capability and reliability of the VSP under continuous operation. Once proven, it becomes possible to proceed with confidence at subsequent work on flocculant optimization.

Table 3.3. Formal experimental cases in field study.

Flocculant	Dosage (g/t), dry basis									
Anionic PAM	300	500	300	500	300	500	300	500	300	500
Cationic PAM	0		1000		2000		3000		4000	

In this work, each formal experiment case is codenamed as follows: a letter *A* that is immediately followed by the applied A-PAM dosage in g/t, a dash, and a letter *C* followed by the corresponding C-PAM dosage in g/t. If no C-PAM was applied, the dash and the second C-PAM dosage portion are omitted. Thus all ten formal cases in **Table 3.3** are listed below for clarity.

- A300
- A500
- A300-C1000
- A500-C1000
- A300-C2000
- A500-C2000
- A300-C3000
- A500-C3000
- A300-C4000
- A500-C4000

Both A-PAM and C-PAM flocculant solutions for the upcoming CVST experiment must be prepared in advance. For this work, the A-PAM and C-PAM solutions were prepared in batches of 50 g or greater. Due to the low concentration of 300 ppmw (ppm, weight basis) for the A-PAM solution (2000 ppmw for C-PAM solution), the amount of dry powder needed is in the order of milligrams. Even with the use of precision balance, there may exist errors in weighing dry powders – especially so for A-PAM. Subsequent variations in flocculant solution concentrations are highly likely to occur if one prepares

only a small amount of solution. Thus, in general it is prudent to produce large batches of A-PAM and C-PAM to minimize associated experimental errors.

Horizon pond water sourced on site was vacuum-filtered with Whatman #5 Qualitative filter paper and used for flocculant dissolution at aforementioned concentrations. Since each volume of pond water contain variable amount of suspended solids that will interact with flocculants, filtration was deemed necessary to remove such experimental variability without impacting the pond water chemistry. To further minimize experimental errors from contamination, a dedicated set of container and magnetic stir bar was used for A-PAM and C-PAM solution preparation. Mixing of both flocculant solutions were carried out at 500 RPM over 12 h.

When the flocculant solutions were ready to use, pre-dilution of raw Horizon MFT to 60 g batch at 5 wt% solids was carried out in a 100 mL beaker with the same filtered Horizon pond water. The dilution target of 5 wt% was selected based on experiences from the preliminary study. In short, this value represented a compromise between the use of less flocculants on a dry solids basis (requires more MFT dilution), and the practical need of minimizing transport of process materials (requires less MFT dilution). Note that this value depends on the nature of MFT and flocculants used – past experiences with Syncrude and Suncor MFT indicated much higher compromises at 10-15 wt% with the same flocculants.

For the CVST study, the 60 g batch of diluted Horizon MFT was pre-mixed for 5 min at 350 RPM using a small 4-blade impeller mounted on a laboratory mixer.

3.3.3.3. Flocculant addition

The A-PAM solution was added dropwise first to the diluted MFT under mixing, followed by dropwise addition of C-PAM solution (if applicable). Mixing speed remains at 350 RPM throughout this section. For each solution, a dedicated dispenser was used to add the required amount in exactly 1 min. Thus if two types of solution were used, the total amount of time allocated was 2 mins. Mixing was stopped immediately when all required amount of solution has been added.

3.3.3.4. Initial settling rate (ISR) and supernatant turbidity

All content of the 100 mL beaker was transferred to the plexiglass cylinder and top of the cylinder was sealed with Parafilm. At the beginning of each ISR measurement, the initial height of the liquid-air interface was recorded as the solid-liquid interface position (mudline) at time zero. The standard stopwatch app on a smartphone was used to determine the elapsed settling time at chosen heights on the settling column, as it was capable of conveniently recording multiple lap times in rapid succession. Next, the cylinder was inverted three times. Note that one inversion involves flipping the cylinder upside-down, then flipping it upright. Then the cylinder was immediately placed on a flat surface while the stopwatch was simultaneously started. Each lap time was recorded when the mudline reaches integer heights in cm (as marked on the settling column). Data collection continues until a maximum of four lap times were recorded (after which the sediment generally started to consolidate). In the event of extremely rapid solids settling, the author attempted to record at least one lap time to estimate the ISR.

Supernatant samples were collected for turbidity analysis by a Micro 100 Turbidimeter (HF Scientific Inc., USA) after 5 min of settling (inclusive of the time elapsed during the ISR test). The instrument is capable of measuring turbidity from 0.02 up to 1100 NTU. To properly transfer supernatant out of the tall settling column, a long glass tube with a suction bulb is recommended. It must be stressed that the CVST user shall never attempt to tilt the settling column and pour out supernatant – doing so will damage the sediment and invalidate any subsequent CVST data. Once the liquid level inside the column was lower than the top of the sediment chamber, it was possible to remove the settling column and drain any remaining supernatant with a plastic pipet. When the liquid level approaches the top surface of the sediment, a 1-min time window was used to consistently remove the final remainder of supernatant, as the sediment continues to slowly release water over time.

Often it is of interest to determine the dry solids content of the supernatant for mass balance purposes. In this case, all supernatant was removed by the aforementioned method into a dedicated container (with known empty weight) for air-purge oven drying at 105 °C over 12 h.

3.3.3.5. Running the CVST

The CVST user should first check if the sediment sample height is suitable for the experiment. To measure height of the sample, it is required to obtain $SV2$ as indicated by **Eq. 3.2**. Place the sediment chamber (with sample release fastened) inside the pellet press. Next, adjust the slider sensor till bottom of the slider aligns with top of the sample. The current slider sensor output value is recorded as $SV2$, whose acceptable range is 150

to 250 as determined by trial and error. If SV_2 is below 150, the user risks pre-mature outflow of sediment out of the sample chamber (rupture), which terminates the experiment early. On the other hand, if SV_2 is above 250, there may be insufficient vertical travel distance for the piston to cause the maximum desired strain, which results in an incomplete stress-strain curve. Three possibilities thus follow.

1. If SV_2 is within 150 to 250, the user shall record SV_2 and proceed.
2. If SV_2 is below 150, the user must obtain a container and label as “new sediment”.
 - a. Weigh and record the mass of the empty container.
 - b. Remove excess sediment from the top with a plastic pipet and place the material into the container.
 - c. Measure SV_2 again and ensure it is within the acceptable range. Repeat step (b) if otherwise.
 - d. Weigh and record the mass of the filled container.
 - e. Apply air-purge oven drying at 105 °C over 12 h to determine its dry solids content for mass balance purposes.
3. In the unlikely event of $SV_2 > 250$, the user is required to restart and modify the current CVST experiment materials.
 - a. Discard the sediment sample.
 - b. Proceed to cleanup (see **section 3.3.3.6**).
 - c. Increase the sample size of the 5 wt% diluted MFT from 60 g. Exact amount will require further trial and error.

Once $SV2$ is obtained, the slider sensor is moved downward till in contact with the press platform, at which the value of $SV3$ is read.

While the sediment chamber is on a flat surface, carefully and slowly place the piston on top of the sediment sample. The piston will sink immediately due to gravity. Next, visually assess the bottom of the piston for air pockets, which will distort the force sensor readings at initial stage of the measurement. In case of significant air entrapment, slightly nudge and rotate the piston without pressing downwards and attempt to release most of the trapped air. When the piston has been secured, place the sample chamber and piston assembly inside the pellet press. Align the center of the piston to the tip of the force sensor. Initialize the force measurement program and experimental data collection.

For all currently available CVST experiments, strain production started at exactly 3 s following the beginning of data acquisition. As described previously, the upright hydraulic oil lever was first swung to horizontal position over 1 s and caused 110 ± 10 μm of vertical strain. For the next 1 s, the lever was returned to its initial upright position but generated no vertical strain. A steady pace of swing action was maintained throughout the experiment.

On the custom-built LabVIEW force measurement program, a real-time waveform plot of the compression force was used to assess the experimental progress. The user should immediately stop the CVST experiment by opening the oil release valve on the pellet press if any one of the following is observed.

1. Measured force exceeds 2000 N.
2. The slider has almost reached the top-most position on the strain sensor.

3. A plateau on the waveform plot.

Stop conditions #1 and #2 were adopted to protect the sensors from overloading. On the other hand, stop condition #3 indicates a “*plasticity*” event that suggests, at this point in time, any vertical strain applied to the sediment sample causes no more subsequent increase in compressional stress – corresponding to perfect plastic deformation. In terms of flocculated MFT sediments, one of the following must be true.

- A. Release of water, or “*dewatering*” event.
- B. Release of sediment, or “*rupture*” event.

Therefore, without prior knowledge, it is required to stop the CVST and assess the nature of the very first plasticity event. To distinguish between the two types of plasticity events, simply use a plastic pipet to remove all material that was squeezed out of the sample chamber. Visually determine the main component of the material (water or sediment).

For better accuracy and confidence, remove the sediment from sample chamber and apply the aforementioned air-purge oven drying method (105 °C over 12 h) to determine its dry solids content. Then it is possible to determine the water and solids losses caused by the CVST via mass balance. A dewatering event corresponds to the loss of mostly water, while a rupture event will cause significant dry solids escape from the sample.

In the case of a dewatering event, the user should perform additional follow-up experiments and further strain the sample past the first plasticity event (whose type is known). At higher strains, the sample may produce a second unknown plasticity event, at which the experiment should be stopped for assessment. Iterate again and look for additional plasticity events if the second event is caused by dewatering as well. However

if a rupture event has been confirmed, the user should not apply additional vertical strain to this particular sample as the subsequent data will be invalid. It is recommended to replicate this experiment up to the known rupture event for verification purposes only.

At the end of the CVST, the final slider sensor output value should be recorded as $SV4$ for calculation of the maximum applied vertical strain, as stated in **Eq. 3.3**.

3.3.3.6. Notes on cleanup

It is very important that the CVST user shall never use any organic chemical solvent to remove bitumen from the plexiglass cylinder. A recommended method is to use the Sparkleen detergent to rub against the bitumen. Rinse the cylinder well with tap water. Extreme care should be taken to fully rinse the threads, whose spacing is able to trap significant amount of Sparkleen detergent as well as other impurities.

Do not lose or damage any of the two rubber rings.

After cleaning, dry all interior surfaces with paper towel. Pressurized air may be used to dry the top settling column.

Finally, loosely attach the top settling column on the end of the sample chamber that has been marked by arrows. Loosely attach the bottom sample release on the other end (with no markings).

References

- Boxill, L., 2015. Using Imaging to Decode Geotechnical Characterization of Polymer-Amended Fine Tailings, Edmonton, AB: COSIA Clay Workshop.
- Chen, L. et al., 2015. Water Recovery Estimation for Polymer Flocculated Oil Sand Tailings: A comparison between experimental practices and a fluid flow simulation based on Lattice-Boltzmann method, Calgary, AB: COSIA.
- Ng, J. & Xu, Z., 2017. Application of Switchable Hybrid Polymers in Oil Sands, Edmonton: Presentation for NSERC IRC in Oil Sands Engineering.
- Wang, C. et al., 2016. Role of pre-conditioning cationic Zetag® flocculant in enhancing MFT flocculation. *Energy Fuels*, 30(7), p. 5223–5231.

Chapter 4: Volute Screw Press Field Study

4.1. Field study experimental

Field tests with the VSP were carried out in the Horizon Oil Sands Innovation Centre at CNRL (Fort McMurray, AB). The Horizon MFT, pond water, as well as both A-PAM and C-PAM used for VSP field study in this work were of same origin and properties as those described in **section 3.3.3.2**. Main flocculant dosage cases were the same as in the CVST study (see **Table 3.3**). For these dosage cases, **Table 4.1** lists all applied process setpoints.

Table 4.1. VSP normal operation setpoints.

Parameter	Value
FHT feed slurry rate	0.4 m ³ /h
FHT feed slurry dry solids	5 wt%
CT mixer speed	180 RPM (not adjustable)
FT mixer speed	60 RPM (right-side controller setpoint 60)
Endplate gap	2 mm
Screw speed	1.6 RPM (left-side controller setpoint 20)
Volute plate washers	1.85 mm thickness (default)

An additional six (6) trial cases have been included in the field study to obtain preliminary information on the effects of adjustable operating parameters of the VSP under constant dosage, as detailed in **Table 4.2**.

Table 4.2. Trial cases in field study.

Case #	Flocculants dosage (Anionic-Cationic, g/t)	Parameters studied
T1	A300-C0	Full recycle mode (filtrate used for MFT dilution and both flocculant solutions).
T2	A300-C3000	Smaller endplate gap (1 mm).
T3	A300-C3000	Smaller endplate gap (1 mm). Slower FT mixer (45 RPM).
T4	A300-C4000	Full recycle mode.
T5	A300-C4000	Full recycle mode. Longer flocculant solution preparation time (15 h).
T6	A300-C4000	Full recycle mode. Longer flocculant solution preparation time (15 h). Slower FT mixer (45 RPM).

4.2. Flocculant solution preparations

On each day, 300-L batches of A-PAM and C-PAM solution were produced in the test facility. The A-PAM and C-PAM dry powder were both dissolved in Horizon pond water (or in recycle water for some trial cases) over 8-10 h as follows: 300 ppmw concentration for Magnafloc, and 2000 ppmw for Zetag. A dedicated 350-L mixing tank was used for each solution to avoid contamination. The product solutions were pumped to separate 300-L drums for subsequent use.

4.3. Process start-up

Prior to feed to VSP, raw MFT was diluted to 5 wt% solids with Horizon pond water for the start-up run and with the recycle filtrate for all subsequent runs

4.4. Sample collection

After a target dosage was set, VSP cake product was sampled every 30 min, whose dry solids content was analyzed after heating to 160 °C over 15 mins by one of four HB43-S Halogen heated balances (Mettler-Toledo). Solids contents in other process streams were analyzed in the same manner as required. It was determined that a run time of 3.5 h is needed to stabilize the solid content of cake (reaching steady state) after each dosage change (see **Fig. 4.1**). Therefore during the 3.5-h time interval, only filter cake solids content was monitored every 30 min. Upon reaching steady state, both filter cake and filtrate streams were randomly sampled twice per stream for their respective dry solids contents. Also, runoff material (from volute plate self-cleaning cycles) was randomly sampled once to determine its dry solids in order to obtain sufficient information for

process analysis and mass balance. In the meantime, two separate containers were used to collect the produced cake and runoff materials over a set amount of time to obtain their respective rates of production. The apparent increase or decrease in dry solids content over time is indicative of the gradual change in filter cake properties since the previous run. For example, A300-C4000 was executed prior to A300, and the latter run was found to yield much lower dry solids content than the former run.

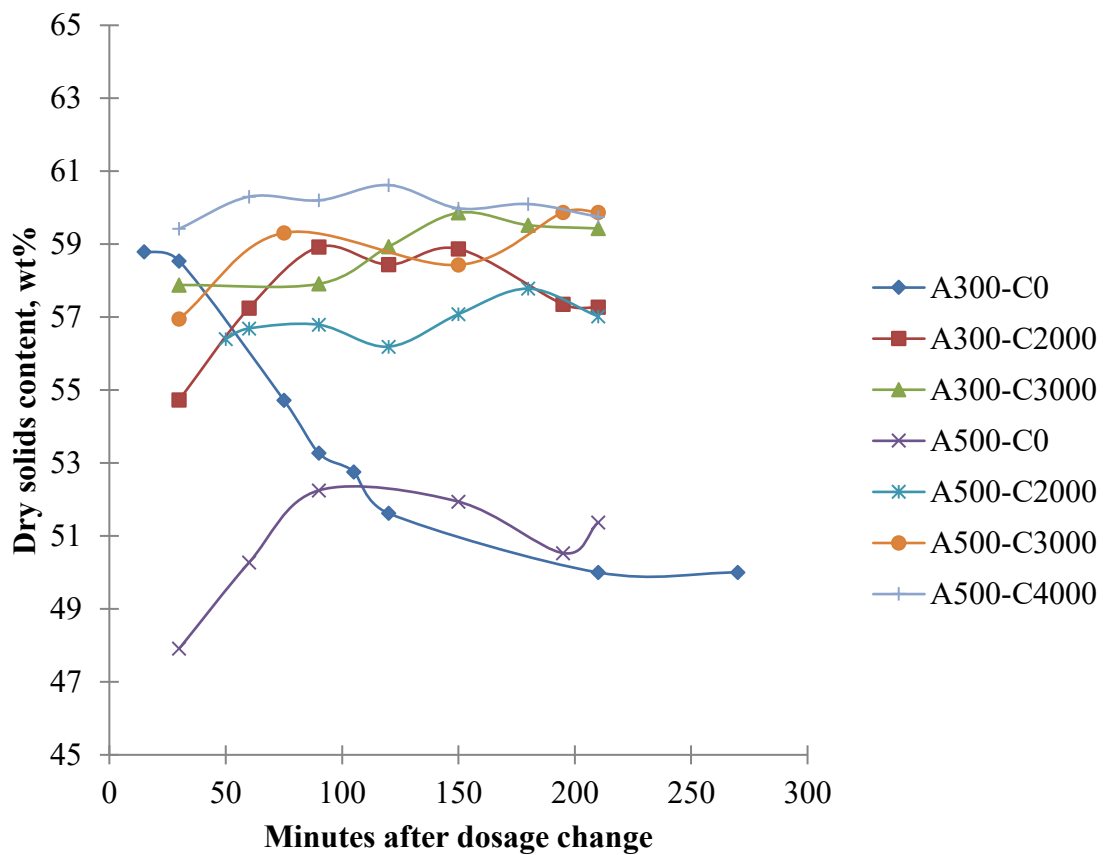


Figure 4.1. Time evolution of VSP product dry solids content after a flocculant dosage change.

Chapter 5: Controlled Vertical Strain Tests

Chapter 5 presents detailed analyses and discussions for the results obtained in the bench-scale study conducted on campus at the University of Alberta.

5.1. Controlled vertical strain test results (10 formal cases)

5.1.1. Flocculation performance

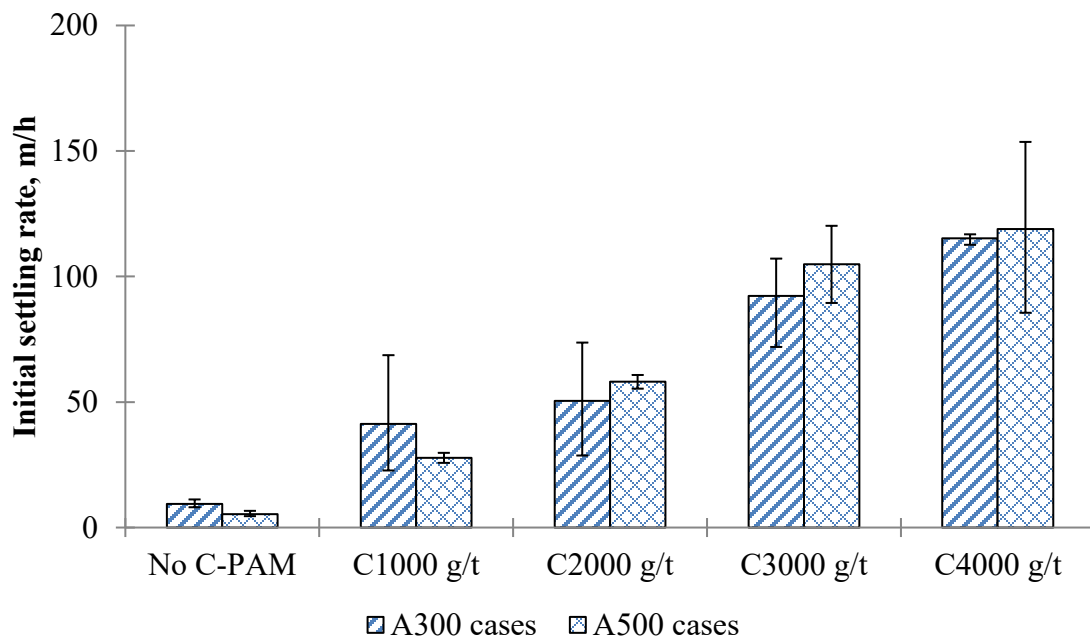


Figure 5.1. Initial settling rate of flocculated sediment solids.

The initial settling rate (ISR) of the flocculated MFT solids is of importance to tailings thickener applications among other gravity-based solid-liquid separation processes. Value of ISR is determined by the slope of the initial linear region of the solids settling curve.

Generally speaking, a large ISR is desired upon addition of polymer flocculants. Thus this parameter has become one of the predominant factors for flocculant selection and optimization in a variety of industry applications.

It was observed the A-PAM in this study was able to flocculate and settle MFT solids at 9.37 m/h with 300 g/t addition. The ISR slowed to 5.35 m/h with 500 g/t dosage of A-PAM, suggesting an overdose from the optimum dosage for sedimentation. The ISR dramatically increased with the subsequent addition of C-PAM across all C-PAM dosages tested. As well, the differences in ISR between A300 and A500 cases became negligible when the large error bars were taken into consideration. From **Fig. 5.1**, it is clear that the use of C-PAM after applying A-PAM significantly improved MFT solids settling, while increasing C-PAM dosages progressively increased the ISR. Extremely fast ISR of 50-120 m/h were measured at C-PAM dosages of 2000 g/t or higher.

Interestingly, rate of increase in ISR per additional 1000 g/t C-PAM becomes slower from 3000 to 4000 g/t, which suggests the approach of an optimum C-PAM dosage in terms of solids sedimentation.

Once the flocculated slurry was transported to the VSP Dewatering Press inlet, faster solids ISR would improve supernatant removal in the same amount of residence time. It was hypothesized such phenomenon would slightly increase the dry solids (DS) content of the post-drainage sediments for use in the Dewatering Press. This may help in the subsequent production of filter cakes with higher DS content. In the upcoming **Chapter 6**, dry solids data in **Fig. 6.1** seems to empirically correlate with ISR shown in **Fig. 5.1**.

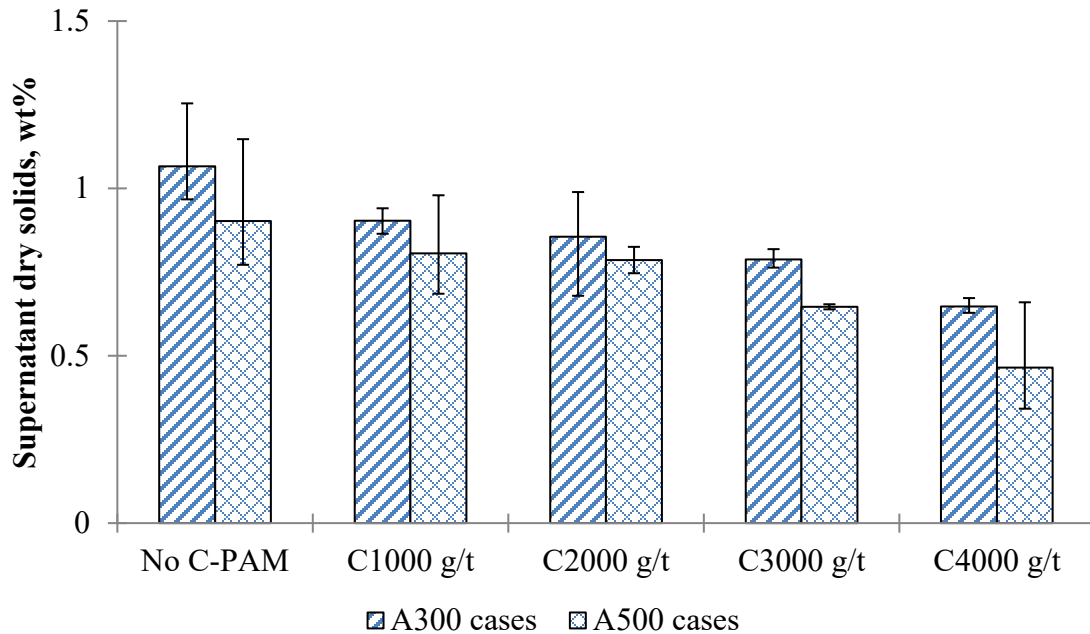


Figure 5.2. Supernatant dry solids.

Quality of supernatant (in terms of DS) is also an important process variable as it affects the overall mass balance and the feasibility of recycling. Unfortunately it was not possible to remove all DS in the supernatant for all A-PAM and C-PAM dosages tested in this study. None of the supernatant samples could be directly measured for turbidity, and the DS data was presented instead in **Fig 5.2**. This may be a consequence of elevated monovalent cation concentration in conjunction with the low divalent cation concentration in Horizon pond water, plus the abundance of $< 2 \mu\text{m}$ clays as shown in **Chapter 3**. The generally poor filtrate quality in the upcoming **Chapter 6** may also be explained in a similar manner.

Use of A-PAM resulted in an extremely turbid supernatant of about 1 wt% DS that showed little sensitivity to 300 or 500 g/t dosages. Subsequent addition of C-PAM gradually reduced the supernatant DS to 0.65 wt% for A300-C4000 and ~ 0.5 wt% for

A500-C4000. The increased removal of DS is likely due to charge neutralization and bridging between C-PAM and suspended solids. An interesting observation at C-PAM dosages of 3000-4000 g/t showed the beneficial effect of initially using 500 g/t A-PAM as opposed to 300 g/t, suggesting the A-PAM carries limited negative charge that can be counteracted with sufficient C-PAM.

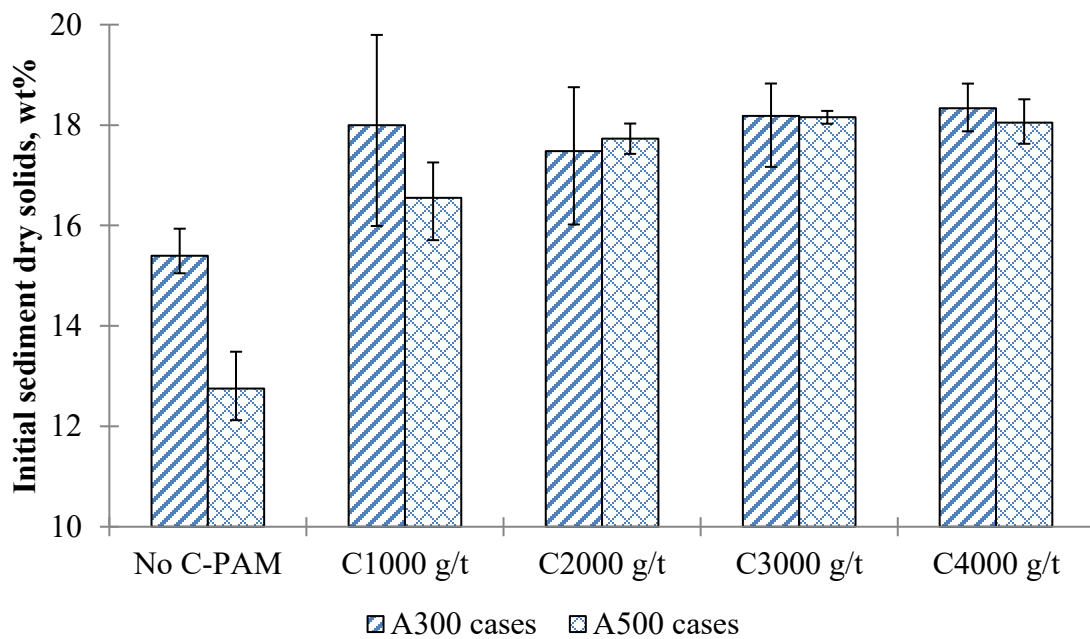


Figure 5.3. Initial sediment dry solids.

The controlled vertical strain test (CVST) procedure in **Chapter 3** disallows sediment sampling from the sample chamber, as the user risks damaging the sediment and invalidates the subsequent CVST data. Instead, a mass balance was performed for each sample as follows to determine the initial sediment DS prior to compression.

1. Mass of slurry was added to the combined mass of A-PAM and C-PAM used.

2. Mass of supernatant was subtracted from the quantity in step #1 to get mass of initial sediment.
3. Total amount of DS is known.
4. Mass of DS in supernatant is obtained with data from **Fig. 5.2** and step #2.
5. Subtract DS in step 4 from the quantity in step 3 to get DS in the initial sediment.

Data in **Fig. 5.3** was calculated by the ratio between initial sediment DS mass and initial sediment mass. In the absence of C-PAM, clearly the use of 300 g/t A-PAM is a superior choice than 500 g/t in terms of initial sediment DS. The difference becomes negligible with the addition of the first 1000 g/t C-PAM, in which both experiment cases saw significant improvements. As the C-PAM dosages further increased, the initial sediment DS stabilized to ~18 wt% irrespective of A-PAM dosages. Relevant discussions after **Fig. 5.1** hypothesized a connection between faster ISR and higher initial sediment DS across the same amount of sedimentation time. This appears to be true up to ISR of ~90-100 m/h, at which large measurement uncertainties interfered with any meaningful correlations.

5.1.2. CVST stress-strain curves

5.1.2.1. Identifying the nature of a plasticity event

The iterative process for distinguishing between two different types of plasticity events during CVST is best illustrated by the example for case A300-C1000. Left inset of **Fig 5.4** shows the second observed plasticity event: an unknown plateau at ~5 vol% of applied vertical strain and a response stress slightly over 150 kPa (significance of the first

plateau will be discussed in the upcoming sub-section). The experiment was stopped immediately followed by a close examination of the material inside the effluent trap on top of the sample chamber. For this example, it was found that all effluent material at the second plasticity event was liquid. Right inset of **Fig. 5.4** shows the status of the effluent trap after all liquid has been removed. A small amount of effluent leaked out as the photograph was taken. However, the residual effluent was transparent and no solid sediment material could be found, both of which suggests a dewatering event has occurred.

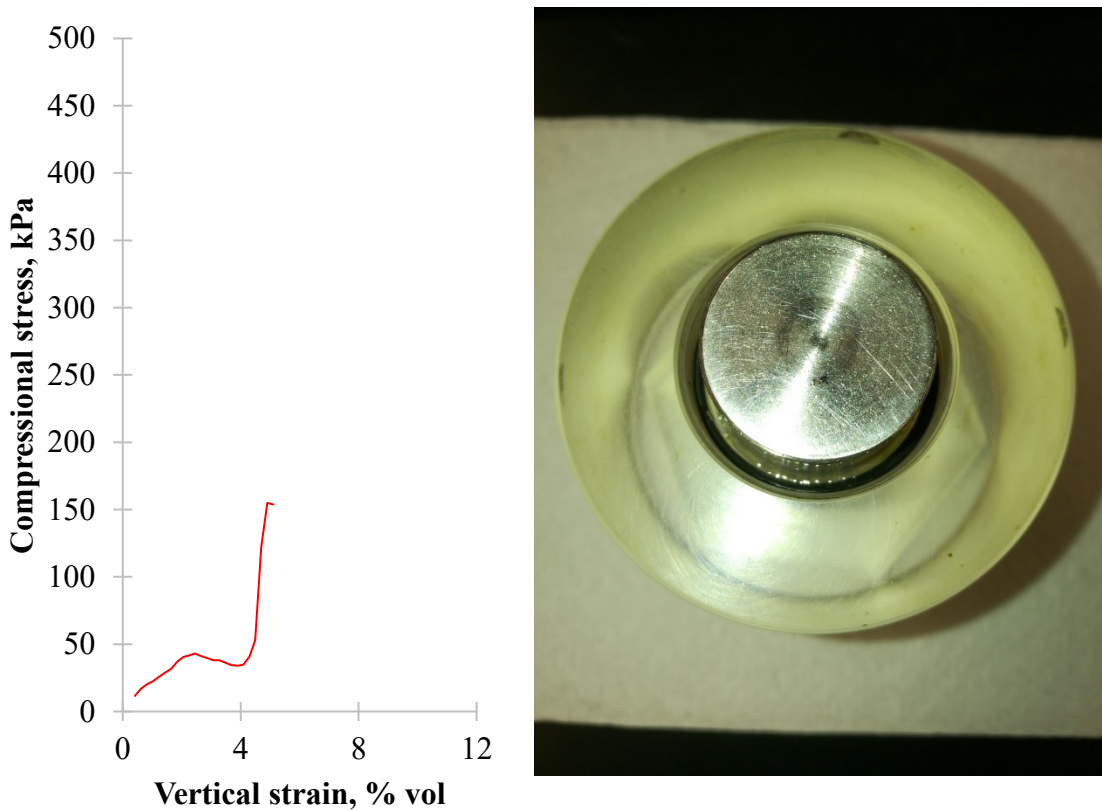


Figure 5.4. Second plasticity event characterization for case A300-C1000. Left: a CVST stress-strain curve for A300-C1000, indicating an unknown plasticity event. Right: top-

down view of the sample chamber effluent trap for this experiment. After liquid removal, the remaining residual material was transparent. This plateau indicated a dewatering event.

Following the above discovery, additional vertical strain was applied to replicate A300-C1000 experiments past a response stress of 150 kPa to find the next plasticity event. Left inset of **Fig. 5.5** shows a third plasticity event on the CVST stress-strain curve for A300-C1000 sediments. This time the response stress plateaued at ~400 kPa near 7 vol% vertical strain. Right inset of **Fig. 5.5** visualizes the effluent trap after liquid removal. It was discovered that a small amount of solid sediment material escaped the sample chamber, which signals the onset of a rupture event. Therefore the CVST for A300-C1000 has been completed at this point.

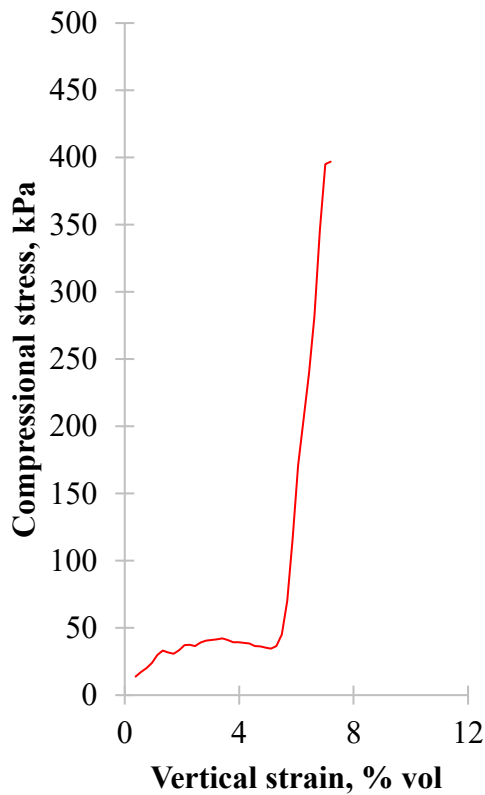


Figure 5.5. Third plasticity event characterization for case A300-C1000. Left: an additional CVST stress-strain curve for A300-C1000, indicating an unknown plasticity event at higher response stress. Right: top-down view of the sample chamber effluent trap for this experiment. After liquid removal, small amount of solid sediment was visible. This plateau indicated the onset of a rupture event.

Note the rupture event shown on the right inset of **Fig. 5.5** may not be immediately obvious to new CVST users. Thus another example (A300) was selected to illustrate a sediment sample that easily undergoes rupture. Left inset of **Fig. 5.6** shows a second stress plateau at ~150 kPa that occurred shortly after experiment was started. Since the A300 sediments were known to be plastic for compressive dewatering, its second plasticity event was expected as rupture. As shown on the right inset of **Fig 5.6**, sediment

material was clearly visible in the effluent trap, which indeed suggests the occurrence of a rupture event.

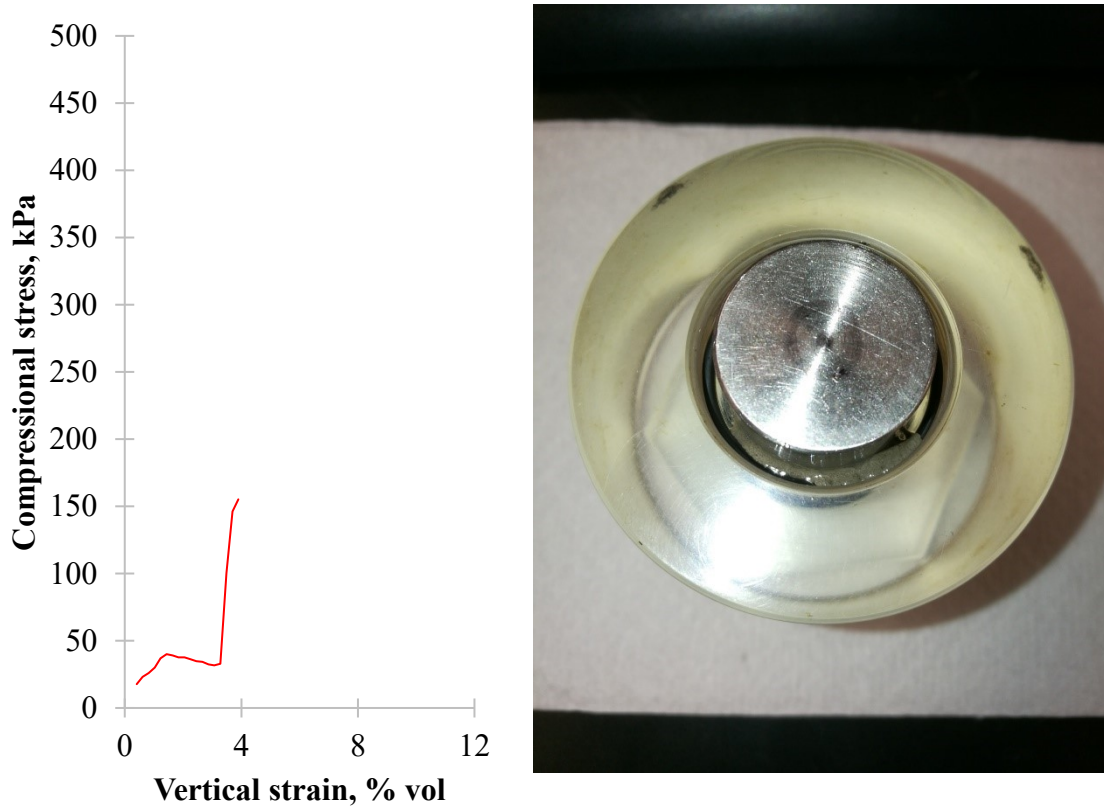


Figure 5.6. Second plasticity event characterization for case A300. Left: a CVST stress-strain curve for A300, indicating an unknown plasticity event. Right: top-down view of the sample chamber effluent trap for this experiment. After liquid removal, solid sediment material was clearly visible. This plateau indicated a rupture event.

Using the aforementioned identification methods for plasticity events, complete CVST stress-strain response curves were established for all 10 formal experiment cases, as shown in **Fig. 5.7A** to **5.7E**. Despite different degrees of variations across replicates, there is a general agreement in the overall response trend for a given dosage case.

Experimental errors using the current CVST setup is inevitable due to the manual step-up process for vertical strain production.

It is apparent that dosage cases without C-PAM addition (A300 and A500, **Fig. 5.7A**) produces sediments that ruptures under significantly less strain and stress than all other cases where C-PAM was subsequently used (**Figs. 5.7B/C/D/E**). Methods of curve analysis and data extraction will be discussed in the upcoming sub-sections.

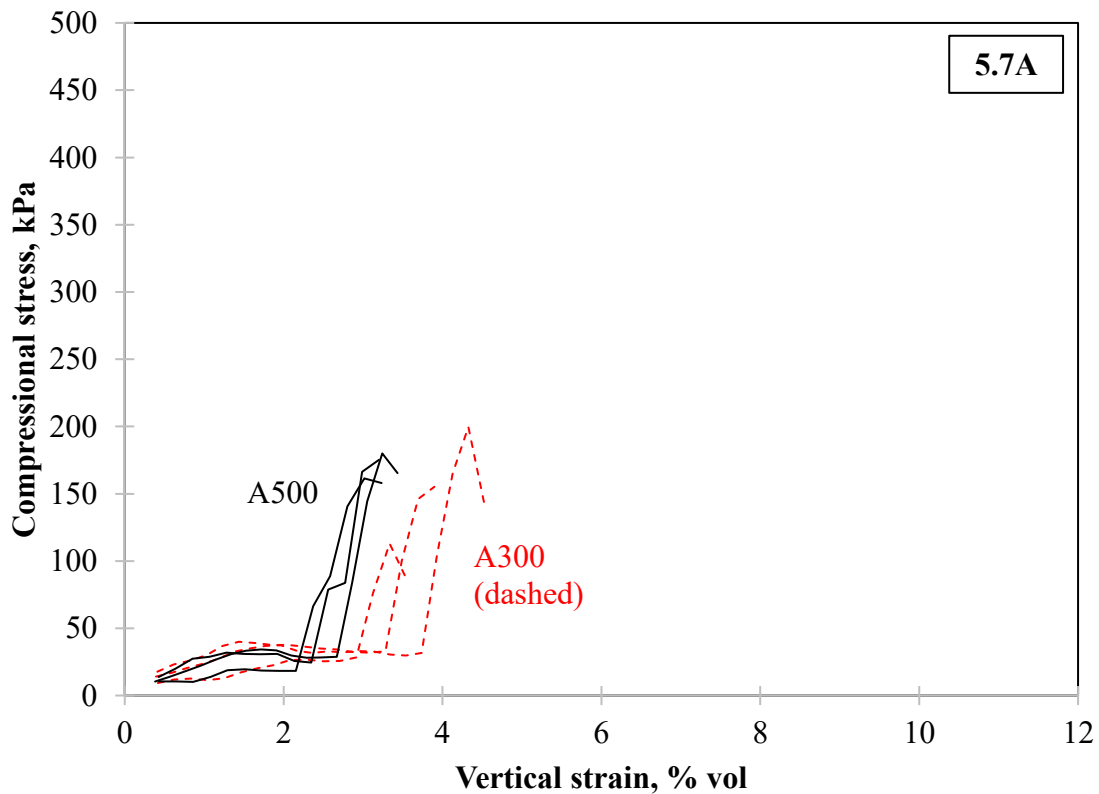


Figure 5.7A. Complete CVST stress-strain curves for A300 and A500.

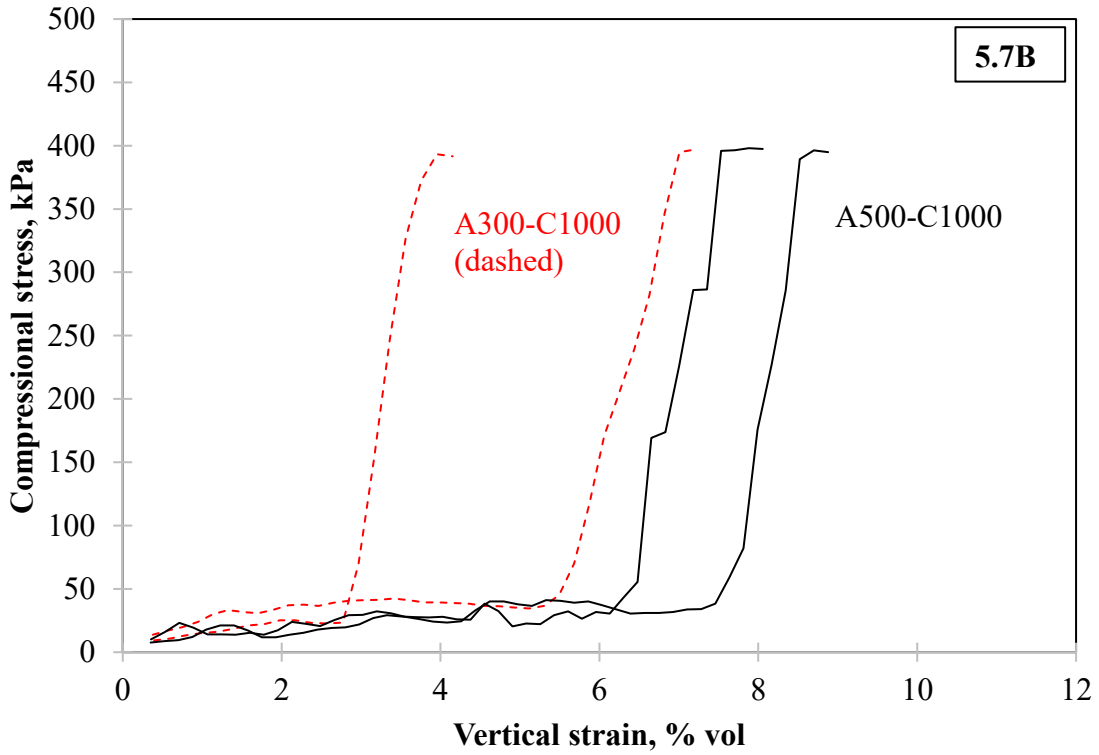


Figure 5.7B. Complete CVST stress-strain curves for A300-C1000 and A500-C1000.

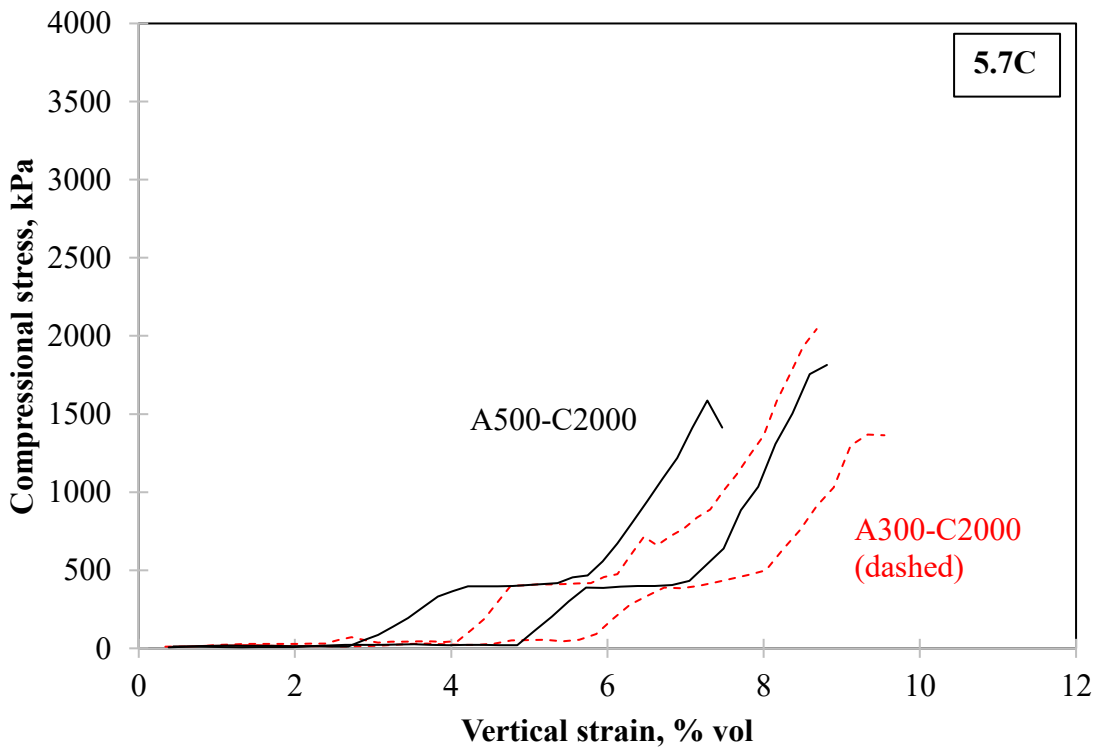


Figure 5.7C. Complete CVST stress-strain curves for A300-C2000 and A500-C2000.

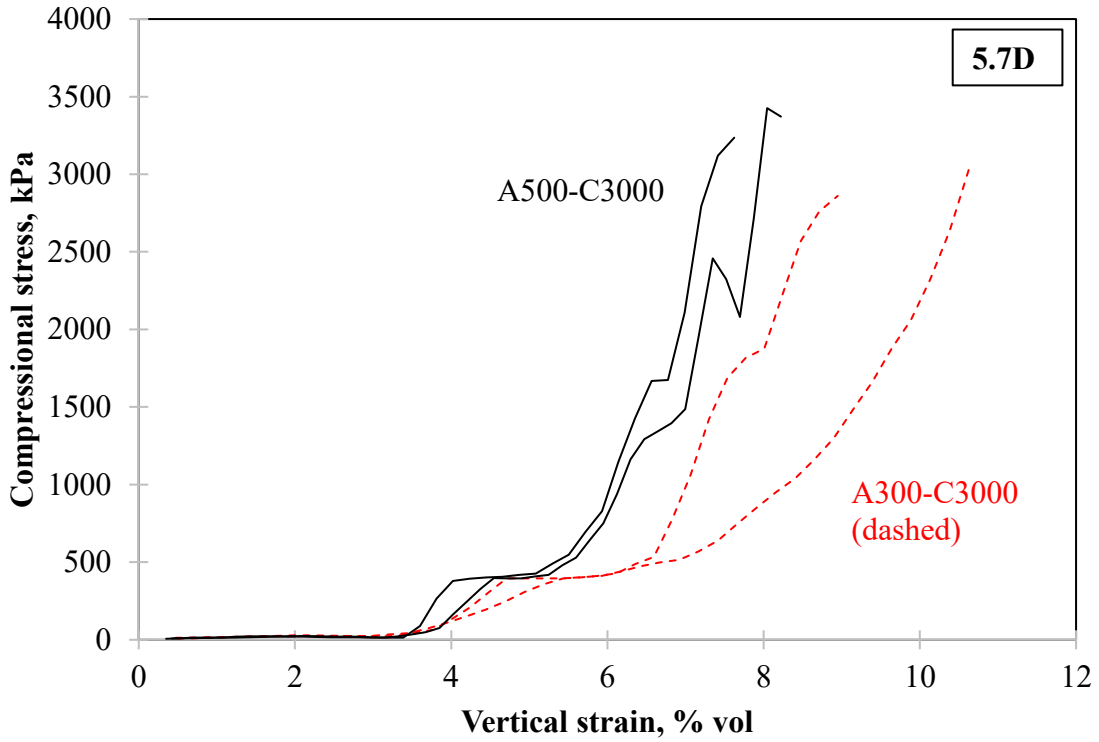


Figure 5.7D. Complete CVST stress-strain curves for A300-C3000 and A500-C3000.

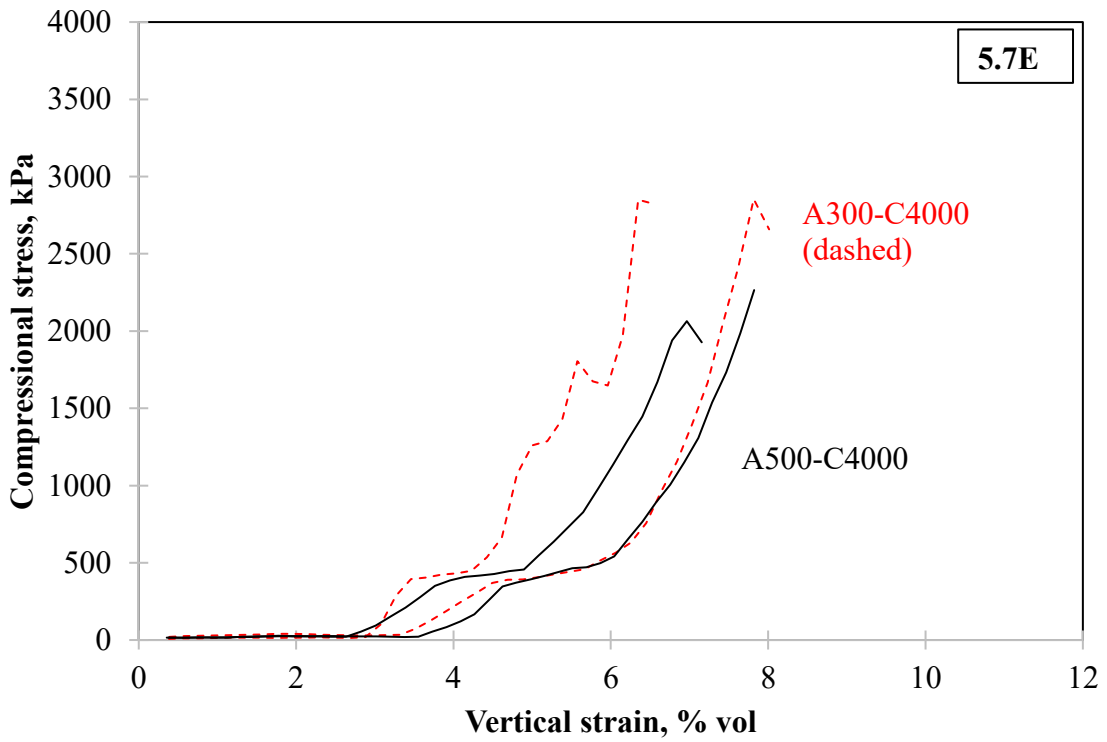


Figure 5.7E. Complete CVST stress-strain curves for A300-C4000 and A500-C4000.

5.1.2.2. Empirical curve classification and analysis

Figure 5.8 presents one of the complete CVST stress-strain curves for case A500-C3000 from Fig 5.7D. This example will also be used for subsequent definitions on the constituents of all CVST stress-strain curves.

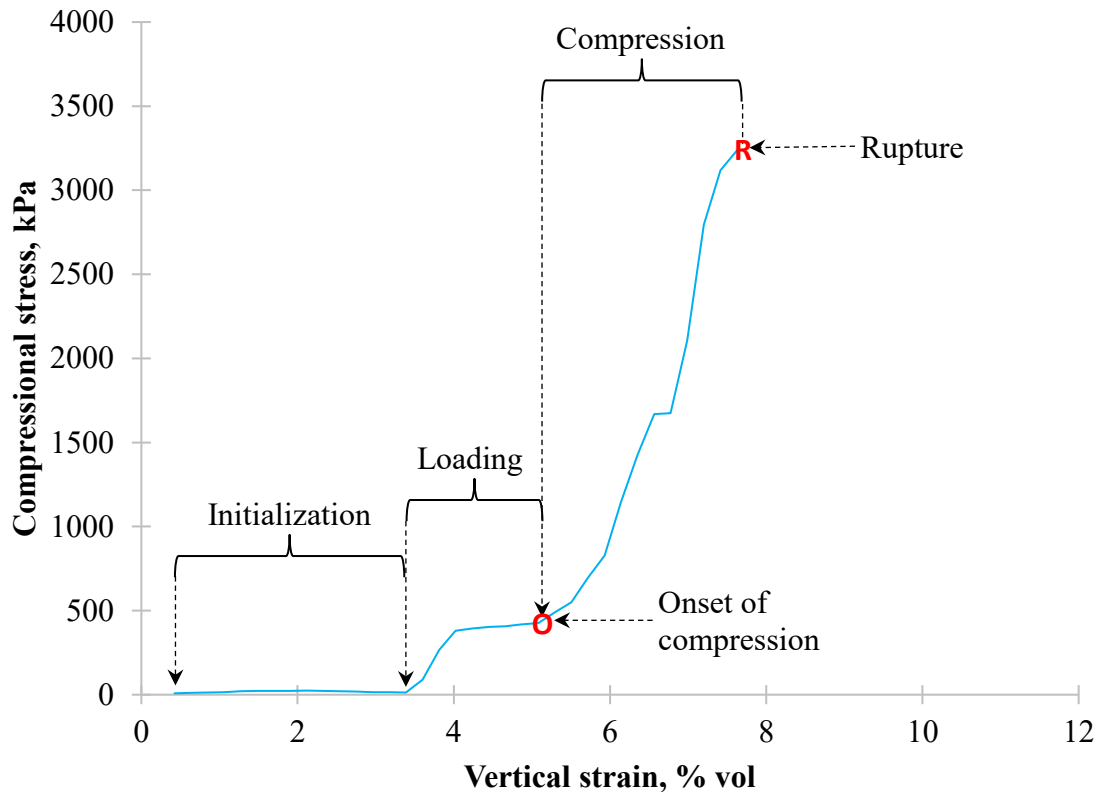


Figure 5.8. A complete and classified CVST stress-strain curve for A500-C3000.

There are three distinct parts on each CVST stress-strain curve that are common to all experiment cases tested, as outlined on Fig. 5.8.

- Initialization: occurs at the beginning of CVST. This stage involves de-aeration of the sediment chamber, as well as removal of any supernatant that has been

released by the sediment prior to compression. Due to the incompressibility of both air and supernatant, the response stress remains close to zero as the vertical strain increases in this stage.

- Loading: present as a ramp-up in response stress, followed by the first stress plateau (plasticity event). All experiments have been stopped here and assessed for rupture. However no rupture event has been found at the first plasticity event for all cases, suggesting this plateau is essentially some form of water removal under low compressive stress. Therefore all previous discussions in **section 5.1.2.1** focused on identifying only the second or third plasticity event. It was hypothesized the loading stage involved closure of relatively large (on the order of ~0.1 to ~1 mm) water channels. This would explain the occurrence of a stress plateau, as the trapped water at sediment interior is incompressible but requires slight external pressure to be liberated. Sometimes a loss of stress was observed in the loading stage, possibly due to a disproportionately excess amount of water being liberated from the sample chamber whenever the vertical strain increased in this stage.
- Compression: a significant ramp-up in response stress that occurs after the loading stage. This stage is the core of CVST and most important in characterizing sediment dewatering elasticity or plasticity. It is defined as the region between the “onset of compression” (inflection point at the end of the first plateau, denoted by point *O*) and the rupture point (as assessed in **section 5.1.2.1**,

denoted by point R). Here the sediment remains inside the sample chamber while its volume gradually reduces via release of internal water. The size distribution of water channels is hypothesized to be reduced to smaller sizes (on the order of $\sim 10^{-2}$ to $\sim 10^{-3}$ mm) during this period, which increases the pressure required to liberate the remaining internal water, while the bulk sediment compressive yield strength increases due to the loss of water. The two processes co-exist until the applied stress becomes sufficient to destroy the integrity of the sediment. At this point, a rupture event occurs for CVST.

Once a complete stress-strain curve has been classified, it becomes possible to define the *compressive dewatering index* (CDI) of this sediment as follows.

$$CDI = \frac{\sigma(R) - \sigma(O)}{\varepsilon(R) - \varepsilon(O)} \quad (5.1)$$

Equation 5.1 essentially linearizes the compression stage of the CVST stress-strain curve. As discussed in **Chapter 3**, a linear stress-strain relation indicates compressional elasticity. On the other hand, no mathematical relation could describe a plastic response as the resultant stress becomes independent of applied strain. Nevertheless, several factors are evident in the context of CVST results.

1. Compression of sediments without C-PAM (A300 and A500) involves very small (< 1%) step-up in vertical strain, and causes a nominal increase in response stress ($\sim 10^2$ kPa). The resultant CDI is expected to be numerically small.

2. Compression of sediments with high subsequent C-PAM dosages (A300 or A500 with C2000 and above) produces relatively high response stress values ($\sim 10^3$ kPa) across slightly larger vertical strains (~ 1.5 - 3.5%). Thus the resultant CDI should be larger.
3. Close scrutiny will be placed for the analyses across A300/A500 and A300/A500-C1000 cases, whose CDI values appear similar but their respective VSP dewatering outcomes are very different.

Therefore, for the CVST with flocculated MFT sediments, a lower CDI generally indicates relatively plastic sediments that respond poorly to mechanical compression dewatering, and vice versa. High CDI values would suggest the sediment is able to remain stationary inside containment and dewater under elevated compressive stress.

In conjunction with the CDI, it is often prudent to consider the position of the rupture point R on the CVST stress-strain curve while assessing the overall compressive dewaterability of sediments. Ideally a high rupture stress (y -value of point R) located at a large rupture strain (x -value of point R) in combination with a large CDI is highly promising for VSP application. Desired range of values for these criteria will be discussed in the upcoming sub-section.

5.1.2.3. Onset of compression, rupture point, and CDI results

Table 5.1 shows the respective strain and stress values obtained graphically from **Fig. 5.7**. Results in **Table 5.1** were subsequently used in **Fig. 5.9**, which plots the CDI values

as a function of C-PAM dosage. Clearly, increasing C-PAM dosages past 1000 g/t significantly increased the sediment CDI, whose effects will be elaborated in **Chapter 7**.

Table 5.1. Properties of point *O* and point *R* for each experiment case.

Experiment case	Onset of Compression (Point <i>O</i>)		Rupture (Point <i>R</i>)	
	Strain, vol%	Stress, kPa	Strain, vol%	Stress, kPa
A300	2.91	29	3.32	112
	3.29	32	3.7	146
	3.73	31	4.31	200
A300-C1000	2.78	26	3.95	392
	5.4	40	7	395
A300-C2000	5.8	420	8.61	2050
	8.02	500	9.32	1375
A300-C3000	6.6	520	8.95	2860
	6.9	510	10.61	3020
A300-C4000	4.22	460	6.34	2860
	5.68	470	7.81	2860
A500	2.16	19	3.01	161
	2.35	26	2.99	166
	2.67	29	3.25	180

A500-C1000	6.11	30	7.52	396
	7.47	38.5	8.51	390
A500-C2000	5.75	460	7.28	1585
	7.05	430	8.81	1810
A500-C3000	5.1	425	7.61	3240
	5.25	420	8.03	3420
A500-C4000	4.91	470	6.97	2070
	6.06	540	7.82	2270

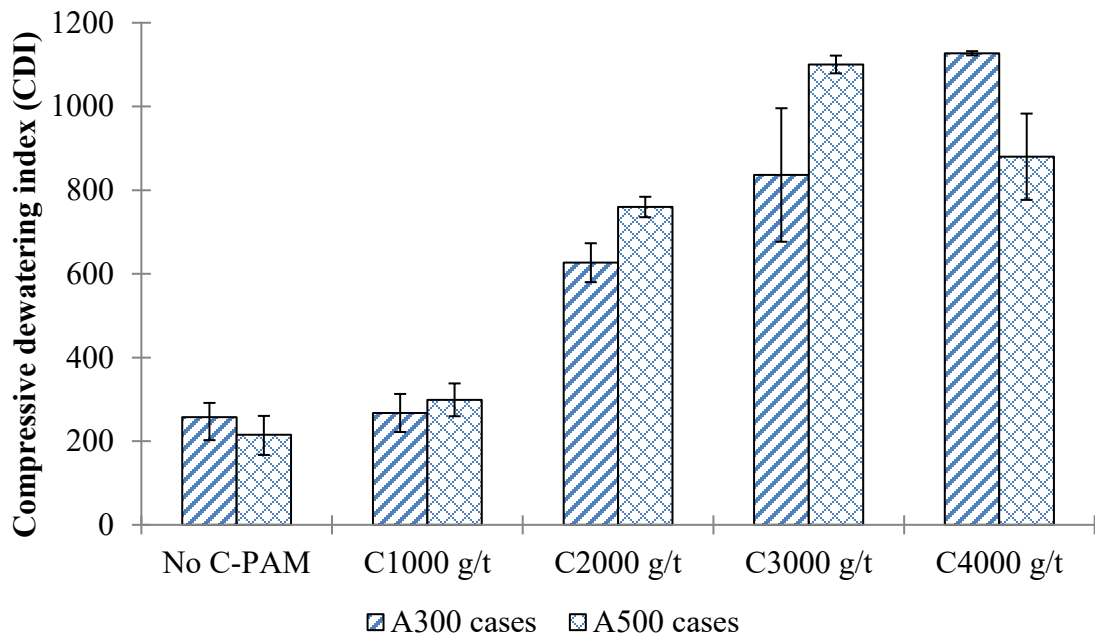


Figure 5.9. Compressive dewatering indices for all 10 formal experiment cases.

Chapter 6: Volute Screw Press Dewatering Tests

Chapter 6 provides results and relevant discussions in detail for the field study conducted on-site at Canadian Naturals Horizon Oil Sands Innovation Centre.

6.1. Effects of A-PAM and C-PAM (10 formal cases)

6.1.1. Filter cake product dry solids

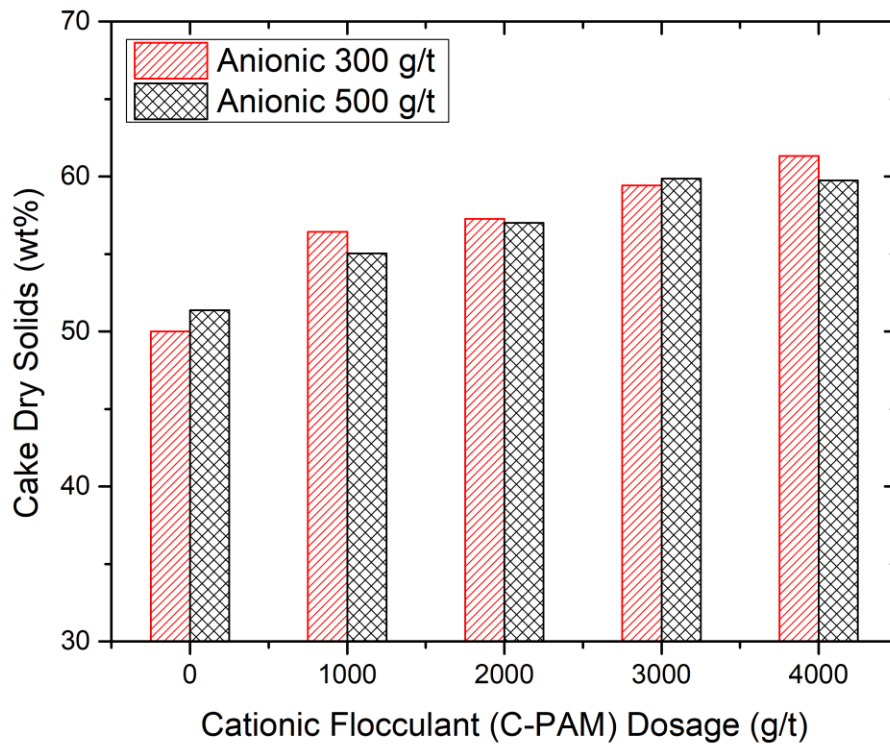


Figure 6.1. Impact of A-PAM and C-PAM dosages on filter cake dry solids content.

In this work, analysis and prediction of filter cake dry solids content are of primary importance. As observed from **Fig. 6.1**, in the absence of C-PAM, the sole use of A-PAM

combined with the dewatering capabilities of volute screw press produced 50 - 51 wt% dry solids in filter cake. Physical properties of such products are similar to solid cakes produced from decanter-type centrifuges used elsewhere in the industry for tailings treatment. This is achieved despite the volute screw press normally operates at much lower rotational speeds (< 2 RPM) than industrial centrifuges (~1800 RPM).

When C-PAM was introduced to the feed slurry and the resultant sediment goes through the same DP unit, the filter cake becomes noticeably dry. A significant step-up in cake dry solids to 55-56 wt% was found after dosing 1000 g/t C-PAM after the use of A-PAM. With each 1000 g/t increase in C-PAM dosage, dry solids content in the filter cake progressively increased till an apparent plateau at about 60-61 wt% was reached at 3000-4000 g/t C-PAM.

An important observation from the results in **Fig. 6.1** suggests that, with increasing C-PAM dosage, the flocculated sediment become more susceptible to volume loss (via water release) upon mechanical compression. On the other hand, applying 300 or 500 g/t A-PAM made no significant difference in terms of cake dry solids over all C-PAM dosages tested. Thus the *dosage of C-PAM appears to be positively correlated to sediment elasticity of dewatering*. As this particular C-PAM is known to generate increasingly large and strong flocs with increasing dosage (Wang, et al., 2016), it is hypothesized that the average water channel size within the sediment also increases as a result. Such development could explain the apparent acquisition of dewatering elasticity.

6.1.2. Filter cake dry solids throughput

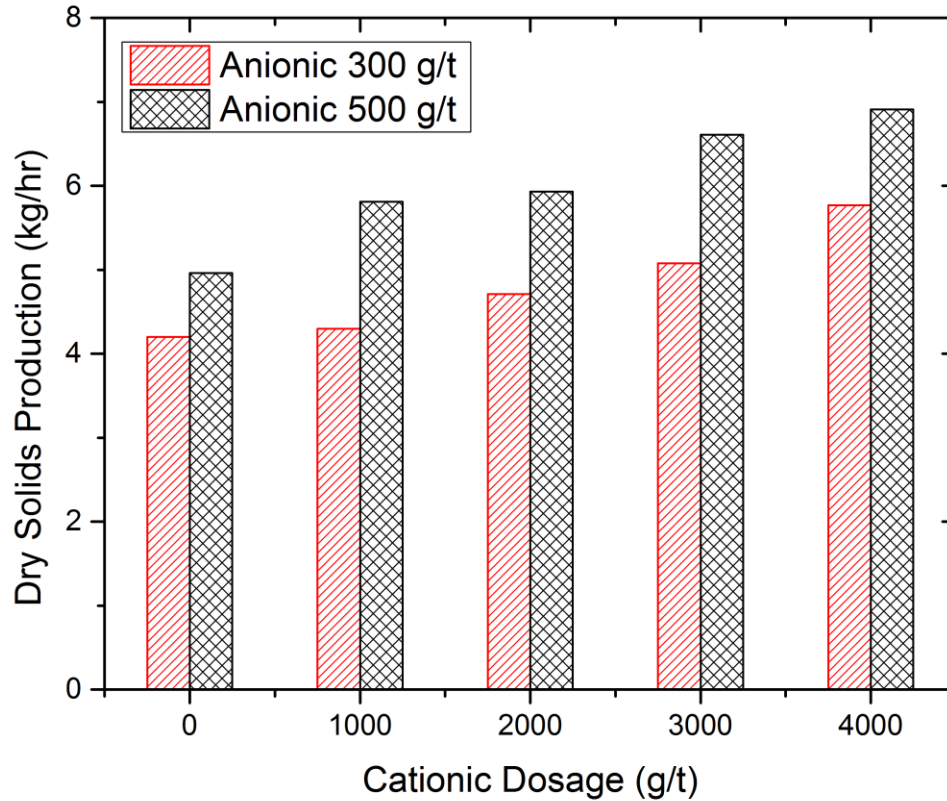


Figure 6.2. Impact of A-PAM and C-PAM dosages on filter cake dry solids production rate (mass throughput).

A closer look at the role of A-PAM revealed its primary function as a “catalyst” for higher rates of filter cake production. **Fig. 6.2** demonstrates the extents of mass-based throughput enhancement for using 500 g/t A-PAM compared to 300 g/t. Effects range from ~18% more dry solids at zero C-PAM to ~35% more at 1000 g/t C-PAM. Although it appeared at the same A-PAM dosage, increasing C-PAM dosages also appeared to improve dry solids throughput. However this was a direct consequence of increased cake

dry solids content and subsequently, higher cake density. As discussed in **section 6.1.1**, more usage of the A-PAM across all C-PAM dosages tested caused little difference in cake dry solids content. By assuming a constant dry solids density of 2650 kg/m^3 and 1000 kg/m^3 for water, the weight-based production data in **Fig. 6.2** can be converted to volumetric basis (detailed steps in **section 6.3.2.2**), as shown in **Fig. 6.3**.

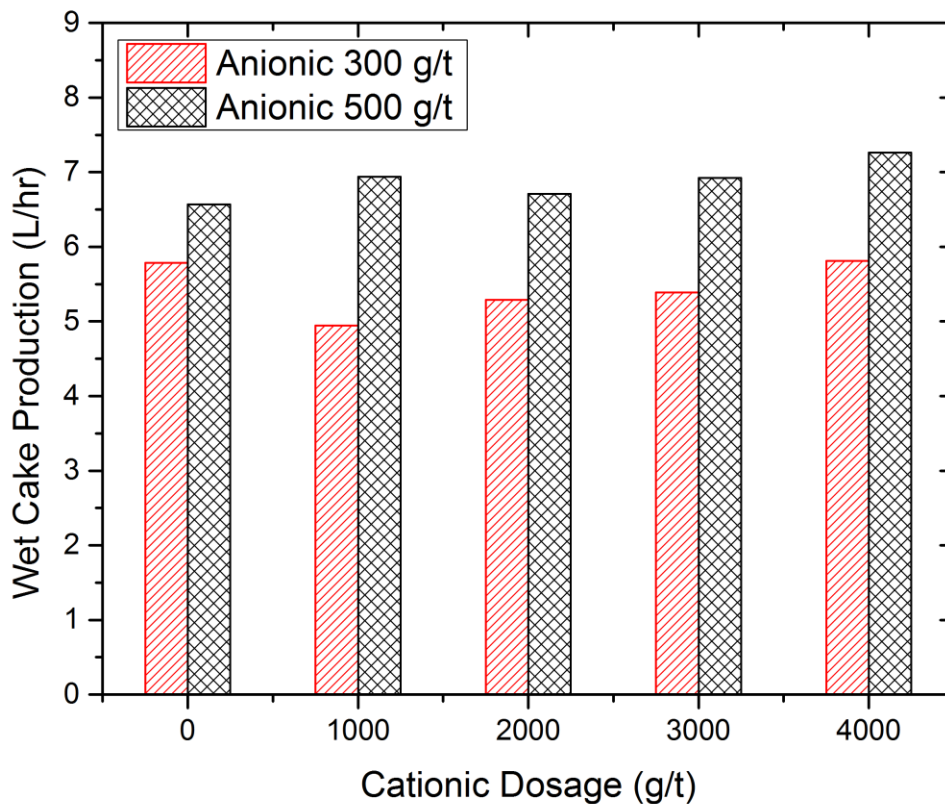


Figure 6.3. Impact of A-PAM and C-PAM dosages on filter cake dry solids production rate (volumetric throughput).

It is evident from **Fig. 6.3** that application of 500 g/t A-PAM significantly increased the *volumetric* flow of cake products than those cases with 300 g/t A-PAM. In contrast,

higher dosages of C-PAM had no clear impact on the volume-based cake throughput. Therefore the role of A-PAM dosage is positively correlated to the bulk movement ability of sediments – in other words, *plasticity of dewatering*.

6.1.3. Filtrate quality

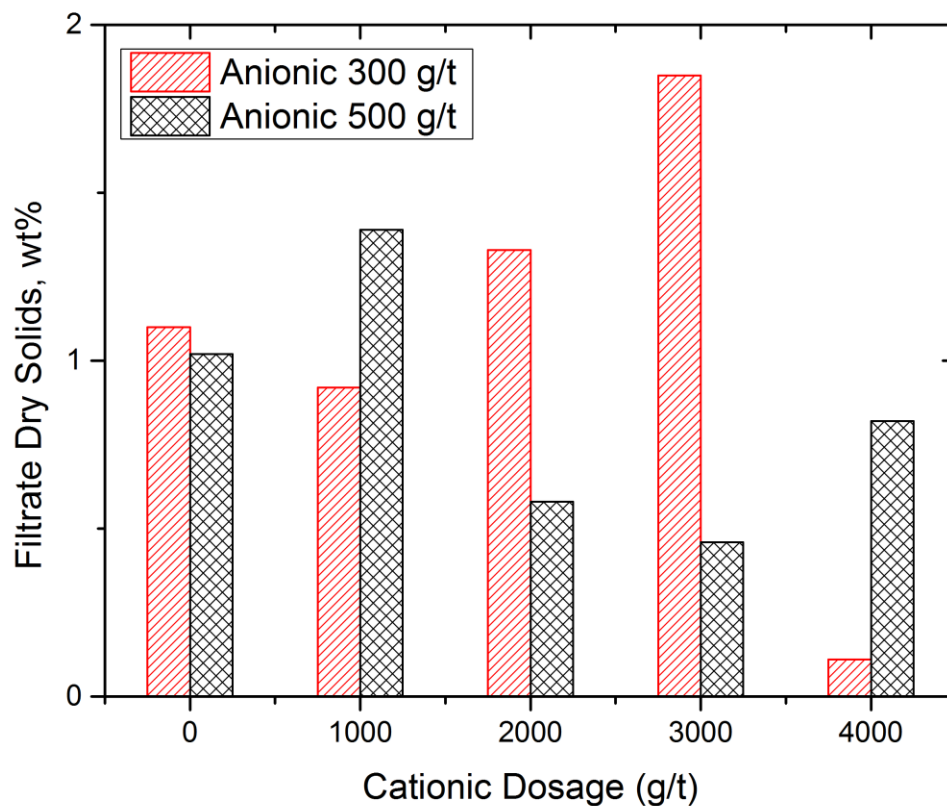


Figure 6.4. Impact of A-PAM and C-PAM dosages on filtrate quality.

It was expected that, with the use of higher doses of C-PAM, greater amounts of suspended solids would be flocculated and removed from the feed slurry. This would result in much lower solids in the supernatant as well as the resultant filtrate.

Unfortunately, four practical factors severely limited the extent of suspended solids removal in normal operations.

1. Low concentration of divalent cations in the Horizon pond water hindered the coagulation of suspended solids.
2. Low D_{50} and high clay-to-water ratio in Horizon MFT.
3. Filtrate stream always washed past the volute plate runoff materials, which re-captured some of the solids (see **section 6.1.4**).
4. VSP was operated intermittently by automatic controls, resulting in over-shearing of flocs and re-dispersion of flocculated solids (see **section 6.3.1**).

Therefore, no clear trend in filtrate quality can be observed against different A-PAM or C-PAM dosages in **Fig. 6.4**. Only one of the formal experiment cases (A300-C4000) matched the previous expectations.

For future VSP studies it may be best to sample the filtrate stream more frequently and at multiple locations along the DP unit once the circuit stabilizes.

6.1.4. Volute plate runoff losses

Runoff materials are a by-product of the volute plate self-cleaning cycle. During normal operations, sediment at interior of the DP unit is compressed against the volute plates, which can leave a minor amount of solids in the drainage slits. The self-cleaning cycle constantly ejects these fugitive solids from the drainage slits and keeps the filter medium clean for unimpeded outflow of filtrate.

There are a number of reasons for a VSP operator to monitor the runoff materials.

1. To gauge the internal compression stress of the DP. Too much stress will cause severe loss of solids via runoff, as well as excessive wear to the volute plates and auger screw.
2. To quickly estimate the product cake dry solids content. It was observed that higher cake dry solids caused – intuitively – an increase of dry solids content in the runoff material.

Generally speaking, as long as the dry solids mass flow ratio between the runoff stream and product cake stream is small, both can be co-mixed for deposition without reducing the mixture solids content over a tolerance limit. Suppose an arbitrary but reasonable 2% limit is proposed (for example, co-mix runoff with 60 wt% cake such that the mixture contains at least 58 wt% dry solids), it was estimated that the threshold runoff-to-cake dry solids ratio would be ~10% based on actual operating data, as shown in **Table 6.1**. As observed from columns *C* and *F*, none of the formal cases in the field study exceeded the aforementioned target, suggesting the DP unit was indeed operating normally.

Table 6.1. Process data for runoff calculations. Operating scenario is desired if data in column *C* and column *F* differ by $\leq 2\%$.

<i>A</i>	<i>B</i>	<i>C</i>	<i>D</i>	<i>E</i>	<i>F</i>	<i>G</i>
Case	Cake (kg/h)	Cake solids (wt% dry)	Runoff (kg/h)	Runoff solids (wt% dry)	Mixture solids (wt% dry)	Runoff-to-cake dry solids ratio
A300	8.40	50.00%	0.69	42.00%	49.39%	6.90%
A300-C1000	7.62	56.43%	0.72	43.52%	55.32%	7.29%
A300-C2000	8.22	57.27%	0.78	43.08%	56.04%	7.14%
A300-C3000	8.55	59.43%	0.98	43.21%	57.77%	8.29%
A300-C4000	9.40	61.33%	1.07	47.03%	59.87%	8.70%
A500	9.66	51.37%	0.82	41.12%	50.57%	6.76%
A500-C1000	10.56	55.05%	0.73	42.29%	54.23%	5.30%
A500-C2000	10.40	57.02%	1.01	43.86%	55.85%	7.50%
A500-C3000	11.04	59.87%	1.44	44.36%	58.08%	9.66%
A500-C4000	11.56	59.75%	0.90	45.18%	58.70%	5.89%

In addition to the aforementioned positive dependence between cake product and runoff dry solids content, the following observations can be made.

1. All A300 cases showed a gradual increase in the runoff-to-cake dry solids ratio as C-PAM dosage is increased. This suggests a gradual ramp-up in the internal DP stress which coincided with the densification of product cake.
2. All A500 cases followed similar trend until the maximum C-PAM dosage was applied (A500-C4000). The sudden drop in runoff-to-cake dry solids ratio may be a result of sampling errors in the determination of runoff flow rate for the previous case (A500-C3000). A runoff production rate of 1.44 kg/h seems abnormally high and requires further verification.

3. There is little difference in terms of runoff production between A300 and A500 cases.

6.2. Effects of other adjustable operating parameters (6 trial cases)

Table 6.2 presents operating results for trial cases T1 – T6.

Table 6.2. Operating results for six trial cases.

Case	Cake (kg/h)	Cake solids (wt% dry)	Filtrate solids (wt% dry)	Runoff solids (wt% dry)	Runoff-to-cake dry solids ratio
T1	7.44	48.36%	3.26%	43.01%	5.38%
T2	5.76	61.62%	0.90%	47.66%	24.71%
T3	4.29	59.36%	1.82%	45.64%	41.26%
T4	9.60	58.73%	0.82%	45.91%	5.37%
T5	7.80	64.57%	1.72%	46.57%	9.99%
T6	6.60	61.59%	1.34%	46.07%	10.88%

6.2.1. Full recycle operating mode

It is of interest to reduce fresh pond water intake by the VSP process with the full water recycle operating mode. By comparing trial cases T1 and T4 respectively against formal cases A300 and A300-C4000, the following effects can be observed.

1. Reduction in cake dry solids, compared to A300 (50 wt%) and A300-C4000 (61.33 wt%).
2. Increased filtrate solids, versus A300 (1.10 wt%) and A300-C4000 (0.25 wt%).
3. Reduced runoff-to-cake dry solids ratio, from A300 (6.90%) and A300-C4000 (8.70%).

Overall, the VSP circuit would suffer from minor degradation in cake quality and significantly worse filtrate quality if fresh pond water is replaced by filtrate for flocculant solution preparation. As the filtrate contains increased amount of dry solids that pre-emptively adsorbs to the flocculant molecules prior to use in the VSP, efficacy of the resultant flocculant solution is suppressed. This decreases the actual flocculant dosage delivered to the feed MFT slurry and causes the aforementioned performance deteriorations. For long-term operations under the full recycle mode, it is recommended to dose extra amount of A-PAM and C-PAM solutions or dry powders (during preparation) in order to offset the decrease in solution efficacy.

In general, it is more prudent to reuse the filtrate only for feed MFT dilution, and only use fresh pond water for flocculant preparation, as the latter process has shown to be extremely sensitive to water quality.

6.2.2. Flocculant solution preparation time

The C-PAM flocculant has been known to undergo ageing in its aqueous solution, which causes an increase in its flocculation performance at the same applied dosage (Wang, et al., 2016). On the other hand, no efficacy change was previously observed for ageing of A-PAM solution. The following are found by comparing trial cases T5 and T4 (under full recycle mode).

1. Significant increase in cake dry solids, from T4 (58.73 wt%).
2. Reduced dry solids mass throughput, compared to T4 (5.64 kg/h).
3. Elevated filtrate dry solids, versus T4 (0.82 wt%).

4. Nominally acceptable runoff-to-cake dry solids ratio, as opposed to T4 (5.37%)

Relevant operating data for trial case T5 indeed confirmed the C-PAM ageing phenomenon, which helped to achieve the maximum cake dry solids content encountered in the field study (64.57 wt%). Both observations 2 and 4 above suggest an increase in the DP internal stress that reflects the production of the much denser cake. However, the filtrate dry solid content was determined to be unacceptably high for further flocculant solution preparation.

For future studies, it may be of benefit to extend the preparation time of both A-PAM and C-PAM solutions to 15 hours or more in order further verify the above discovery.

6.2.3. Endplate gap distance

It was hypothesized that adjustment of endplate gap would dramatically affect the DP internal stress and therefore affect cake dry solids. The gap was reduced from 2 mm in formal case A300-C3000 to 1 mm for trial case T2. The following was observed.

1. Increased cake dry solids, versus A300-C3000 (59.43 wt%).
2. Significant loss of cake throughput, from A300-C3000 (8.55 kg/h).
3. Dramatic increase in runoff-to-cake dry solids ratio, compared to A300-C3000 (8.29%).
4. Reduced filtrate solids, as opposed to A300-C3000 (1.85 wt%).

Improvements in cake dry solids were discovered as gap distance was reduced. However, this drastically increased the amount of runoff materials beyond normally acceptable range and subsequently suppressed cake throughput. Interestingly the filtrate quality was

unaffected by the exodus of runoff from the drainage slits, which may be attributed to insufficient filtrate sampling. In consideration with the overall cake production process, it is not recommended to use endplate gap distances smaller than 2 mm with the current volute plate setup.

6.2.4. FT mixer speed

The sweeping action of the large and wide FT mixer blades is the primary mechanism for sending the flocculated slurry towards the overflow weir and into the DP unit. Therefore, adjusting the FT mixer speed should have an impact on cake production. Both trial cases T3 and T6 involve slowing down the FT mixer to 45 RPM with the following effects.

1. Reduction in cake dry solids, from trial cases T2 (61.62 wt%) and T5 (64.57 wt%).
2. Further reduced dry solids throughput, as opposed to T2 (3.55 kg/h) and T5 (5.04 kg/h).
3. Increased runoff-to-cake dry solids ratio, versus T2 (24.71%) and T5 (9.99%).
4. Filtrate quality fluctuated, possibly due to insufficient sampling.

Thus it is best to operate the FT mixer at maximum allowed speed of 60 RPM in order to transfer more materials to the DP unit in a given amount of time. However, this necessitates the use of flocculants that can generate flocs with increased tolerance for shearing.

6.3. Process mass balance (10 formal cases)

6.3.1. Process and stream analyses

Figure 6.5 shows the overall process flow of the entire VSP circuit. For the purposes of mass balance, each process stream is considered to contain two material species: dry solids (DS) and water (W). Note that any fugitive bitumen throughout the circuit is treated as dry solids in terms of flocculation and compressive dewatering. Additional details about each process stream have been listed in **Table 6.3**.

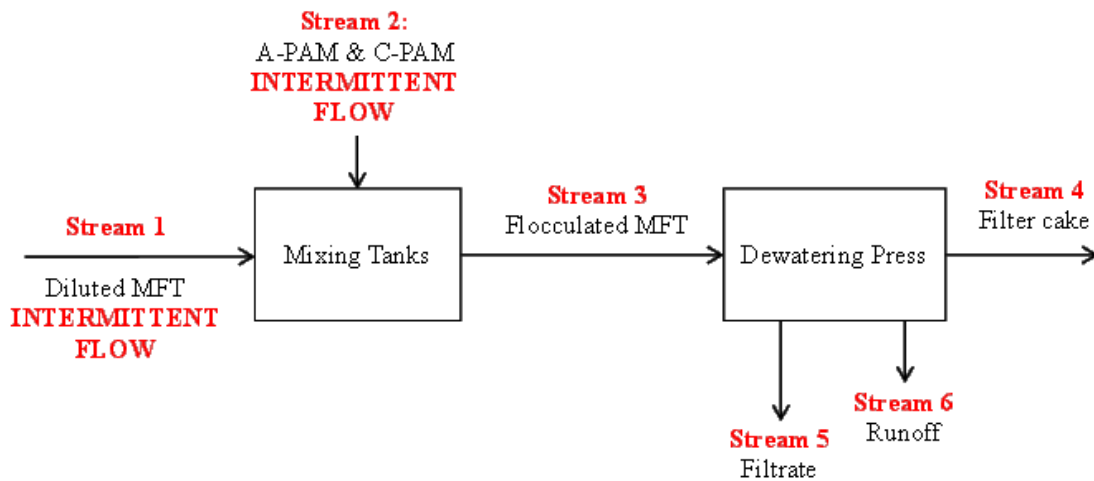


Figure 6.5. Process flow diagram of the VSP circuit.

Table 6.3. Details of each process stream in the VSP circuit.

Stream	Dry solids	Mass flow rate	Continuous or Intermittent Service
1	Sampled	Known instantaneous rate	Intermittent
2	Negligible	Known instantaneous rate	Intermittent
3	Same as S1	Unknown	Continuous
4	Assayed	Assayed	Continuous
5	Assayed	Unknown	Continuous
6	Assayed	Assayed	Continuous

As both Streams 1 and 2 were at intermittent service mode for all 10 formal experiments, it was not possible to directly determine the actual mass flow per hour for these two streams. Instead, a workaround was developed to partially solve Stream 3 with available information from Streams 1 and 2. Subsequently there was sufficient information to fully complete the mass balance and material distributions around the Dewatering Press. Finally, time-averaged mass flows of Streams 1 and 2 were found with the help from now-known Stream 3, plus several verifiable assumptions.

6.3.2. Detailed calculations

6.3.2.1. Assumptions

Three major assumptions were used for all subsequent analyses. First, dry solids content in Stream 1 was always taken to be a constant 5 wt%. Although Stream 1 was not assayed on a regular basis throughout the test due to time and apparatus constraints, Stream 1 was

sampled three times across three separate days during the field study. Results indicate an average DS of 4.8 ± 0.3 wt%, which validates the previous assumption.

Next, there shall be negligible dry solids contributions from Stream 2. It was observed that any solids present in pond water (or filtrate for full recycle mode) were preemptively flocculated during flocculant solutions preparation. These flocculated solids settled to the bottom of solution drums for both A-PAM and C-PAM and were not pumped into the VSP circuit. As a result, the second assumption was also considered to be valid.

Lastly, there was no material leak from the Mixing Tanks or the Dewatering Press. Evaporative losses of water throughout VSP circuit were assumed to be negligible.

6.3.2.2. Dry solids in Dewatering Press feed (Stream 3)

As described in **Chapter 2**, slurry level in the flocculation tank (FT) is used to control the operations of the VSP under automatic mode. If the FT level is low, both Streams 1 and 2 remain in operation at their respective instantaneous flow rates. Otherwise Streams 1 and 2 are simultaneously shut off once the FT level is high. Therefore, it is apparent that dry solids content of the mixture slurry in the FT is not affected by such intermittent service mode.

For all VSP process streams in MFT dewatering service, it was possible to convert between mass flow and volume flow by assuming a constant dry solids density of 2650 kg/m^3 and water density of 1000 kg/m^3 , as shown in **section 6.1.2**. Given the

instantaneous volumetric flow rate for Stream 1 was 0.4 m³/h (at 5 wt% DS), the corresponding instantaneous mass and DS flow rates was determined as follows.

$$\rho_1 = \frac{100 \text{ kg slurry basis}}{\frac{5 \text{ kg DS}}{2650 \text{ kg/m}^3} + \frac{95 \text{ kg W}}{1000 \text{ kg/m}^3}} = 1032.13 \text{ kg/m}^3 \quad (6.1)$$

$$\dot{m}_{1,inst} = \rho_1 \dot{V}_{1,inst} = 1032.13 \frac{\text{kg}}{\text{m}^3} * 0.4 \frac{\text{m}^3}{\text{h}} = 412.85 \text{ kg/h} \quad (6.2)$$

$$\dot{m}_{1,DS,inst} = DS_1 * \dot{m}_{1,inst} = 0.05 \dot{m}_{1,inst} = 20.64 \text{ kg/h} \quad (6.3)$$

For Stream 2, both A-PAM and C-PAM solution streams were dosed according to **Eq. 6.3** for all 10 formal cases, as follows.

$$\frac{\dot{m}_{2,A-PAM,inst} * 300 \text{ ppmw}}{\frac{\dot{m}_{1,DS,inst}}{1000 \text{ kg/t}}} = 300 \text{ or } 500 \frac{\text{g dry A - PAM}}{\text{t DS}} \quad (6.4)$$

$$\frac{\dot{m}_{2,C-PAM,inst} * 2000 \text{ ppmw}}{\frac{\dot{m}_{1,DS,inst}}{1000 \text{ kg/t}}} = 0, 1000 \text{ or } 2000 \text{ or } 3000 \text{ or } 4000 \frac{\text{g dry C - PAM}}{\text{t DS}} \quad (6.5)$$

After a desired dosage combination has been selected, it becomes possible to calculate the combined instantaneous mass flow rate for Stream 2, and subsequently, Stream 3. Ultimately one may obtain the corresponding DS content for all dosage cases in Stream 3, as shown in **Table 6.4** via **Eq. 6.6**.

$$DS_3 = \frac{\dot{m}_{3,DS,inst}}{\dot{m}_{3,inst}} = \frac{\dot{m}_{1,DS,inst} + \dot{m}_{2,DS,inst}}{\dot{m}_{1,inst} + \dot{m}_{2,inst}} = \frac{\dot{m}_{1,DS,inst}}{\dot{m}_{1,inst} + \dot{m}_{2,inst}} \quad (6.6)$$

Table 6.4. Determination of dry solids content for Stream 3.

<i>A</i>	<i>B</i>	<i>C</i>	<i>D = B + C</i>	<i>E</i>	<i>F</i>
Case	A-PAM (kg/h, inst.)	C-PAM (kg/h, inst.)	Stream 2 (kg/h, inst.)	Stream 1 (kg/h, inst.)	Dry solids of Stream 3 (wt%)
A300	20.64	0	20.64	412.85	4.762%
A300- C1000	20.64	10.32	30.96	412.85	4.651%
A300- C2000	20.64	20.64	41.29	412.85	4.545%
A300- C3000	20.64	30.96	51.61	412.85	4.444%
A300- C4000	20.64	41.29	61.93	412.85	4.348%
A500	34.40	0	34.40	412.85	4.615%
A500- C1000	34.40	10.32	44.73	412.85	4.511%
A500- C2000	34.40	20.64	55.05	412.85	4.412%
A500- C3000	34.40	30.96	65.37	412.85	4.317%
A500- C4000	34.40	41.29	75.69	412.85	4.225%

6.3.2.3. Mass and material flows of Dewatering Press

Equations 6.7 and 6.8 respectively show the continuous mass and DS balances around the Dewatering Press.

$$\dot{m}_3 = \dot{m}_4 + \dot{m}_5 + \dot{m}_6 \quad (6.7)$$

$$DS_3 \dot{m}_3 = DS_4 \dot{m}_4 + DS_5 \dot{m}_5 + DS_6 \dot{m}_6 \quad (6.8)$$

At this point, the only unknown quantities are \dot{m}_3 and \dot{m}_5 . Thus it is possible to solve for both unknowns and complete the mass and DS balances.

Since \dot{m}_5 is an intrinsically continuous service stream, **Eq. 6.7** was used in **Eq. 6.8** to eliminate \dot{m}_3 and solve for \dot{m}_5 as follows.

$$DS_3(\dot{m}_4 + \dot{m}_5 + \dot{m}_6) = DS_4\dot{m}_4 + DS_5\dot{m}_5 + DS_6\dot{m}_6 \quad (6.9)$$

Equation 6.10 was subsequently obtained by re-arranging **Eq. 6.9**.

$$\dot{m}_5 = \frac{(DS_4 - DS_3)\dot{m}_4 + (DS_6 - DS_3)\dot{m}_6}{DS_3 - DS_5} \quad (6.10)$$

Therefore, mass flow rate of filtrate for all 10 formal cases were determined with the corresponding values of DS_3 from **Table 6.4**, as well as assay values obtained during the field study. Afterwards, **Eq. 6.7** was used again to find the time-averaged “continuous” mass flow rates of Stream 3. **Table 6.5** presents the completed mass and DS balances for the Dewatering Press of the VSP circuit. These results were subsequently used for all upcoming analyses in this chapter.

Table 6.5. Mass and dry solids balances for Dewatering Press.

CASE	DP FEED (STREAM 3)		FILTER CAKE (STREAM 4)		FILTRATE (STREAM 5)		RUNOFF (STREAM 6)	
	kg/h	<i>DS</i> wt%	kg/h	<i>DS</i> wt%	kg/h	<i>DS</i> wt%	kg/h	<i>DS</i> wt%
A300	120	4.8%	8.4	50.0%	111	1.10%	0.7	42.0%
A300 – C1000	122	4.7%	7.6	56.4%	113	0.92%	0.7	43.5%
A300 – C2000	153	4.6%	8.2	57.3%	144	1.33%	0.8	43.1%
A300 – C3000	205	4.4%	8.6	59.4%	196	1.85%	1.0	43.2%
A300 – C4000	152	4.4%	9.4	61.3%	142	0.25%	1.1	47.0%
A500	144	4.6%	9.7	51.4%	134	1.02%	0.8	41.1%
A500 – C1000	191	4.5%	10.6	55.1%	180	1.39%	0.7	42.3%
A500 – C2000	165	4.4%	10.4	57.0%	153	0.58%	1.0	43.9%
A500 – C3000	186	4.3%	11.0	59.9%	174	0.46%	1.4	44.4%
A500 – C4000	212	4.2%	11.6	59.8%	199	0.82%	0.9	45.2%

6.3.2.4. Mass and material flows in Mixing Tanks

With information from **Table 6.5**, time-averaged “continuous” flow rates of Streams 1 and 2 can be found. In addition to completing the circuit balances around the Mixing Tanks of the VSP, these flow rates allow the determination of the average VSP uptime under intermittent service. **Equations 6.11** and **6.12** shows the mass and DS balances around the Mixing Tanks assuming the material flows were fully continuous.

$$\dot{m}_1 = \dot{m}_2 + \dot{m}_3 \quad (6.11)$$

$$DS_1\dot{m}_1 = DS_2\dot{m}_2 + DS_3\dot{m}_3 = DS_3\dot{m}_3 \quad (6.12)$$

Since DS_1 , DS_3 , and \dot{m}_3 are already known for all dosage cases, it becomes fairly straightforward to solve for \dot{m}_1 and \dot{m}_2 . **Table 6.6** presents the corresponding results.

Table 6.6. Mass and dry solids balances for Mixing Tanks (continuous basis).

CASE	M. TANKS FEED (STREAM 1)		FLOCCULANTS (STREAM 2)		DP FEED (STREAM 3)	
	kg/h	<i>DS</i> wt%	kg/h	<i>DS</i> wt%	kg/h	<i>DS</i> wt%
A300	114	5.0%	5.7	0	120	4.8%
A300 – C1000	113	5.0%	8.5	0	122	4.7%
A300 – C2000	139	5.0%	13.9	0	153	4.6%
A300 – C3000	182	5.0%	22.8	0	205	4.4%
A300 – C4000	132	5.0%	19.9	0	152	4.4%
A500	133	5.0%	11.1	0	144	4.6%
A500 – C1000	172	5.0%	18.7	0	191	4.5%
A500 – C2000	145	5.0%	19.4	0	165	4.4%
A500 – C3000	161	5.0%	25.5	0	186	4.3%
A500 – C4000	179	5.0%	32.8	0	212	4.2%

The VSP operational uptime can be determined by the ratio between time-averaged Stream 1 flow rates in **Table 6.6** against the instantaneous flow rate setpoint of 412.85 kg/h, as shown in **Table 6.7**. In general, it is highly desired to operate the VSP as possibly close to 100% uptime in order to maximize dry solids throughput in a timely manner. Also, such an operating scenario would minimize residence time of flocculated solids in the flocculation tank (FT), which avoids over-shearing of flocs. Once the “high slurry level” event triggers in the FT, it was observed that no flocculants or dilute MFT would enter the Mixing Tanks. Consequently, the flocculated solids undergo prolonged mixing in the CT and FT before being processed by the downstream DP.

Therefore, minimizing the delay between floc production and sediment dewatering (by maximizing device uptime) will help to maintain the general floc size and integrity, both of which may contribute to higher DS in the filter cake product at the same flocculant dosage. However, any direct connections between cake product DS content and device uptime (at the same dosage) are outside the scope of the current study.

Table 6.7. Average VSP operational uptime under automatic mode.

Case	Average VSP uptime, %
A300	27.65%
A300-C1000	27.40%
A300-C2000	33.72%
A300-C3000	44.20%
A300-C4000	32.08%
A500	32.28%
A500-C1000	41.76%
A500-C2000	35.19%
A500-C3000	38.99%
A500-C4000	43.36%

6.3.3. Dry solids distribution in Dewatering Press

For most chemical engineering processes it is very important to know the conversion rate of feed materials to desired products and by-products. In terms of VSP for MFT dewatering service, the material of interest is DS. The following parameters were developed to better understand the process efficiency of the VSP Dewatering Press (as the conversion between wet sediment into dry cake only happens there).

Equation 6.13 is the generalized method for determination of single-pass DS conversion (X) between any two continuous streams A and B . Here, stream B has been assigned as the basis stream (Stream 3), whose corresponding values have been previously determined in **Table 6.5**.

$$X_A = \frac{DS_A \dot{m}_A}{DS_B \dot{m}_B} = \frac{DS_A \dot{m}_A}{DS_3 \dot{m}_3} \quad (6.13)$$

For instance, to determine the single-pass DS conversion from Stream 3 to filter cake (Stream 4), simply replace $DS_A \dot{m}_A$ by $DS_4 \dot{m}_4$ in **Eq. 6.13**. Results for all DP output streams (4, 5, and 6) are shown in **Table 6.8** in the form of DS distribution.

Table 6.8. Dry solids distribution in Dewatering Press.

CASE	DP FEED (STREAM 3)		FILTER CAKE (STREAM 4)		FILTRATE (STREAM 5)		RUNOFF (STREAM 6)	
	kg DS/h	X%	kg DS/h	X%	kg DS/h	X%	kg DS/h	X%
A300	5.7	100%	4.2	74%	1.2	21%	0.29	5.1%
A300 – C1000	5.7	100%	4.3	76%	1.0	18%	0.30	5.4%
A300 – C2000	7.0	100%	4.7	67%	1.9	28%	0.34	5.0%
A300 – C3000	9.1	100%	5.1	56%	3.6	40%	0.43	4.7%
A300 – C4000	6.6	100%	5.8	87%	0.4	5.4%	0.52	7.8%
A500	6.7	100%	5.0	75%	1.4	21%	0.33	4.9%
A500 – C1000	8.6	100%	5.8	68%	2.5	29%	0.30	3.4%
A500 – C2000	7.3	100%	5.9	81%	0.9	12%	0.44	6.0%
A500 – C3000	8.0	100%	6.6	82%	0.8	10%	0.62	7.7%
A500 – C4000	9.0	100%	6.9	77%	1.6	18%	0.41	4.5%

As discussed in **section 6.1**, additional C-PAM helped in producing progressively dry filter cake. Here, it also seems to improve the single-pass DS conversion from Stream 3 to Stream 4 by reducing the DS lost in Stream 5 while the losses to Stream 6 fluctuates around 5.6% (A300 cases) and 5.3% (A500 cases). For the case A300-C3000 there seems to be a great deal of deviation from the aforementioned trend, which is likely a result of sampling error in determining the DS content of Stream 5. Nevertheless the VSP circuit achieved an average single-pass DS conversion of 74.3% across the 10 formal cases prior to any sort of process or equipment optimization. Since the feed MFT contains essentially no sand in the field study, the $< 44 \mu\text{m}$ fines capture rate of the VSP is the same (74.3%). This value is critical in evaluating the potential of any MFT dewatering process, for which the VSP shows great promise.

6.3.4. Water balance

To quantitatively determine whether the VSP circuit achieved net surplus or deficit of water across all 10 formal cases on a continuous basis, consider the following internal process steps.

1. Filtrate was produced as Stream 5, with flow rates and solids contents in **Table 6.5**.
2. Stream 5 was diverted into Streams 5A and 5B for recycle.
3. Stream 5A was used to dilute feed MFT from 30 wt% to 5 wt%.
4. Stream 5B was returned to tailings pond for clarification.

5. An equal mass of pond water as Stream 5B was withdrawn elsewhere from the same tailings pond. Subsequently it was used in the preparation of flocculant solutions.
6. Flow rate of Stream 5B is exactly equal to that of Stream 2 in **Table 6.6**. Masses of dry A-PAM or C-PAM powders are negligible in their respective solutions.

Note that the actual course of action in the field study involved storage of Stream 5 in the test facility and withdrawing Stream 5A from said storage. Additionally, pond water was provided in separate containers. So, steps 4 and 5 never occurred in the field study operations, rather it has been included as intermediate hypothetical (and plausible) stages that simplifies the water cycle analysis. Based on the above considerations, the net change in water due to the operation of VSP can be determined by comparing the flow rate of Stream 5 against those of Streams 5A and 5B.

First, Stream 5A is solved using information from Streams 1 and 5, feed MFT, and dilution target.

$$DS_{5A}\dot{m}_{5A} + DS_{MFT}\dot{m}_{MFT} = DS_1\dot{m}_1 \quad (6.14)$$

Equation 6.14 can be further simplified by substituting known relations and quantities.

$$DS_5\dot{m}_{5A} + 0.3\dot{m}_{MFT} = 0.05\dot{m}_1 \quad (6.15)$$

Mass balance in **Eq. 6.16** is used in conjunction with data from **Tables 6.5** and **6.6** to determine the mass flows of Stream 5A and feed MFT across the 10 formal cases.

$$\dot{m}_{5A} + \dot{m}_{MFT} = \dot{m}_1 \quad (6.16)$$

Combined with the water requirement of flocculant solutions in **Table 6.6**, the following **Table 6.9** shows the overall water balance around the VSP circuit. A negative flow rate has been assigned in case of water demand (i.e. Streams 5A and 5B), whereas a positive flow indicates water supply (Stream 5).

Table 6.9. Water balance for the VSP circuit.

CASE	FILTRATE (STREAM 5)		DILUTION (STREAM 5A)		FLOCCULANTS (STREAM 5B)		NET CHANGE	
	kg/h	<i>DS</i> wt%	kg/h	<i>DS</i> wt%	kg/h	<i>DS</i> wt%	kg/h	%
A300	111	1.10%	-99	1.10%	-5.7	0	6.67	6.01%
A300 – C1000	113	0.92%	-97	0.92%	-8.5	0	7.37	6.53%
A300 – C2000	144	1.33%	-121	1.33%	-13.9	0	8.89	6.18%
A300 – C3000	196	1.85%	-162	1.85%	-22.8	0	11.57	5.90%
A300 – C4000	142	0.25%	-111	0.25%	-19.9	0	11.18	7.87%
A500	134	1.02%	-115	1.02%	-11.1	0	8.17	6.09%
A500 – C1000	180	1.39%	-150	1.39%	-18.7	0	11.00	6.11%
A500 – C2000	153	0.58%	-123	0.58%	-19.4	0	10.38	6.79%
A500 – C3000	174	0.46%	-136	0.46%	-25.5	0	12.24	7.04%
A500 – C4000	199	0.82%	-153	0.82%	-32.8	0	12.84	6.45%

Clearly, net water surplus was achieved for all 10 formal experiment cases.

Quantitatively the excess water averaged about 6.5 wt% of produced filtrate from the Dewatering Press. Increasing A-PAM or C-PAM dosages did not result in significant changes to the ratio of surplus water.

References

Wang, C. et al., 2016. Role of pre-conditioning cationic Zetag® flocculant in enhancing MFT flocculation. *Energy Fuels*, 30(7), p. 5223–5231.

Chapter 7: Predictive Modeling of VSP Filter Cake Quality

7.1. Correlations between CVST results and VSP filter cake quality

In this study, extreme emphasis was placed on maximizing the VSP filter cake DS as well as the *a priori* prediction of VSP filter cake DS. **Figure 7.1** shows the relations between the average measured sediment CDI and corresponding VSP filter cake quality for all 10 formal experiment cases. A clear linear correlation exists between the two quantities for experiment cases with both A-PAM and C-PAM added. However, cases with no C-PAM (A300/A500) do not follow this correlation at all.

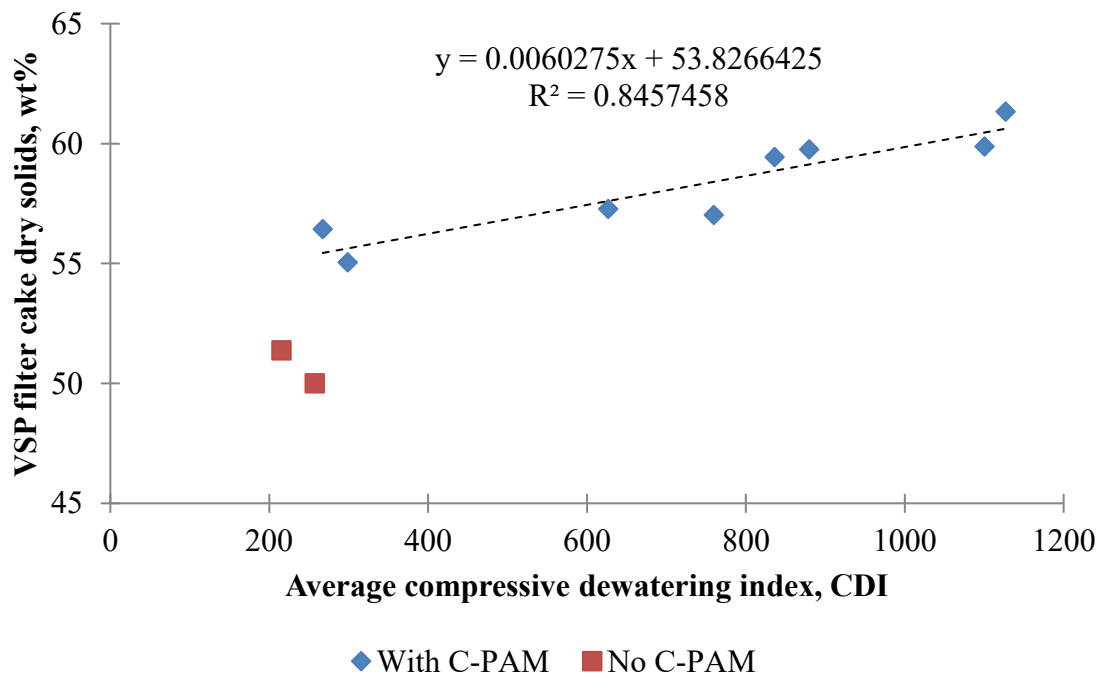


Figure 7.1. Correlation between average sediment CDI and VSP filter cake quality.

Since the derivation of CDI assumes a linear stress-strain response for sediments undergoing compressive dewatering, it would appear that cases A300 and A500 do not

satisfy the elasticity assumption. Therefore, sediments for A300 and A500 must be non-elastic for compressive dewatering. In other words, they are significantly plastic sediments and their respective CDI values have no real physical meaning compared to other experiment cases.

As discussed in **Chapter 5**, in the absence of C-PAM, the MFT sediment was found to be extremely prone to rupture, which again indicated plasticity for compressive dewatering. Thus, at similar CDI values of 200-300 but without C-PAM, the VSP was unable to produce ~55 wt% DS cake as predicted by the linear correlation in **Fig. 7.1**. Once sediments acquire elasticity for dewatering via the use of C-PAM, correlation between CDI and expected VSP filter cake DS becomes valid.

To emphasize, it can be concluded that the introduction of C-PAM to Horizon MFT slurry (already flocculated by A-PAM) brought a definitive change to the sediment dewatering behavior. When subjected to mechanical compression by the CVST, any vertical strain imposed on such sediment will produce a linear response in the compressive stress. The slope of such linear response (CDI) can be confidently used for *a priori* prediction of dewatering performance with the actual VSP device. Higher values of CDI are desired as the contained sediment can absorb more stress per vol% of applied strain by releasing water. Lower values of CDI are indicative of poor VSP performance as the sediment is able to sustain limited amount of stress per vol% of applied strain. Any additional strain will cause the low-CDI sediment to flow instead of further releasing water.

7.2. CDI gain

Once a flocculated sediment acquires dewatering elasticity, the dependence of solids content in VSP cake on CDI (i.e. slope of the best-fit line in **Fig. 7.1**) is currently expected to be characteristic of the slurry material only. Such rate is hereby termed as the *CDI gain* of a given slurry system undergoing flocculation. For a dual-flocculant system such as in this study, the CDI gain of the flocculant pair is meaningful only if the A-PAM is added first to the slurry followed by C-PAM, as was done in the CVST study and VSP field study. Based on **Fig. 7.1**, the CDI gain of sediments upon addition of C-PAM (for dilute Horizon MFT already flocculated by A-PAM) is ~0.6 wt% increase in VSP filter cake DS per 100 unit of increase in average sediment CDI. Equivalently, for the A-PAM and C-PAM tested, every 165.9 (~166) units of increase in average CDI will increase VSP cake DS by 1 wt%.

For simplicity of use, the numeric value of CDI gain will be expressed in the latter manner – the necessary increase in CDI in order to yield a 1 wt% increase in VSP cake DS. Therefore in this study, the CDI gain was determined to be 166.

Note that the value of CDI gain is currently considered as a slurry-specific parameter, and lower CDI values (than 166) are believed to be beneficial in VSP operations. Additional studies should be carried out on more types of flocculants and/or slurries to determine such relations.

Chapter 8: Conclusions and Knowledge Contributions

Chapter 8 summarizes the major findings from preliminary, field, and bench-scale studies. Original contributions to scientific knowledge from this work are stated after the summaries. Also, aspects of possible future work are suggested here.

8.1. Early VSP trials (Phase 1)

Although not mentioned in great detail, the preliminary studies have been instrumental for the subsequent success of our field work. These early trials – while lacking in sufficient materials for properly determining the steady-state time for filter cake DS – nevertheless helped to pinpoint the limitations of the VSP device. These discoveries proved to be invaluable for the field experiment planning and execution.

In terms of feed materials, several observations were noted as follows.

1. The MFT from Coanda / Suncor (which were used in the beginning of the preliminary study) flocculates very differently than Horizon MFT (tested at the end of preliminary study) using the same A-PAM and C-PAM. It was discovered that at similar dosage combinations as outlined in **Chapter 3**, Horizon MFT must be diluted to 5 wt% DS for satisfactory flocculation performance (see **Chapter 5**), whereas Coanda / Suncor MFT only requires dilution to 10 wt% DS.
2. MFT that comes with noticeable amount of sand will cause problems all over the feed dilution and transport circuit. For example, sand accumulation occurred at the bottom of the dilution tank, at which the feed was supposedly to be

withdrawn. This caused immediate plugging and termination of feed materials into the VSP. Fortunately the problem was circumvented via a standing pipe (courtesy of Mr. Artin Afacan at the University of Alberta). Sand accumulation also significantly complicated the shutdown and cleanup efforts.

3. Residual bitumen in MFT – while also complicates cleanup efforts – will not cause pipe plugging, and would become part of the polymer-solids flocs for compression in the VSP Dewatering Press. In normal operation, any bitumen present at the Dewatering Press drainage slits will be rubbed into a thin film via volute plate self-cleaning. In this sense, bitumen would not cause issues with water drainage. However, if these bitumen films were not removed after VSP shutdown (especially under batch operating mode), the volute plates will be glued together by dry bitumen clumps as all water evaporates. Such phenomenon will seal nearly all drainage slits and render the slits hydrophobic, which would severely diminish the formation of filter cake inside the Dewatering Press on the next use. As a best practice, solvent-based bitumen cleaners (degreasers, etc.) were applied to all volute plates immediately after each VSP shutdown while rotation of the center screw was turned on.

4. All dilutions and flocculant dissolution were carried out in tap water. Effects of tap water dilution on MFT (as opposed to dilution with pond/process water) were not well characterized in terms of flocculation performance. On the other hand, A-PAM and C-PAM solutions made with tap water were distinctively different from

their counterparts produced by pond/process water. At a concentration of 500 ppm, the A-PAM solution viscosity became too great for the chemical diaphragm pump to transport into the Conditioning Tank (even at full pump speed). Same problems with C-PAM solution viscosity were also encountered at a concentration of ≥ 2500 ppm. Thus there were practical upper limits on the concentrations of both flocculant solutions made with tap water, which complicated the experimental setup and planning process.

5. At the same operating conditions and MFT feed, different combination of flocculants will yield higher or lower filter cake DS. For example, a cake 68 wt% DS was produced with Coanda/Suncor MFT using two proprietary Japanese flocculants. On the other hand, the A-PAM and C-PAM used in this study resulted in 63-64 wt% DS cake for the same MFT.

Several hardware limitations of the VSP device were also discovered.

6. Minimum flow of the feed pump for Feed Holding Tank is $0.4 \text{ m}^3/\text{h}$, which was found to be oversized for our MFT dewatering service. Also during start-up, the feed pump requires ~ 1 m head at suction side to work properly.
7. Maximum flow for each of A-PAM and C-PAM diaphragm pumps is $\sim 50 \text{ L/h}$. This created a practical lower limit on the concentrations of flocculant solutions.
8. Also, the A-PAM and C-PAM pumps were not only restricted by viscosity. There is a minimum pump speed at which no solution – no matter how dilute – could be

transported into the Condition Tank or Flocculation Tank. The minimum speed was empirically determined to be 30%. Generally, it is not advised to use pump speed of < 40% once solution viscosity is taken into consideration.

Basic dimensions of the device were measured during preliminary studies (for example, tank volume, volute plate thickness, washer thickness, Dewatering Press inclination / inlet and outlet, auger screw pitch, and so on). In one of the trial runs, effect of screw rotation rate was increased to assess its impact on filter cake DS. As expected, faster screw rotation resulted in more wet cake throughput at the cost of significantly deteriorated cake DS. It is possible to optimize between the two variables in this manner. However, this factor was not tested in the field study due to time constraints.

8.2. Field operations (Phase 2)

There were plenty of important findings made during the short weeklong testing at Canadian Naturals Horizon Oil Sands Innovation Centre. The following summarizes these discoveries made with Horizon MFT (diluted to 5 wt% DS) flocculated with A-PAM and C-PAM solutions produced by Horizon pond water.

1. It takes 3.5 h for the VSP filter cake DS to stabilize following any change in A-PAM or C-PAM dosage.
2. At the same A-PAM dosage (300 or 500 g/t), increasing C-PAM dosage immediately improved filter cake DS, from a baseline of 50-51 wt% without C-

PAM to 55-56 wt% with an additional 1000 g/t C-PAM. It is possible to achieve cake DS of ≥ 60 wt% given sufficient C-PAM at ≥ 3000 g/t.

3. At the same C-PAM dosage, increasing A-PAM dosage increased the volumetric throughput of wet filter cake, from 5-5.8 L/h at A-PAM of 300 g/t to 6.6-7.3 L/h for A-PAM at 500 g/t. In terms of cake DS (and thus cake density) there is only a maximum of 1.58 wt% reduction following an increase in A-PAM dosage (between A300-C4000 and A500-C4000, corresponds to a density decrease from 1618 kg/m³ to 1592 kg/m³). Such small density difference could not overcome the significant increase in volumetric rate of wet cake output.
4. Two most important observations from the field work are as follows. The C-PAM dosage seems to be positively correlated to the ability of sediments to dewater under compression (hypothesized sediment elasticity of dewatering). On the other hand, A-PAM dosage directly correlates to the rate of bulk movement of sediments under compression (hypothesized sediment plasticity of dewatering).
5. Dry solids in the filtrate should be minimized if possible. Doing so will minimize complications in filtrate recycling, as well as increasing the conversion rate of feed DS to filter cake.

6. Amount of volute plate runoff materials should be kept reasonably low, at a runoff-to-cake DS ratio of $\leq 10\%$ by weight. Upon co-mixing of filter cake and runoff for disposal, this criterion minimizes DS change from those in filter cake.
7. Other adjustable operating parameters that can increase cake DS are: a) increasing the preparation time of the particular C-PAM used in this study; b) decreasing the endplate gap distance; and c) maximizing the Flocculation Tank mixer speed.
8. Based on the mass balance for the entire VSP circuit, most DS was lost in filtrate instead of runoff.
9. The VSP was running continuously for only 27-44% of the time.
10. Average DS conversion rate from feed to cake was 74.3% by weight, equivalent to the fines capture rate.
11. Water balance around the VSP circuit indicated a net gain of water, whose value varied between 5.9-7.9 wt% of produced filtrate.

In short, once the VSP operator uses a suitable combination of polymers – current belief is adding A-PAM first, C-PAM second – the VSP is capable of achieving continuous dewatering from the flocculated MFT sediments.

However, the act of choosing the best polymers requires a set of metrics for comparison purposes, for which the bench-scale studies endeavored to establish.

8.3. Lab-based CVST studies (Phase 3)

Chapter 3 hypothesized a parameter that can directly indicate the susceptibility of flocculated MFT sediment to compressive dewatering or compression-driven flow. If correctly proposed and formulated, the elasticity of dewatering would be a key metric for assessing the viability of sediments generated by a given combination of flocculants for VSP compressive dewatering. The following were found during the relevant course of investigation.

1. In terms of flocculation performance, using C-PAM following A-PAM greatly enhanced the solids initial settling rate from a mere 5.3-9.4 m/h to 115-119 m/h. Supernatant DS decreased from 0.9-1.1 wt% with only A-PAM to 0.47-0.65 wt%. However all supernatant samples were too turbid for direct measurement. The initial sediment DS increased from 12.8-15.4 wt% with no C-PAM and gradually stabilized to 18.2-18.3 wt% at higher C-PAM dosages.
2. Multiple complete CVST stress-strain curves were generated for each experiment case using an iterative procedure as described in **Chapter 3**. Three distinct regions were identified as common features for all CVST curves: initialization, loading, and compression regions.
3. For sediments that dewatered poorly on the VSP (i.e. A300 and A500), the CVST curves indicated rupture at 110-200 kPa response stress generally occurring on ≤ 4 vol% vertical strain.

4. In contrast, sediments that dewatered well on the VSP (A300-C2000/3000/4000, A500-C2000/3000/4000) showed a rupture point of 1375-3420 kPa at 6.3-10.6 vol% vertical strain.
5. The A300-C1000 and A500-C1000 sediments showed fairly low rupture points occurring at 390-396 kPa and 4-8.5 vol% vertical strain. Despite the similarities in rupture points compared to A300 and A500, these two sets of experiments have quite different outcomes in VSP dewatering, which suggests very different dewatering elasticity properties.
6. By linearizing the compression region on a complete CVST curve, value of the slope known as compressive dewatering index (CDI) can be obtained.
7. When the VSP filter cake DS results were plotted against the corresponding CDI values, a positive linear relation is clearly evident between the two for all experiment cases with C-PAM (A300/A500-C1000/2000/3000/4000). This suggests that all such sediments share a common property for VSP dewatering. Since the CDI values are obtained assuming linear stress-strain responses (which in turn is the definition of elasticity), thus sediments with C-PAM must be elastic upon compressive dewatering. This significant finding validates all previous assertions regarding the elasticity of dewatering for flocculated MFT sediments.

8. The aforementioned differences between A300/A500 and A300/A500-C1000 become obvious on the CDI-cake DS plot. It was observed that A300/A500-C1000 follows the positive linear trend shared with A300/A500-C2000/3000/4000. However, datapoints for A300/A500 cases falls under the line, which suggests these sediments were not of the same degree of elasticity, or quite possibly, not elastic at all. Currently A300/A500 sediments are only considered to be non-elastic (i.e. plastic) for dewatering.
9. The CDI gain for the C-PAM (when applied to dilute Horizon MFT already flocculated by A-PAM) is 166 per 1 wt% increase in VSP cake DS.

There is overwhelming evidence across both field and bench-scale studies to conclude the existence of sediment elasticity of dewatering. The usefulness of the dewatering elasticity concept is further illustrated by the compressive dewatering index (CDI) that can be directly obtained from a complete and classified CVST stress-strain curve. Strong linear correlation between CDI and the VSP filter cake DS for experiment cases with C-PAM offers the final proof on the conceptual validity of the hypothesized sediment elasticity of dewatering. The elasticity concept can also be used to detect non-elastic (i.e. plastic) sediments, which would significantly deviate from the CDI-cake DS correlation. Significance of the CDI gain would become better understood when the dewatering efficacies of different slurries and polymers are tested by both the CVST and the VSP methods.

8.4. Original contributions to scientific knowledge

In this thesis, the following original contributions are believed to be very significant to the overall scientific knowledge in fines and ultra-fines slurry dewatering.

- I. Novel application of the volute screw press for dewatering flocculated CNRL Horizon MFT. It has been demonstrated that, with proper choice of flocculants, it is possible to continuously produce dry stackable MFT filter cake at > 60 wt% dry solids, despite immense challenges from the extremely small D_{90} , high clay-to-water ratio, elevated monovalent cation concentrations in pond water (relative to divalent cations), and presence of bitumen.
- II. New theoretical perspective at characterizing the compressional response of flocculated MFT sediments. Concepts of elastic and plastic deformations of metallic solids were extended and applied to describe mechanical compression dewatering of semi-solid MFT sediments.
- III. Based on Contribution II, a new bench-scale method (CVST, controlled vertical strain test) was developed to assess the qualitative existence and quantitative extent of dewatering elasticity for properly- and improperly-flocculated MFT sediments. It was discovered that the hypothetical descriptions in Contribution II could be experimentally verified with flocculated CNRL Horizon MFT.
- IV. Based on Contribution III, a material-specific parameter (CDI, compressional dewatering index) could be determined from the CVST, whose value is dependent on flocculant dosages.
- V. The CDI parameters obtained in the bench-scale study (from Contribution IV) were shown to have excellent linear correlation against the filter cake dry solids

content obtained in the field study. Such agreement between the bench-scale CVST and pilot-scale VSP experiments enable *a priori* prediction of VSP filter cake dry solids content, and greatly assist the selection of suitable flocculants. Use of the CVST will pre-emptively distinguish between promising flocculants or dosage range (high CDI values) and unsuitable flocculants or dosage range (low CDI values).

- VI. Based on Contribution V, the newly-developed CVST is a useful, rapid, and quantitative method for VSP flocculant screening process, or quite possibly, for flocculant screening of other mechanical/compressive dewatering processes. Results obtained from the CVST can be corroborated with other relevant standard tests (for example, jar test, one-dimensional consolidation test, etc.) to further assess the viability of a given flocculant recipe at mechanical dewatering applications.

8.5. Future work

A list of possible follow-up work has been created following the general order of writing in this chapter, and may include items that were not described previously.

1. Using the same flocculant(s) and feed MFT, for a given basis of flocculation performance, determine the relations between MFT dilution and flocculant dosage (dry basis). It has been postulated that diluting MFT helps to reduce the flocculant dosage. However excessive MFT dilution was found to yield diminishing returns

on dosage reduction. A plot of flocculant dosage versus MFT dilution should be non-linear.

- a. The dosage-dilution plot mentioned in #1 is characteristic of the given MFT. Obtain MFT from different sources and produce its corresponding dosage-dilution curve. It was already known that Coanda/Suncor and Horizon MFT have distinctly different curves. Syncrude Aurora MFT differs from those two as well.
 - b. Fundamentally pinpoint the reason(s) that can cause the differences in dosage-dilution curves. Particle size distribution, sand-to-fines ratio, clay-to-water ratio, types of clay, and water chemistry are all possible factors to investigate.
 - c. Utilize findings in 1(b) and attempt to adjust the MFT and/or dilution procedures so that flocculant dosage can be minimized. This has immense practical applications if successful.
2. Characterize the effect of dilution water (DI/tap vs. pond or process water) on MFT slurry and subsequent flocculation. Again, a basis for flocculation performance is necessary.

3. Investigate the observed viscosity difference in A-PAM and C-PAM solutions made with tap/DI water or pond/process water. Such study would primarily focus on the interactions between soluble ions and polymer molecules.
4. Try using different types of A-PAM and/or C-PAM on both CVST and VSP to optimize the use of flocculants, in terms of dosage and dewatering performance.
 - a. As mentioned in **Chapter 3**, it would be of even more valuable to probe the fundamental factors involved for better or worse performance in compressive dewatering. A good direction to start would be the flocculant molecular properties such as molecular weight, linearity and branching, charge type and density, etc. This would provide flocculant vendors with a scientific basis to tailor their products for compressive dewatering applications.
 - b. Determine the corresponding CDI gain values with a variety of slurries and polymers for better understanding on the roles and effects of sediment dewatering elasticity development.
5. Replace the feed pump under the current VSP for a smaller one to decrease idling. This would also involve re-wiring of the control circuit.

- a. Study the differences in VSP operations and quality of products when the device uptime is increased.
6. Set up formal experiments to determine the operational effects of faster/slower screw rotation. The screw speed controller setpoint can vary between 10% to 120%, but so far only the 20% setpoint (1.6 RPM) has been used.
7. There is an apparent gap in the current CDI-cake DS plot. It may be interesting to study dosage cases of A300/A500 with < 1000 g/t C-PAM added, in order to fill the gap and examine the overall curve. This can provide clues on the rate of elasticity development for Horizon MFT sediments.
8. Leave the C-PAM solution (made with pond water) longer in preparation and confirm its beneficial role for producing higher cake DS.
9. Design formal experiments to assess the operational effects of increased endplate gap distance. So far only 1 mm and 2 mm have been tested.
10. Mechanical improvements and scale-up for the VSP Dewatering Press.

All References

- Abdel-Aal, E.-S.A., 2000. Recovery of phosphoric acid from Egyptian Nile Valley phosphate tailings. *Miner. Eng.* 13 (2), 223–226.
- Alagha, L. et al., 2013. Probing adsorption of polyacrylamide-based polymers on anisotropic basal planes of kaolinite using quartz crystal microbalance. *Langmuir* 29, 3989–3998.
- Alamgir, A., Harbottle, D., Masliyah, J., Xu, Z., 2012. Al-PAM assisted filtration system for abatement of mature fine tailings. *Chem. Eng. Sci.* 80, 91–99.
- Alam, N., Ozdemir, O., Hampton, M.A., Nguyen, A.V., 2011. Dewatering of coal plant tailings: flocculation followed by filtration. *Fuel* 90, 26–35.
- Alberta Energy Regulator, 2012. Directive 074 (Supplemental Information, Tailings Management Assessment Report (2011/2012)). <http://www.aer.ca/rules-andregulations/directives/directive-074> (accessed 2013).
- Alberta Energy Regulator, 2013. ST98: Alberta's Energy Reserves & Supply/Demand Outlook. <http://www.aer.ca/data-and-publications/statistical-reports/st98> (accessed 2013).
- Allen, E.W., 2008. Process water treatment in Canada's oil sands industry: I. Target pollutants and treatment objectives. *J. Environ. Eng. Sci.* 7, 123–138.
- Al, T.A., Blowes, D.W., 1999. The hydrogeology of a tailings impoundment formed by central discharge of thickened tailings: implications for tailings management. *J. Contam. Hydrol.* 38, 489–505.
- Amcon China, 2016. Overseas Subsidiaries - amcon inc.. [Online], Available at: <http://en.amcon.co.jp/company/group/> [Accessed January 2016].
- ASTM, 2011. D2487-11 Standard Practice for Classification of Soils for Engineering Purposes (Unified Soil Classification System). http://enterprise.astm.org/filtrexx40.cgi?+REDLINE_PAGES/D2487.htm (accessed 2013).
- Barraza, J., Guerrero, J., Piñeres, J., 2013. Flotation of a refuse tailing fine coal slurry. *Fuel Process. Technol.* 106, 498–500.
- Beier, N.A., Segó, D.C., 2009. Cyclic freeze–thaw to enhance the stability of coal tailings. *Cold Reg. Sci. Technol.* 55, 278–285.

- Besra, L., Sengupta, D., Roy, S., 2000. Particle characteristics and their influence on dewatering of kaolin, calcite and quartz suspensions. *Int. J. Miner. Process.* 59, 89–112.
- Bethell, P.J., 2012. Dealing with the challenges facing global fine coal processing. In: Bethell, P.J., Arnold, B.J., Klima, M.S. (Eds.), *Challenges in Fine Coal Processing, Dewatering, and Disposal*. Society for Mining, Metallurgy, and Exploration Inc., Englewood, Colorado, pp. 33–45.
- BGC Engineering Inc., 2010. Oil Sands Tailings Technology Review (OSRIN Report No. TR-1). Oil Sands Research and Information Network, University of Alberta, School of Energy and the Environment, Edmonton, Canada.
- Boger, D.V., 2009. Rheology and the resource industries. *Chem. Eng. Sci.* 64, 4525–4536.
- Bott, R., Langeloh, T., 2001. Synergy effects with steam pressure filtration. *Chem. Ing. Tech.* 73, 1323–1327.
- Boxill, L., 2015. Using Imaging to Decode Geotechnical Characterization of Polymer-Amended Fine Tailings, Edmonton, AB: COSIA Clay Workshop.
- Bridge, G., 2000. The social regulation of resource access and environmental impact: production, nature and contradiction in the US copper industry. *Geoforum* 31, 237–256.
- Carrier, W.D., 2001. Rapid Clay Dewatering Phase II: Field-Scale Tests. Florida Institute of Phosphate Research, Bartow, Florida.
- Chaiko, D.J., Kopasz, J.P., Ellison, A.J.G., 1998. Use of sol–gel systems for solid/liquid separation. *Ind. Eng. Chem. Res.* 37, 1071–1078.
- Chen, G., Mujumdar, A.S., 2002. Application of electrical fields in dewatering and drying. *Dev. Chem. Eng. Miner. Process.* 10, 429–441.
- Chen, L. et al., 2015. Water Recovery Estimation for Polymer Flocculated Oil Sand Tailings: A comparison between experimental practices and a fluid flow simulation based on Lattice-Boltzmann method, Calgary, AB: COSIA.
- Ching, H.-W., Tanaka, T.S., Elimelech, M., 1994. Dynamics of coagulation of kaolin particles with ferric chloride. *Water Res.* 28, 559–569.
- Consortium of Tailings Management Consultants, 2012. Alberta Innovates – Energy and Environment Solutions, Featured Reports, Tailings Roadmap and Action Plan. <http://www.ai-ees.ca/reports.aspx> (accessed 2013).

- COSIA, 2013. Centrifuges Used to Release Water from Fluid Fine Tailings. <http://www.cosia.ca/projects/tailings/centrifuges-used-to-release-water> (accessed 2013).
- Crowson, P., 2012. Some observations on copper yields and ore grades. *Resour. Policy* 37, 59–72.
- Davis, R.H., Zhang, X., Agarwala, J.P., 1989. Particle classification for dilute suspensions using an inclined settler. *Ind. Eng. Chem. Res.* 28, 785–793.
- de Kretser, R., Scales, P.J., Boger, D.V., 1997. Improving clay-based tailings disposal: case study on coal tailings. *AIChE J.* 43, 1894–1903.
- Dick, R.I., Ball, R.O., Novak, J.T., 1980. Sludge dewatering. *CRC Crit. Rev. Environ. Control* 10, 269–337.
- Duan, J., Gregory, J., 2003. Coagulation by hydrolysing metal salts. *Adv. Colloid Interf. Sci.* 100–102, 475–502.
- Elimelech, M., Gregory, J., Jia, X., Williams, R.A., 1995. *Particle Deposition and Aggregation Measurement, Modelling and Simulation*. Butterworth-Heinemann, USA.
- ERCB, 2009. Directive 074: Tailings Performance Criteria and Requirements for Oil Sands Mining Schemes. <http://www.aer.ca/rules-and-regulations/directives/directive-074> (accessed 2013).
- Farkish, A., Fall, M., 2013. Rapid dewatering of oil sand mature fine tailings using super absorbent polymer (SAP). *Miner. Eng.* 50–51, 38–47.
- Fenzel, M.S., 2012. Belt filter press in coal tailings dewatering—a comprehensive economic, design, and process analysis. In: Bethell, P.J., Arnold, B.J., Klima, M.S. (Eds.), *Challenges in Fine Coal Processing, Dewatering, and Disposal*. Society for Mining, Metallurgy, and Exploration Inc., pp. 309–327.
- Franks, G.V., Li, H., O’Shea, J.-P., Qiao, G.G., 2009. Temperature responsive polymers as multiple function reagents in mineral processing. *Adv. Powder Technol.* 20, 273–279.
- Franks, G.V., Yates, P.D., Lambert, N.W., Jameson, G.J., 2005. Aggregate size and density after shearing, implications for dewatering fine tailings with hydrocyclones. *Int. J. Miner. Process.* 77, 46–52.
- Gao, W., Smith, D., Segó, D., 2004. Treatment of pulp mill and oil sands industrial wastewaters by the partial spray freezing process. *Water Res.* 38, 579–584.

Gaudreault, R., van de Ven, T.G., Whitehead, M., 2005. Mechanisms of flocculation with poly(ethylene oxide) and novel cofactors. *Colloids Surf. A: Physicochem. Eng. Aspects* 268, 131–146.

Gentes, M.-L., Waldner, C., Papp, Z., Smits, J.E., 2006. Effects of oil sands tailings compounds and harsh weather on mortality rates, growth and detoxification efforts in nestling tree swallows (*Tachycineta bicolor*). *Environ. Pollut.* 142, 24–33.

Giese, R.F., 2002. *Colloid and Surface Phenomena in Clays and Related Materials*. Marcel Dekkar Inc., New York, USA.

Golder Associates, 2009. Reclamation and Closure in Oil Sands Development Areas. http://www.golder.ca/en/modules.php?name=Newsletters&op=viewarticle&sp_id=114&page_id=1100&article_id=124 (accessed 2013).

Gordon, R.B., 2002. Production residues in copper technological cycles. *Resour. Conserv. Recycl.* 36, 87–106.

Gräfe, M., Power, G., Klauber, C., 2011. Bauxite residue issues: III. Alkalinity and associated chemistry. *Hydrometallurgy* 108, 60–79.

Gupta, V. et al., 2011. Particle interactions in kaolinite suspensions and corresponding aggregate structures. *J. Colloid Interf. Sci.* 359, 95–103.

Gupta, V., Miller, J.D., 2010. Surface force measurements at the basal planes of ordered kaolinite particles. *J. Colloid Interf. Sci.* 344, 362–371.

Hansen, H.K., Yianatos, J.B., Ottosen, L.M., 2005. Speciation and leachability of copper in mine tailings from porphyry copper mining: influence of particle size. *Chemosphere* 60, 1497–1503.

Harbottle, D., Biggs, S., Fairweather, M., 2011a. Fine particle turbulence modulation. *AIChE J.* 57 (7), 1693–1699.

Harbottle, D., Fairweather, M., Biggs, S., 2011b. The minimum transport velocity of colloidal silica suspensions. *Chem. Eng. Sci.* 66, 2309–2316.

Harbour, P.J., Dixon, D.R., Scales, P.J., 2007. The role of natural organic matter in suspension stability: 1. Electrokinetic–rheology relationships. *Colloids Surf. A: Physicochem. Eng. Aspects* 295, 38–48.

Hogg, R., 2000. Flocculation and dewatering. *Int. J. Miner. Process.* 58, 223–236.

- International Fertilizer Industry Association, 2010. <http://www.fertilizer.org>.
<http://www.fertilizer.org/ifa/HomePage/STATISTICS/Production-and-trade> (accessed 2013).
- ISO, 2002. ISO 14688-1:2002 Geotechnical Investigation and Testing – Identification and Classification of Soil – Part 1: Identification and Description.
http://www.iso.org/iso/catalogue_detail.htm?csnumber=25260 (accessed 2013).
- Israelachvili, J.N., 2011. *Intermolecular and Surface Forces*, third ed. Elsevier Inc..
- Iwata, M., 2003. Solid–liquid separation by use of particle immobilization in calcium alginate gel. *Sep. Sci. Technol.* 38, 837–850.
- Ji, Y., Lu, Q., Liu, Q., Zeng, H., 2013. Effect of solution salinity on settling of mineral tailings by polymer flocculants. *Colloids Surf. A: Physicochem. Eng. Aspects* 430, 29–38.
- Johnson, S.B. et al., 2000. Surface chemistry–rheology relationships in concentrated mineral suspensions. *Int. J. Miner. Process.* 58, 267–304.
- Jones, B.E.H., Haynes, R.J., 2011. Bauxite processing residue: a critical review of its formation, properties, storage, and revegetation. *Crit. Rev. Environ. Sci. Technol.* 41, 271–315.
- Jones, H., Boger, D.V., 2012. Sustainability and waste management in the resource industries. *Ind. Eng. Chem. Res.* 51, 10057–10065.
- Kalkan, E., 2006. Utilization of red mud as a stabilization material for the preparation of clay liners. *Eng. Geol.* 87, 220–229.
- Keles, S. et al., 2010. Development of the centribaric (TM) dewatering technology. In: *Proceedings from International Coal Preparation Congress*, pp. 488–495.
- Klein, C., Harbottle, D., Alagha, L., Xu, Z., 2013. Impact of fugitive bitumen on polymer-based flocculation of mature fine tailings. *Can. J. Chem. Eng.* 91, 1427–1432.
- Konan, K.L. et al., 2007. Surface properties of kaolin and illite suspensions in concentrated calcium hydroxide medium. *J. Colloid Interf. Sci.* 307, 101–108.
- Kulkarni, S.G., Ramarao, B.V., Hassett, J.M., Tien, C., 1993. Dynamic modeling of the sedimentation of concentrated bidispersed suspensions. *Sep. Technol.* 3, 12–24.
- Kumar, S., Kumar, R., Bandopadhyay, A., 2006. Innovative methodologies for the utilisation of wastes from metallurgical and allied industries. *Resour. Conserv. Recycl.* 48, 301–314.

- Lee, M.R., Correa, J.A., 2005. Effects of copper mine tailings disposal on littoral meiofaunal assemblages in the Atacama region of northern Chile. *Mar. Environ. Res.* 59, 1–18.
- Leong, Y.-K., Boger, D.V., 1990. Surface chemistry effects on concentrated suspension rheology. *J. Colloid Interf. Sci.* 136, 249–258.
- Leung, W.-F., 1998. *Industrial Centrifugation Technology*. McGraw-Hill, New York.
- Li, H., Long, J., Xu, Z., Masliyah, J.H., 2007. Flocculation of kaolinite clay suspensions using a temperature-sensitive polymer. *AIChE J.* 53, 479–488.
- Liu, W., Yang, J., Xiao, B., 2009. Review on treatment and utilization of bauxite residues in China. *Int. J. Miner. Process.* 93, 220–231.
- Liu, Y.-C. et al., 2013. Leaching kinetics of copper flotation tailings in aqueous ammonia/ammonium carbonate solution. *Can. J. Chem. Eng.* 91, 770–775.
- Lockhart, N.C., Veal, C., 1996. Coal dewatering: Australian R&D trends. *Coal Prep.* 17, 5–24.
- Loginov, M., Citeau, M., Lebovka, N., Vorobiev, E., 2013. Electro-dewatering of drilling sludge with liming and electrode heating. *Sep. Purif. Technol.* 104, 89–99.
- Mahmoud, A., Olivier, J., Vaxelaire, J., Hoadley, A.F., 2010. Electrical field: a historical review of its application and contributions in wastewater sludge dewatering. *Water Res.* 44, 2381–2407.
- Masala, S., Dhadli, N., 2012. Correlations of shear strengths of soft oil sands tailings assessed by different in situ methods. In: *Proceedings from 3rd International Oil Sand Tailings Conference*, Edmonton, Canada.
- Masliyah, J.H., Bhattacharjee, S., 2006. *Electrokinetic and Colloid Transport Phenomena*. Wiley-Interscience, Hoboken, NJ.
- Masliyah, J.H., Czarnecki, J., Xu, Z., 2011. *Handbook on Theory and Practice of Bitumen Recovery from Athabasca Oil Sands: Theoretical Basis*, vol. I. Kingsley Knowledge Publishing, Canada.
- Mikula, R., Munoz, V., Omotoso, O., 2008. Centrifuge options for production of dry stackable tailings in surface mined oil sands tailings management. In: *Proceedings from Canadian International Petroleum Conference*, Calgary, AB, Canada.
- Morey, B., 2013. Dewatering. In: *Kirk–Othmer Encyclopedia of Chemical Technology*. John Wiley and Sons Inc., pp. 310–339.

- Murphy, C., Bennett, C., Olinger, G., Cousins, B., 2012. Alternatives to coal mine tailings impoundment – evaluation of three dewatering methods at rockspring coal mine. In: *Proceedings from Water in Mineral Processing*, Seattle, WA, pp. 301–309.
- Nasr-El-Din, H.A., Masliyah, J.H., Nandakumar, K., 1990. Continuous gravity separation of concentrated bidisperse suspensions in an inclined plate settler. *Int. J. Multiph. Flow* 16, 909–919.
- National Research Council, 2002. *Coal Waste Impoundments: Risks, Responses, and Alternatives*. National Academy Press, Washington, DC.
- Nenu, R., Hayase, Y., Yoshida, H., Yamamoto, T., 2010. Influence of inlet flow rate, pH, and beads mill operating condition on separation performance of submicron particles by electrical hydrocyclone. *Adv. Powder Technol.* 21, 246–255.
- Nesbitt, C.C., 2007. Waste reduction in metals manufacturing. In: *Environmentally Conscious Materials and Chemicals Processing*. John Wiley & Sons Inc., pp. 33–58.
- Ng, J. & Xu, Z., 2017. *Application of Switchable Hybrid Polymers in Oil Sands*, Edmonton: Presentation for NSERC IRC in Oil Sands Engineering.
- Nguyen, Q., Boger, D., 1998. Application of rheology to solving tailings disposal problems. *Int. J. Miner. Process.* 54, 217–233.
- O’Shea, J.-P., Qiao, G.G., Franks, G.V., 2010. Solid–liquid separations with a temperature-responsive polymeric flocculant: effect of temperature and molecular weight on polymer adsorption and deposition. *J. Colloid Interf. Sci.* 348, 9–23.
- Ofori, P. et al., 2011. Shear-induced floc structure changes for enhanced dewatering of coal preparation plant tailings. *Chem. Eng. J.* 172, 914–923.
- Oliveira, M.S., Santana, R.C., Ataíde, C.H., Barrozo, M.A., 2011. Recovery of apatite from flotation tailings. *Sep. Purif. Technol.* 79, 79–84.
- Onuaguluchi, O., Eren, Ö., 2012. Recycling of copper tailings as an additive in cement mortars. *Constr. Build. Mater.* 37, 723–727.
- Ortega-Rivas, E., 2012. Hydrocyclones. In: *Ullmann’s Encyclopedia of Industrial Chemistry*. Wiley-VCH Verlag GmbH & Co. KGaA, Weinheim, pp. 208–233.
- Penner, D., Lagaly, G., 2001. Influence of anions on the rheological properties of clay mineral dispersions. *Appl. Clay Sci.* 19, 131–142.
- Percy, K., Hansen, M., Dann, T., 2012. Air quality in the Athabasca oil sands region 2011. In: *Developments in Environmental Science*. Elsevier Ltd., pp. 47–91.

Peuker, U.A., Stahl, W., 1999. Scale-up of steam pressure filtration. *Chem. Eng. Process.* 38, 611–619.

Poulin, É., Blais, J.-F., Mercier, G., 2008. Transformation of red mud from aluminium industry into a coagulant for wastewater treatment. *Hydrometallurgy* 92, 16–25.

Power, G., Gräfe, M., Klauber, C., 2011. Bauxite residue issues: I. Current management, disposal and storage practices. *Hydrometallurgy* 108, 33–45.

Prat, G., 2012. Dewatering fine coal and tailings with a filter press. In: Bethell, P.J., Arnold, B.J., Klima, M.S. (Eds.), *Challenges in Fine Coal Processing, Dewatering, and Disposal*. Society for Mining, Metallurgy, and Exploration Inc., pp. 279–292.

Proskin, S., Segó, D., Alostaz, M., 2010. Freeze–thaw and consolidation tests on Suncor mature fine tailings (MFT). *Cold Reg. Sci. Technol.* 63, 110–120.

Raats, M., van Diemen, A., Laven, J., Stein, H., 2002. Full scale electrokinetic dewatering of waste sludge. *Colloids Surf. A: Physicochem. Eng. Aspects* 210, 231–241.

Ramirez, M., Massolo, S., Frache, R., Correa, J.A., 2005. Metal speciation and environmental impact on sandy beaches due to El Salvador copper mine, Chile. *Mar. Pollut. Bull.* 50, 62–72.

Rayhani, M., Yanful, E., Fakher, A., 2007. Desiccation-induced cracking and its effect on the hydraulic conductivity of clayey soils from Iran. *Can. Geotech. J.* 44, 276–283.

Renault, S., Zwiazek, J., Fung, M., Tuttle, S., 2000. Germination, growth and gas exchange of selected boreal forest seedlings in soil containing oil sands tailings. *Environ. Pollut.* 107, 357–365.

Ruyters, S. et al., 2011. The red mud accident in Ajka (Hungary): plant toxicity and trace metal bioavailability in red mud contaminated soil. *Environ. Sci. Technol.* 45, 1616–1622.

Ryu, C., Finney, K., Sharifi, V.N., Swithenbank, J., 2008. Pelletised fuel production from coal tailings and spent mushroom compost – Part I: Identification of pelletisation parameters. *Fuel Process. Technol.* 89, 269–275.

Sabah, E., Cengiz, I., 2004. An evaluation procedure for flocculation of coal preparation plant tailings. *Water Res.* 38, 1542–1549.

Sabah, E., Yuzer, H., Celik, M., 2004. Characterization and dewatering of fine coal tailings by dual-flocculant systems. *Int. J. Miner. Process.* 74, 303–315.

- Samal, S., Ray, A.K., Bandopadhyay, A., 2013. Proposal for resources, utilization and processes of red mud in India – a review. *Int. J. Miner. Process.* 118, 43–55.
- Singer, M.J., Munns, D.N., 1996. *Soils: An Introduction*, third ed. Prentice-Hall Inc., New Jersey, USA.
- Smith-Palmer, T., Pelton, R., 2012. Flocculation of particles. In: Somasundaran, P., Hubbard, A. (Eds.), *Encyclopedia of Surface and Colloid Science*. Taylor & Francis, pp. 2584–2599.
- Smuda, J., Dold, B., Spangenberg, J.E., Pfeifer, H.-R., 2008. Geochemistry and stable isotope composition of fresh alkaline porphyry copper tailings: implications on sources and mobility of elements during transport and early stages of deposition. *Chem. Geol.* 256, 62–76.
- Stancyzyk, M., Field, I., Collins, E., 1971. *Dewatering Florida Phosphate Pebble Rock Slime by Freezing Techniques*. US Bureau of Mines, Washington, DC (Report of Investigations 7520).
- Stroh, G., Stahl, W., 1990. Effect of surfactants on the filtration properties of fine particles. *Filtr. Sep.* 27, 197–199.
- Sung, D.-J., Turian, R.M., 1994. Chemically enhanced filtration and dewatering of narrow-sized coal particles. *Sep. Technol.* 4, 130–143.
- Tadros, T., 2011. Interparticle interactions in concentrated suspensions and their bulk (rheological) properties. *Adv. Colloid Interf. Sci.* 168, 263–277.
- Tao, D., Parekh, B., Honaker, R., 2008. *Development and Pilot-Scale Demonstration of Deep-Cone (TM) Paste Thickening Process for Phosphatic Clay Disposal*. Florida Institute of Phosphate Research, Bartow, Florida.
- Therriault, Y. et al., 1995. The effect of chemical, physical and enzymatic treatments on the dewatering of tar sands tailings. *Fuel* 74, 1404–1412.
- Timoney, K.P., Lee, P., 2009. Does the Alberta tar sands industry pollute? The scientific evidence. *Open Conserv. Biol. J.* 3, 65–81.
- Tu, Y. et al., 2005. Recovery of bitumen from oilsands: gelation of ultra-fine clay in the primary separation vessel. *Fuel* 84, 653–660.
- Venkataraman, S., Weiland, R.H., 1985. Buoyant-particle-promoted settling of industrial suspensions. *Ind. Eng. Chem. Process Des. Dev.* 24, 966–970.

- Verma, S., Klima, M.S., 2010. Evaluation of a pilot-scale plate-and-frame filter press for dewatering fine anthracite refuse. In: Proceedings from International Coal Preparation Congress, pp. 516–524.
- Voordouw, G., 2013. Interaction of oil sands tailings particles with polymers and microbial cells: first steps toward reclamation to soil. *Biopolymers* 99, 257–262.
- Wakeman, R., 2007. The influence of particle properties on filtration. *Sep. Purif. Technol.* 58, 234–241.
- Wang, C. et al., 2016. Role of pre-conditioning cationic Zetag® flocculant in enhancing MFT flocculation. *Energy Fuels*, 30(7), p. 5223–5231.
- Wang, S., Ang, H., Tadé, M., 2008a. Novel applications of red mud as coagulant, adsorbent and catalyst for environmentally benign processes. *Chemosphere* 72, 1621–1635.
- Wang, X., Feng, X., Xu, Z., Masliyah, J.H., 2010. Polymer aids for settling and filtration of oil sands tailings. *Can. J. Chem. Eng.* 88, 403–410.
- Wang, X. et al., 2008b. Particle characteristics and rheological constitutive relations of high concentration red mud. *J. China Univ. Min. Technol.* 18, 0266–0270.
- Watson, A. et al., 2010. A comparison of alternative tailings disposal methods – the promises and realities. In: Proceedings from Mine Waste, Perth, Australia.
- Weber, K., Stahl, W., 2002. Improvement of filtration kinetics by pressure electrofiltration. *Sep. Purif. Technol.* 26, 69–80.
- Whitmore, W.L., 1955. The sedimentation of suspensions of spheres. *Br. J. Appl. Phys.* 6, 239–245.
- WISE Uranium Project, 2012. Chronology of Major Tailings Dam Failures. <http://www.wise-uranium.org/mdaf.html> (accessed 2013).
- Wong, R. et al., 2004. Calcined oil sands fine tailings as a supplementary cementing material for concrete. *Cem. Concr. Res.* 34, 1235–1242.
- Wu, Z.H. et al., 2010. Dewatering and drying in mineral processing industry: potential for innovation. *Dry. Technol.* 28, 834–842.
- Xu, Y., Dabros, T., Kan, J., 2008. Filterability of oil sands tailings. *Process Saf. Environ. Prot.* 86, 268–276.
- Xu, Z., Zhang, Q., Lin, H., Qiu, Y., 2012. Application of reverse flotation to recover phosphate minerals from plant tailings. In: El-Shall, H.E., Miller, J.D., Zhang, P. (Eds.),

- Beneficiation of Phosphates: New Thought, New Technology, New Development. Society for Mining, Metallurgy, and Exploration Inc., pp. 275–279.
- Yang, Q., Li, Z., Lv, W., Wang, H., 2013. On the laboratory and field studies of removing fine particles suspended in wastewater using mini-hydrocyclone. *Sep. Purif. Technol.* 110, 93–100.
- Yan, L., Englert, A.H., Masliyah, J.H., Xu, Z., 2011. Determination of anisotropic surface characteristics of different phyllosilicates by direct force measurements. *Langmuir* 27, 12996–13007.
- Yan, L., Masliyah, J.H., Xu, Z., 2013. Understanding suspension rheology of anisotropically-charged platy minerals from direct interaction force measurement using AFM. *Curr. Opin. Colloid Interf. Sci.* 18, 149–156.
- Yuan, X., Shaw, W., 2007. Novel processes for treatment of syncrude fine transition and marine ore tailings. *Can. Metall. Quat.* 46, 265–272.
- Yukawa, H. et al., 1976. Analysis of batch electrokinetic filtration. *J. Chem. Eng. Jpn.* 9, 396–401.
- Zhang, P., Stana, R., 2012. Phosphogypsum management and utilization: a review of research and industry practice. In: El-Shall, H.E., Miller, J.D., Zhang, P. (Eds.), *Beneficiation of Phosphates: New Thought, New Technology, New Development*. Society for Mining, Metallurgy, and Exploration Inc., pp. 309–322.
- Zhao, L., Jiang, M., Wang, Y., 2008. Experimental study of a hydrocyclone under cyclic flow conditions for fine particle separation. *Sep. Purif. Technol.* 59, 183–189.
- Zhu, R. et al., 2011. Role of dissolving carbon dioxide in densification of oil sands tailings. *Energy Fuels* 25, 2049–2057.

Appendix A: Some Geotechnical Considerations

Appendix A provides the author's attempts at connecting the CVST with some of the well-known geotechnical aspects of soil consolidation.

A.1. One-dimensional consolidation test (oedometer test)

In soil mechanics and soil consolidation studies, an established technique is the one-dimensional consolidation test or oedometer test (ASTM standard testing procedure D2435). The incremental loading method is normally applied in the oedometer test in which a constant load is applied to the soil sample. Any drainage is allowed to leave the test system through porous media at the top and bottom of the sample. Once the resultant strain stabilizes over time, the load is further increased proportional to the previous value. Upon completion of the oedometer test, the applied load is also removed incrementally (i.e. reversal of the load application process).

Clearly, the newly-developed CVST differs from the oedometer test in the following aspects:

1. The CVST system confines the sample in an air- and water-tight cell, whereas the oedometer sample cell is neither air- nor water-tight.
2. The CVST involves controlled and continuous application of strain, whereas the oedometer applies a series of controlled load to the sample.
3. The CVST measures output stress in real-time, but the oedometer generates strain data over time.
4. Drainage is not allowed in the CVST, as opposed to the oedometer.

5. Flocculated sediment sample is formed inside the CVST apparatus, whereas soil samples for the oedometer comes from ex-situ environments.

In this thesis, the material of interest is the semi-solid polymer-flocculated wet sediments, which renders these samples initially weak in material strength and causes significant drainage over time. So it is apparent that for wet sediment applications, the standard oedometer test apparatus and procedure would need to be modified to a significant degree in order to accommodate the wet sediments encountered in this thesis. Direct application of the wet sediments to the oedometer would foreseeably cause at least three issues: (a) sediment escape through porous media in test cell (b) variable period of drainage, depending on the applied load, and (c) higher margin of error by transferring ex-situ sediment samples into test cell. Unless these issues are resolved, any results and subsequent conclusions from applying the standard oedometer to wet sediment is questionable. At this time, it is far easier and more prudent to apply the CVST for wet sediment applications.

A.2. Sediment dewatering characteristics prior to CVST compression regime

At low-strain environments, it was desired to examine the dewatering properties of wet sediment in order to reveal any connections to the final VSP filter cake dry solids. The hypothesis goes as follows: if a wet sediment shows extensive dewatering (i.e. large volumetric reduction) without accumulating too much stress, it would be an indication of desirable drainage channels at interior of this sediment. Consequently such sediment would perform better under high-strain dewatering processes such as the VSP.

From **Table 5.1**, it is possible to obtain the extent of volumetric reduction prior to compression regime from the strain values of “Onset of Compression” (Point *O*). Average value for each experiment case is used for subsequent analyses. **Figure A1** plots the VSP filter cake dry solids results against the average strain of Point *O* for all of the experiment cases. Interestingly, there seems to be an optimum for CVST pre-compression strain of about 5 vol%, from which the best filter cake has been obtained on the VSP. However, data shown in **Fig. A1** also pointed out the weakness of the original hypothesis – higher extent of pre-compression strain is not the best indicator of VSP product quality when compared to the compression dewatering index.

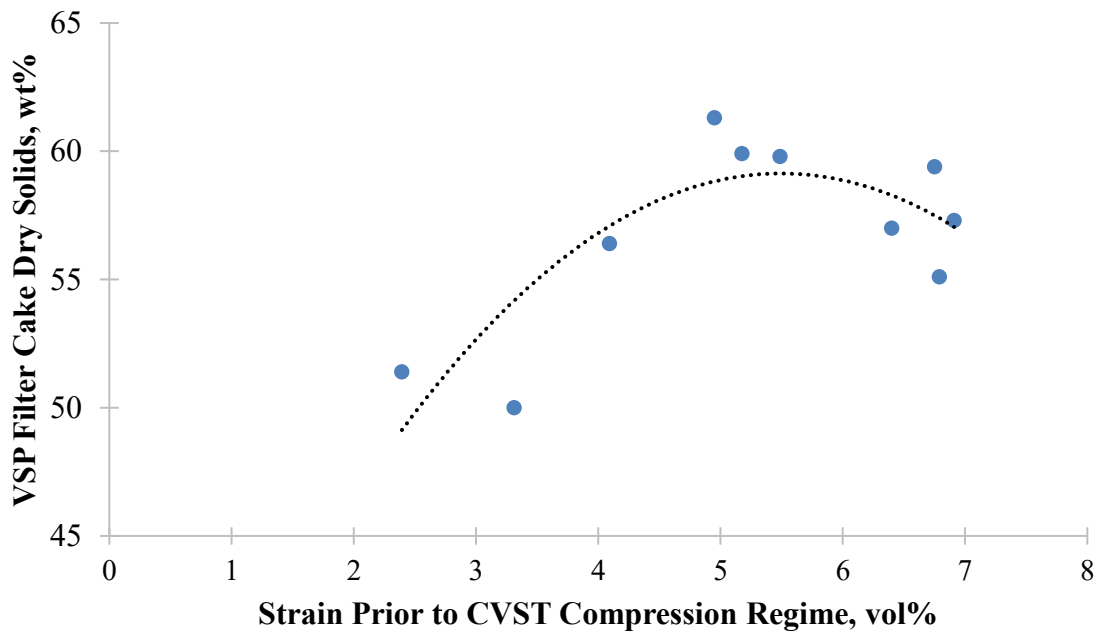


Figure A1. Relations between CVST pre-compression strain and VSP cake dry solids.

A.3. Evolution of sediment void ratio in CVST

Due to the variable amount of flocculant solutions present in each experiment case for the CVST, the total system volume across all 10 cases are different. Therefore it was of interest to examine the sediments in terms of their void ratio (e) defined as follows:

$$e = \frac{V_V}{V_S} = \frac{V_W}{V_S} \quad (\text{A.1})$$

In the context of CVST and this thesis, the void volume (V_V) is assumed to be equal to the volume of water (V_W) due to the insignificant concentration of residual solids in the supernatant and pore fluid (see **Fig. 5.2**). Initial volumetric content of solids ($V_{S,i}$) can be determined from **Fig. 5.3** and mass-volume conversion method in **section 6.3.2.2**. Time-evolution of the volume of solids (V_S) can be calculated from the CVST data prior to sediment rupture, again by assuming any sediment strain results in a corresponding volumetric loss of solids-free water. **Table A1** summarizes the initial values of $V_{S,i}$ for all experimental cases via their respective dry solids content in volumetric basis, from which their initial void ratio (e_i) can be determined by **Eq. A.1**.

Table A1. Initial sediment volumetric dry solids and void ratio for all experimental cases.

Case	Average sediment dry solids (wt%)	Average sediment dry solids (vol%), $V_{s,i}$	Initial void ratio, e_i
A300	15.398%	6.427%	14.56
A300-C1000	17.995%	7.647%	12.08
A300-C2000	17.482%	7.403%	12.51
A300-C3000	18.181%	7.737%	11.93
A300-C4000	18.339%	7.812%	11.80
A500	12.752%	5.227%	18.13
A500-C1000	16.549%	6.962%	13.36
A500-C2000	17.729%	7.520%	12.30
A500-C3000	18.155%	7.724%	11.95
A500-C4000	18.046%	7.672%	12.03

Several observations are evident from **Table A1**. As discussed, the A-PAM appeared to be overdosed at 500 g/t from initial settling rate data. Here, the overdosing of A-PAM seems to also significantly increased the void ratio of the wet sediments formed shortly after flocculation. Upon introduction of C-PAM, the differences in initial sediment void ratio between A300 and A500 samples becomes smaller and eventually negligible at C-PAM dosages 2000 g/t and above. This suggests the increasingly dominating role of C-PAM in altering the sediment internal void structures at higher C-PAM doses, as one would expect.

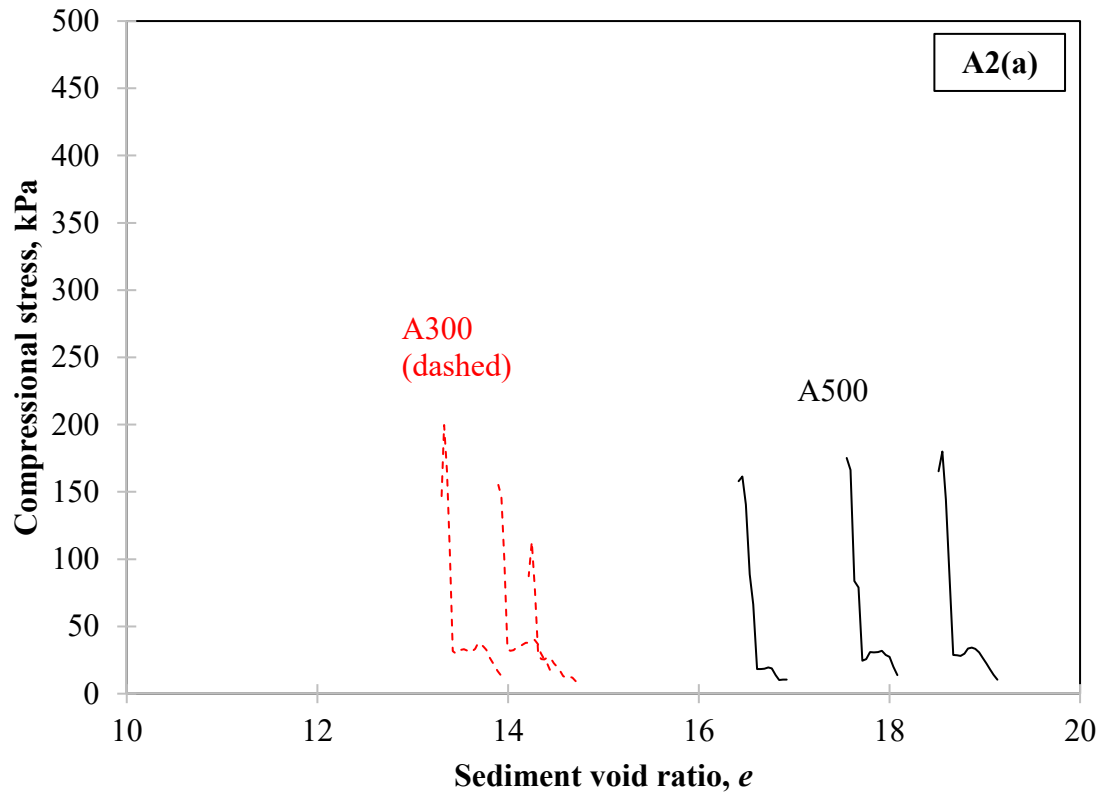


Figure A2(a). Complete stress-void ratio curves for A300 and A500.

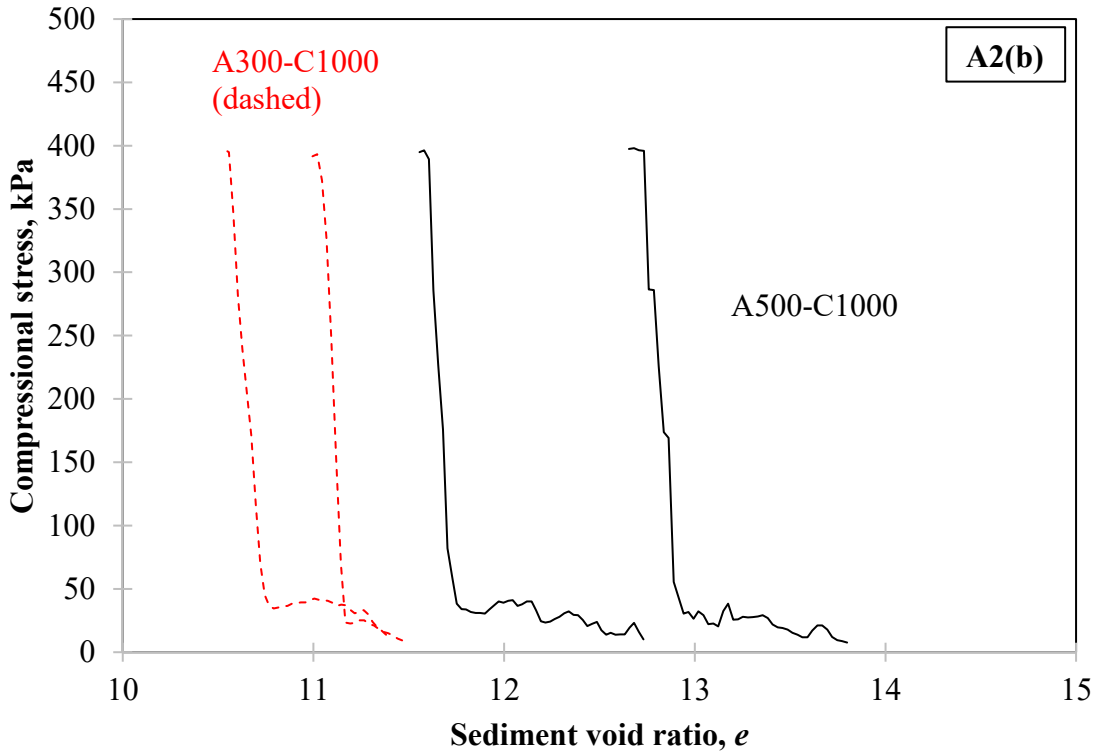


Figure A2(b). Complete stress-void ratio curves for A300-C1000 and A500-C1000.

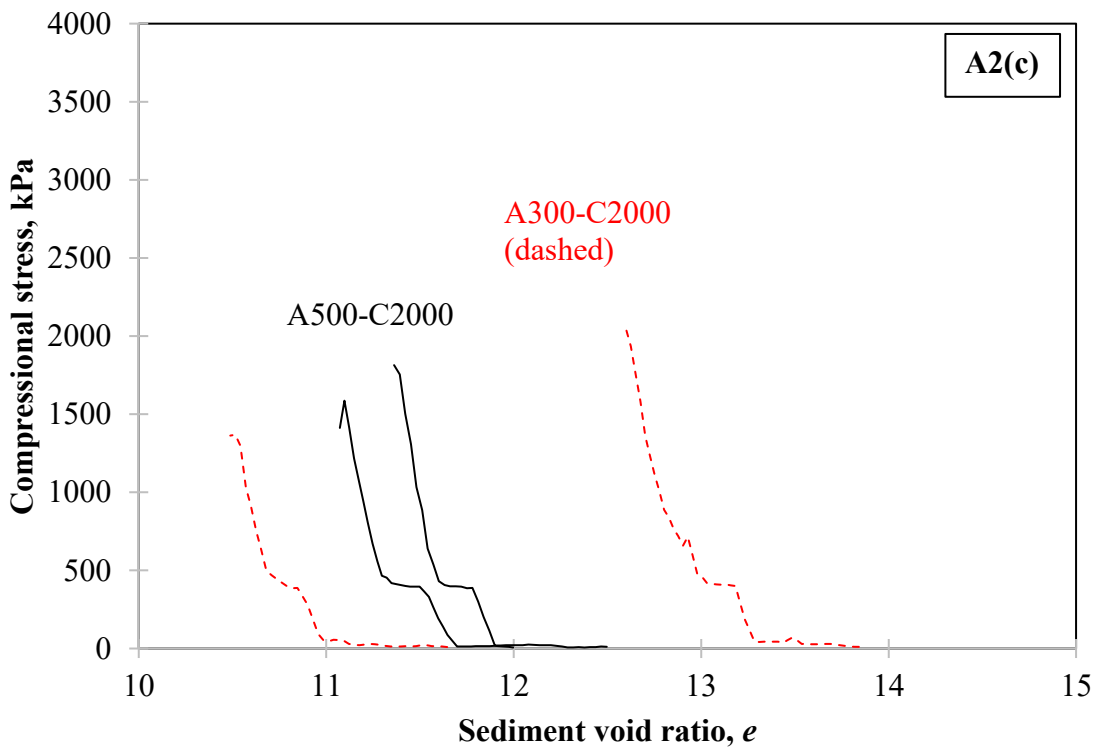


Figure A2(c). Complete stress-void ratio curves for A300-C2000 and A500-C2000.

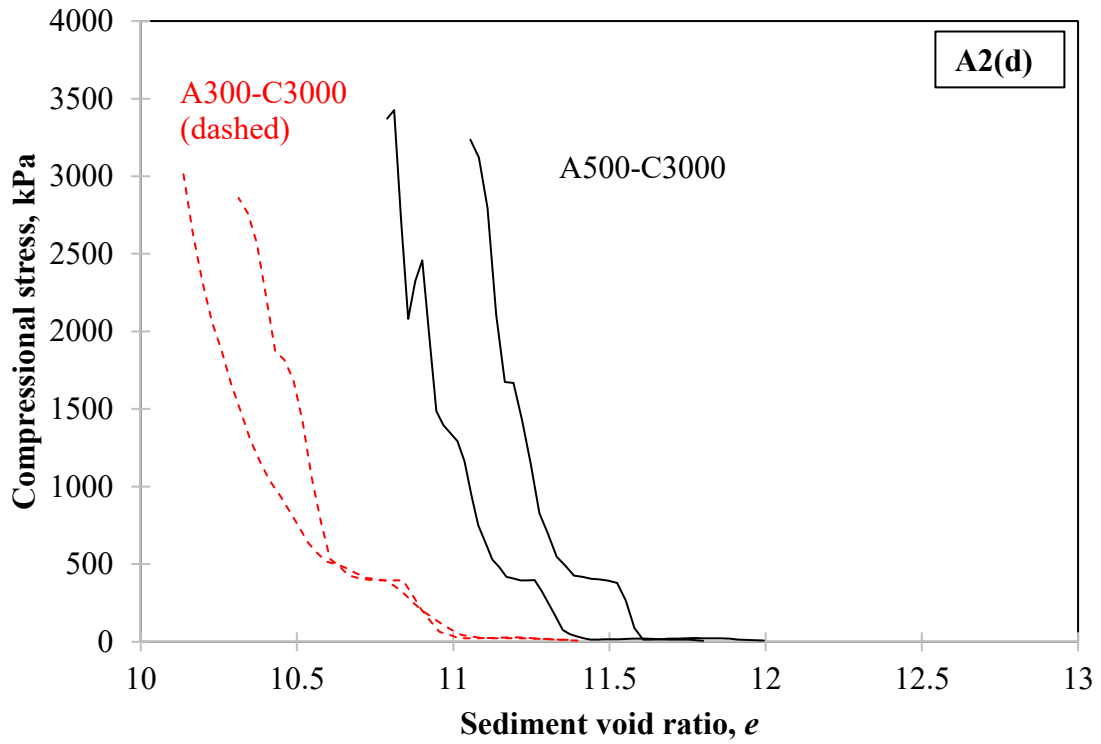


Figure A2(d). Complete stress-void ratio curves for A300-C3000 and A500-C3000.

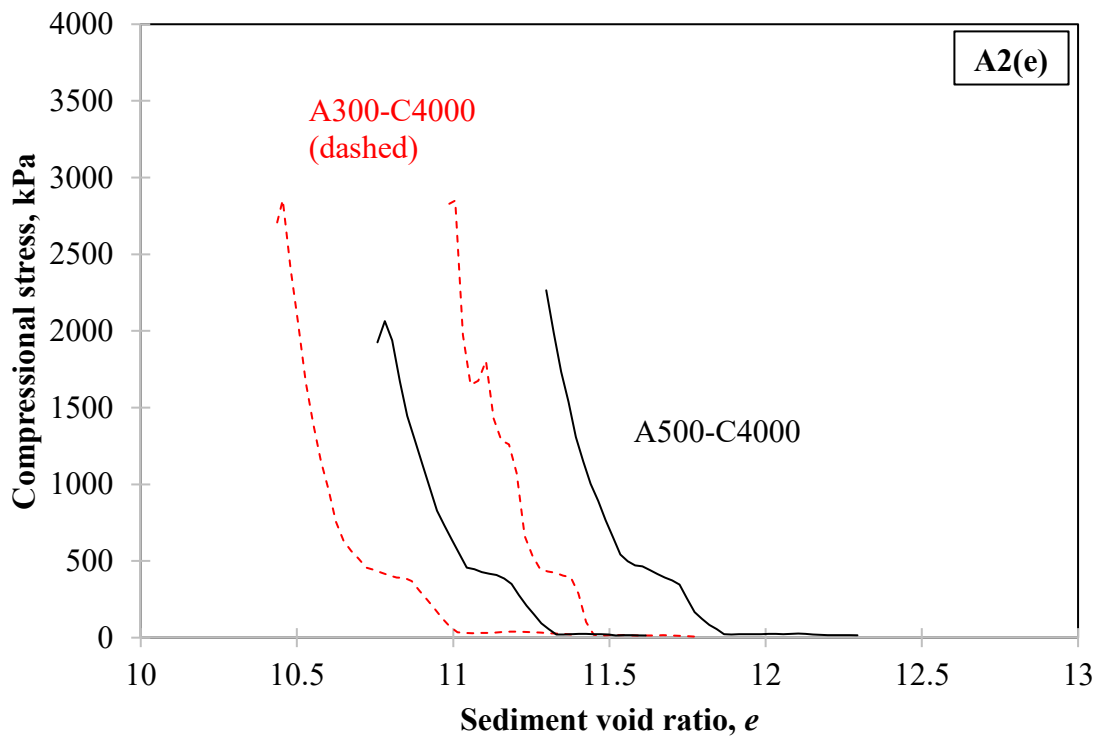


Figure A2(e). Complete stress-void ratio curves for A300-C4000 and A500-C4000.

Based on **Figs. A2 (a) to A2(e)**, the following are observed.

1. Sediment void ratio values encountered in the CVST is between 10 and 20.
2. Sediment void ratio decreases from its initial value as CVST progresses for all experimental cases in this thesis.
3. Compared to the CVST stress-strain curves, the stress-void ratio curves appear as mirror image of the former. Therefore the general trend of both curves are very similar across all experimental cases – reduced volume of water in the sediment samples eventually leads to a significant ramp-up in resultant stress experienced by the sample.
4. However, analysis and linearization of the ramp-up regime on the stress-void ratio curves require alternative theoretical treatment, which is beyond the scope of this thesis.

References

ASTM D2435, ASTM International. <https://www.astm.org/Standards/D2435.htm>
<accessed Sept 2017>.